THESIS FOR THE DEGREE OF DOCTOR OF PHILOSOPHY

Interplay of Nanostructure and Molecular Doping of Poly(3-hexylthiophene)

JONNA HYNYNEN

CHALMERS

Department of Chemistry and Chemical Engineering

CHALMERS UNIVERSITY OF TECHNOLOGY

Gothenburg, Sweden 2019

Interplay of Nanostructure and Molecular Doping of Poly(3-hexylthiophene)
JONNA HYNYNEN
ISBN 978-91-7905-161-7

Doktorsavhandlingar vid Chalmers tekniska högskola
Ny serie nr 4628
ISSN 0346-718X

Department of Chemistry and Chemical Engineering
Chalmers University of Technology
SE-412 96 Gothenburg
Sweden
Telephone + 46 (0)31-772 1000

Cover: *"Horsepower" Illustration by Mattias Larson*

30 years ago no one believed that the internet would fit in your pocket.
Who knows what the future will bring?

Chalmers Reproservice
Gothenburg, Sweden 2019

Interplay of Nanostructure and Molecular Doping of Poly(3-hexylthiophene)

Jonna Hynynen

Department of Chemistry and Chemical Engineering

Chalmers University of Technology

SE-412 96 Gothenburg, Sweden

ABSTRACT

The accelerating growth of the number of inter-connected small devices, which together make up the so-called *Internet of Things*, is increasing the need for autonomous power sources. Heat is an abundant and often wasted source of energy. Thermoelectric generators could be used to harvest this waste energy. Small devices could potentially be powered by low-grade heat sources using flexible plastic thermoelectric generators.

This thesis discusses thermoelectric plastics and in particular the semiconducting polymer poly(3-hexylthiophene) (P3HT). P3HT is a model conjugated polymer that is commercially available and has become an important reference material for the study of optoelectronic processes in organic semiconductors.

At first, I investigated isotropic thin films of P3HT doped with 2,3,5,6-Tetrafluoro-7,7,8,8-tetracyanoquinodimethane (F4TCNQ). I chose doping from the vapour phase as this allowed me to disentangle the influence of polymer processing and doping. I demonstrate that by improving the degree of solid state order of P3HT it is possible to strongly increase the electrical conductivity, which enhances the thermoelectric power factor from 0.2 to 2.7 μW m^{-1} K^{-2}.

Secondly, I explored the impact of orientation on the thermoelectric properties of P3HT. I chose to study highly anisotropic thin films of P3HT, aligned using a high temperature rubbing technique. Further, I investigated free-standing bulk tapes that where uniaxially oriented through tensile drawing. Sequential doping from solution with F4TCNQ or a molybdenum dithiolene complex allowed me to preserve the anisotropy of both thin films and stretched tapes. I found that orientation of the polymer allows to further increase the thermoelectric properties in the direction of alignment. As a result, a power factor of 16 μW m^{-1} K^{-2} for tensile drawn tapes and ~ 100 μW m^{-1} K^{-2} for rubbed thin films is obtained. Furthermore, oriented P3HT tapes show no change in the glass transition temperature of about 20 °C upon doping with a molybdenum dithiolene complex, which suggests that tensile drawing can be used to prepare flexible thermoelectric materials.

Keywords: Thermoelectric plastic, semiconducting polymer, doping, P3HT, F4TCNQ, Mo(tfd-$COCF_3$)$_3$, structure-property relationships

ACKNOWLEDGEMENT

There are many people that I owe a great debt of gratitude.

First of all I would like to express my gratitude to my supervisor **Christian Müller**. Thanks for taking me in as a PhD student and for the support during the years.

I would also like to thank the people that I have worked very closely with at Chalmers, So thank you:

Mattan who supervised me during my graduate MSc-work and who encouraged me to stay in the group to do a PhD; **Renee** for being a friend and for answering all my stupid questions; **Liyang** for your patience; **David K** for all your help and your company during AWs; **Ida** for keeping me company in the early hours at work and for a lot of nice discussions (work and non-work related); **Lotta** for helping out with all the practical stuff regarding work and I'm sorry I didn't bring Tuva in to work as much as I should have; **Anna H**. for not killing me the last month and I'll never forget the Malbec; **Anja** for all your help and nice discussions both at work and at AWs; **Jason** for all the fun; **Johnas** for all your "English translations" and for making lunchtime at work very joyful and **Massi** for setting the standard.

And thanks to all the amazing ladies that I have shared my time with at Chalmers: **Alicja, Amaia, Ambra, Anna P, Emmy, Maria Q, Mariza, Sarah, Sandra, Sepideh, Sozan and Yingwei**, you rock! For the rest of the **floor 8 colleges**, thank you for creating an amazing work environment and thanks for all the lovely fredags-fika!

I would also like to thank those people outside of Chalmers that I have had the privilege to collaborate with; Mario C. and Davide B. at IIT PoliMi; Rahim M. and Aram A. from KAUST; Martijn K. from LiU; Yadong Z., Stephen B. and Seth M. from Georgia Tech and thank you Martin B., Laure B. and Viktoriia U. CNRS for really engaging in our project.

Nina, **Meiju** och **Melinda** utan er är jag ingenting.
Mattias du är mitt hjärta.

And last but not least

Tack till alla kvinnor i mitt liv. Tack för att ni har visat mig era olika sidor: starka, roliga, sköra, ångestfyllda. Trötta, omtänksamma, fokuserade, målmedvetna. Tack för att ni har lärt och fortfarande lär mig saker. Funnits där, peppat. Tagit med mig på äventyr, fått mig känna trygghet, lånat ut soffa och säng. Dansat cancan, bjudit på te, sjungit finska sånger, och fått mig att andas. Ni betyder allt.

Our lives begin to end the day we become silent about things that matter.

NOMENCLATURE

α	Seebeck coefficient
α-NPD	N,N’-di-[1-naphthyl)-N,N’-diphenyl]-1,1’-biphenyl-4’4’-diamine
AcN	acetonitrile
CB	chlorobenzene
CF	chloroform
CHN	cyclohexanone
CTC	charge transfer complex
CV	cyclic voltammetry
DDB	dodecaborane
DMA	dynamic mechanical analysis
DDQ	2,3-Dichloro-5,6-dicyano-1,4-benzoquinone
DOS	density of states
DSC	differential scanning calorimetry
DPP	diketopyrrolopyrrole
EA	electron affinity
ED	electron diffraction
EDX	energy dispersive X-ray spectroscopy
F2TCNQ	2,5-difluoro-7,7,8,8- tetracyanoquinodimethane
F4TCNQ	2,3,5,6-tetrafluoro-7,7,8,8-tetracyanoquinodimethane
FETs	field effect transistors
FTS	fluoroalkyl trichlorosilane
GIWAXS	gracing-incidence wide-angle X-ray scattering
ΔH	heat of enthalpy
HH	head-head
HOMO	highest occupied molecular orbital
HT	head-tail
ICT	integer charge transfer

IDT	indacenodithiophene
IE	ionization energy
IoTs	internet of things
k	thermal conductivity
LUMO	lowest unoccupied molecular orbital
μ	charge carrier mobility
M_n	number average molecular weight
M_w	weight average molecular weight
Mo(tfd-$COCF_3$)$_3$	molybdenum tris[1-(trifluoroacetyl)-2-(trifluoromethyl)ethane-1,2-dithiolene]
oCVD	oxidative chemical vapour deposition
oDCB	*o*-dichlorobenzene
OFETs	organic field effect transistors
OLEDs	organic light emitting diodes
OSCs	organic solar cells
P3DDT	poly(3-dodecyl-thiophene)
P3HT	poly(3-hexylthiophene)
PBTTT	poly(2,5-bis(3-tetradecylthiophen-2-yl)thieno[3,2-b]thiophene)
PAc	polyacetylene
PAGs	photoacid generators
PE	polyethylene
PEO	poly(ethylene oxide)
PEDOT	poly(3,4-ethylenedioxythiophene)
PF	power factor
PSS	polystyrene sulfonate
PVC	polyvinyl chloride
RR	regioregularity
RSoXS	resonant soft X-ray scattering
RT	room temperature
σ	electrical conductivity

SEM	scanning electron microscopy
T_g	glass transition temperature
T_m	melting temperature
TAGs	thermal acid generators
TCB	1,2,4-trichlorobenzene
TDAE	tetrakis(dimethylamino)ethylene
TEM	transmission electron microscopy
TFSI	bis(trifluoromethylsulfonyl)imide
TGA	thermogravimetric analysis
Tol	toluene
Tos	tosylate
TT	tail-tail
UV-vis	ultraviolet-visible
W	free exciton bandwidth
WAXS	wide angle X-ray scattering
ZT	figure of merit

LIST OF PUBLICATIONS

This thesis consists of an extended summary and the following appended papers:

Paper I **Enhanced Electrical Conductivity of Molecularly p-Doped Poly(3-hexylthiophene) through Understanding the Correlation with Solid-State Order**.
Jonna Hynynen, David Kiefer, Liyang Yu, Renee Kroon, Rahim Munir, Aram Amassian, Martijn Kemerink, Christian Müller
Macromolecules, **2017**, 20, 8140-8148

Paper II **Influence of crystallinity on the thermoelectric power factor of P3HT vapour-doped with F4TCNQ.**
Jonna Hynynen, David Kiefer, Christian Müller
RSC Advances, **2018**, 3, 1593-1599

Paper III **Improved thermoelectric power factor of poly(3-hexylthiophene) through in-plane alignment and doping with a molybdenum dithiolene complex.**
Viktoriia Untilova, Jonna Hynynen, Anna I. Hofmann, Laure Biniek, Stephen Barlow, Seth Marder, Christian Müller, Martin Brinkmann
Manuscript in preparation

Paper IV **Enhanced Thermoelectric Power Factor of Tensile Drawn Poly(3-hexylthiophene).**
Jonna Hynynen, Emmy Järsvall, Renee Kroon, Yadong Zhang, Stephen J. Barlow, Seth R. Marder, Martijn Kemerink, Anja Lund, Christian Müller
ACS Macro Letters, **2019**, 1, 70-76

CONTRIBUTION REPORT

Paper I	Main author. Preparation of samples and doping. Optical, electrical and thermal measurements. Calculations of dopant concentration made by D.K. Models by M.K. Most of the data analysis and interpretation. Compiled the data and wrote the paper together with C.M. and M.K.
Paper II	Main author. Preparation of samples and doping. Optical and electrical measurements. Most of the data analysis and interpretation. Calculations of dopant concentration made by D.K. Compiled the data and wrote the paper together with C.M.
Paper III	*manuscript in preparation*. Co-author. Experimental set-up together with V.U. Performed doping of samples. Compiled the data and did the analysis together with V.U. Wrote the paper together with C.M., V.U. and A.H.
Paper IV	Main author. Preparation of films, tensile drawing and doping of samples. Electrical and WAXS measurements. Data analysis and interpretation together with C.M. and A.L. Compiled the data and wrote the paper together with C.M., M.K. and A.L.

Related publications not included in thesis

Paper 5 **Thermoelectric plastics: from design to synthesis, processing and structure-property relationships.**
Renee Kroon, Desalegn Alemu Mengistie, David Kiefer, Jonna Hynynen, Jason D. Ryan, Liyang Yu, Christian Müller
Chemical Society Reviews, **2016**, 45, 6147-6164

Paper 6 **Highly Insulating Polyethylene Blends for High-Voltage Direct-Current Cables.**
Mattias G. Andersson, Jonna Hynynen, Mats R. Andersson, Villgot Englund, Per-Ola Hagstrand, Thomas Gkourmpis, Christian Müller
ACS Macro Letters, **2017**, 6, 78-82

Paper 7 **Additive-Like Amounts of HDPE Prevent Creep of Molten LDPE: Phase-Behaviour and Thermo-Mechanical Properties of a Melt-Miscible Blend.**
Mattias G. Andersson, Jonna Hynynen, Mats R. Andersson, Per-Ola Hagstrand, Thomas Gkourmpis, Christian Müller
Journal of Polymer Science, Part B: Polymer Physics, **2017**, 55, 146-156

Paper 8 **Bulk Doping of Millimetre-Thick Conjugated Polymer Foams for Plastic Thermoelectrics.**
Renee Kroon, Jason D. Ryan, David Kiefer, Jonna Hynynen, Eva Olsson, Christian Müller
Advances Functional Materials, **2017**, 27, 1704183

Paper 9 **Double doping of conjugated polymers with monomer molecular dopants.**
David Kiefer, Renee Kroon, Anna I. Hofmann, Hengda Sun, Xianjie Liu, Alexander Giovannitti, Dominik Stegerer, Alexander Cano, Jonna Hynynen, Liyang Yu, Yadong Zhang, Dingqi Nai, Thomas F. Harrelson, Michael Sommer, Adam J. Moulé, Martijn Kemerink, Seth R. Marder, Iain McCulloch, Mats Fahlman, Simone Fabiano, Christian Müller.
Nature Materials, **2019**, 18, 149-155

Patent Applications

PA 1 **EP3261096 – Cable and Composition**

Per-Ola Hagstrand, Villgot Englund, Thomas Gkourmpis, Mattias Andersson, Jonna Hynynen, Christian Müller.

2017 European Patent EP3261096

Retrieved from https://register.epo.org/application?number=EP16175588

PA 2 **US2019206588 – Cable with Improved Electrical Properties**

Per-Ola Hagstrand, Thomas Gkourmpis, Antonios Gitsas, Villgot Englund, Ulf Nilsson, Mattias Andersson, Jonna Hynynen, Christian Müller

2019 United States Patent US20190206588

Retrieved from https://worldwide.espacenet.com/publicationDetails/biblio?CC=US&NR=201920658 8A1&KC=A1&FT=D

TABLE OF CONTENTS

ABSTRACT iii
NOMENCLATURE vi
LIST OF PUBLICATIONS ix

1. INTRODUCTION 1
   1.1 Conjugated Polymers 2
   1.2 Poly(3-hexylthiophene) 2
   1.3 Doping of Conjugated Polymers 6
   1.4 Interplay of Solid State Order and Molecular Doping 10
   1.5 Aims of This Thesis 16

2. ISOTROPIC THIN FILMS OF P3HT 17
   2.1 Solid State Structure Modification of Thin Films of P3HT 17
   2.2 Characterisation of Solid State Order and Change Upon Doping 21
   2.3 Thermoelectric Properties of Isotropic Thin Films 23

3. ANISOTROPIC THIN FILMS OF P3HT 29
   3.1 High Temperature Rubbing of P3HT 30
   3.2 Characterisation of Solid State Order and Change upon Doping 30
   3.3 Thermoelectric Properties of Rubbed P3HT 32

4. BULK PROCESSING OF P3HT 37
   4.1 Anisotropic Bulk Films 37
   4.2 Tensile Drawn P3HT 38
   4.3 Characterisation of Solid State Order and Change upon Doping 41
   4.4 Thermoelectric Properties of Tensile Drawn P3HT 44
   4.5 Mechanical Properties of Doped P3HT Tapes 46

5. P3HT FIBRES 49
6. CONCLUSIONS 57
7. OUTLOOK 60
BIBLIOGRAPHY 62

1. INTRODUCTION

”It’s about electric plastics”, that is how Bengt Nordén described the discovery of electrically conducting polymers, when the Nobel Prize in chemistry in 2000 was awarded jointly to Alan J. Heeger, Alan G. MacDiarmid and Hideki Shirakawa “for the discovery and development of conductive polymers.”[1-2] Since the discovery in the mid-1970s, the field of organic electronics has yielded a multitude of important devices such as organic light emitting diodes (OLEDs),[3-5] organic solar cells (OSCs)[6-8] and organic field effect transistors (OFETs).[9-11] Moreover, semiconducting polymers could pave the way for environmentally friendly and biocompatible electronics in applications such as organic batteries,[12-13] organic bioelectronics[14-17] and organic thermoelectrics.[18-20]

Thermoelectric devices exploit the so-called Seebeck effect, which allows direct conversion of heat into electrical energy or vice versa (i.e. Peltier effect). This opens up the possibility to increase the energy efficiency of e.g. combustion engines by turning waste heat into electrical power. Further, low grade heat gradients could be used to autonomously power the myriad of distributed microelectronic devices that are to make up the *Internet of Things* (IoT).

As of today thermoelectrics are based on inorganic compounds such as PbTe and Bi_2Te_3, with a conversion efficiency of 5 - 20% (depending on the operating temperature).[21] Just as for all heat engines the efficiency is limited by the Carnot efficiency (cf. section 1.4.3). However, inorganic thermoelectric materials suffer from some inherent drawbacks such as high processing cost, and they comprise of rare and often toxic elements, which limits the use to high value applications. Organic semiconductors, such as conjugated polymers, are an attractive alternative to inorganic materials since they consist of earth abundant non-toxic elements (carbon, oxygen, sulphur and nitrogen), and allow for cost-effective processing from solution or melt. While organic materials cannot withstand high temperatures above 200 °C, which rules out their use in combustion engines, they may allow to harvest low-grade industrial heat sources as well as e.g. body heat.

This thesis will focus on establishing structure-property relationships relevant for organic thermoelectric materials. The conjugated polymer poly(3-hexylthiophene) (P3HT) will be used as a model material to explore how the thermoelectric performance depends on the solid state nano- and micro-structure and the degree of molecular doping.

1.1 Conjugated Polymers

Polymers are macromolecules, i.e. molecules of high molecular mass, that consist of repetitive units of one or more building blocks, so-called monomers. Most polymers do not conduct electricity and are therefore commonly used as insulators. For instance, the jacketing of power cables is typically composed of polyvinyl chloride (PVC) or polyethylene (PE). In the 1970's it was discovered that polyacetylene (PAc) could be made electrically conducting by oxidation of the polymer with bromine or iodine vapour.[1] A key property of semiconducting polymers is their conjugated backbone that comprises alternating single and double bonds, leading to delocalisation of π-electrons along its length (Figure 1.1). Energy level splitting results in a bonding π-orbital and an anti-bonding π*-orbital, i.e. a highest occupied molecular orbital (HOMO) and lowest unoccupied molecular orbital (LUMO) (Figure 1.2). The energy gap between the LUMO and HOMO is called the bandgap (E_g), which in case of conjugated polymers is typically about 1.5 to 2.5 eV.[22-23] The smaller bandgap as compared to saturated polymers permits the excitation of electrons from the HOMO to the LUMO as well as charge injection, resulting in a semiconducting material. To turn a conjugated polymer into a conducting material, charges need to be created through doping, i.e. the transfer of charges in the form of electrons or protons to or from the conjugated backbone (cf. section 1.3).

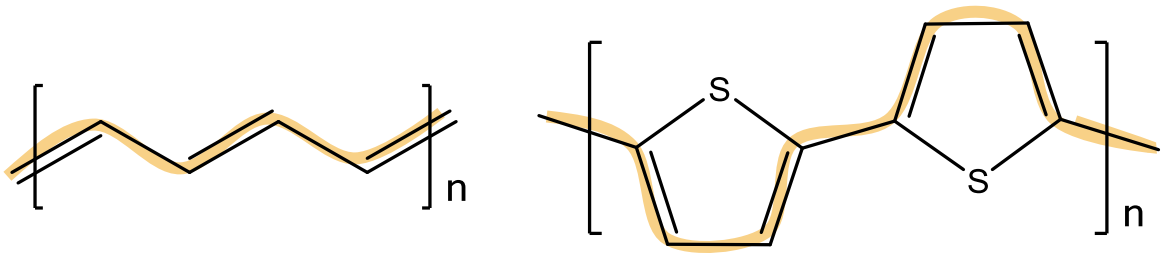

Figure 1.1. Alternating single-double bonds that form the conjugated backbone of PAc (left) and polytiophene (right)

1.2 Poly(3-hexylthiophene)

P3HT is a model conjugated polymer that is commercially available on the gram to kilogram scale. The backbone of P3HT consists of thiophene units with a hexyl side chain (Figure 1.3), the length of which reflects a compromise between ease of processing and a maximal volume fraction of the charge conducting backbone.[24-26] The addition of alkyl side chains is a common means to enhance the solubility of conjugated polymers in organic solvents, and enables the synthesis of high molecular weight materials.[27-29]

Both, the glass transition and melting temperature of poly(3-alkylthiophene)s decrease with side chain length, with P3HT showing values of typically about T_g, ~ 20°C and T_m ~ 220 - 250°C.[30-31]

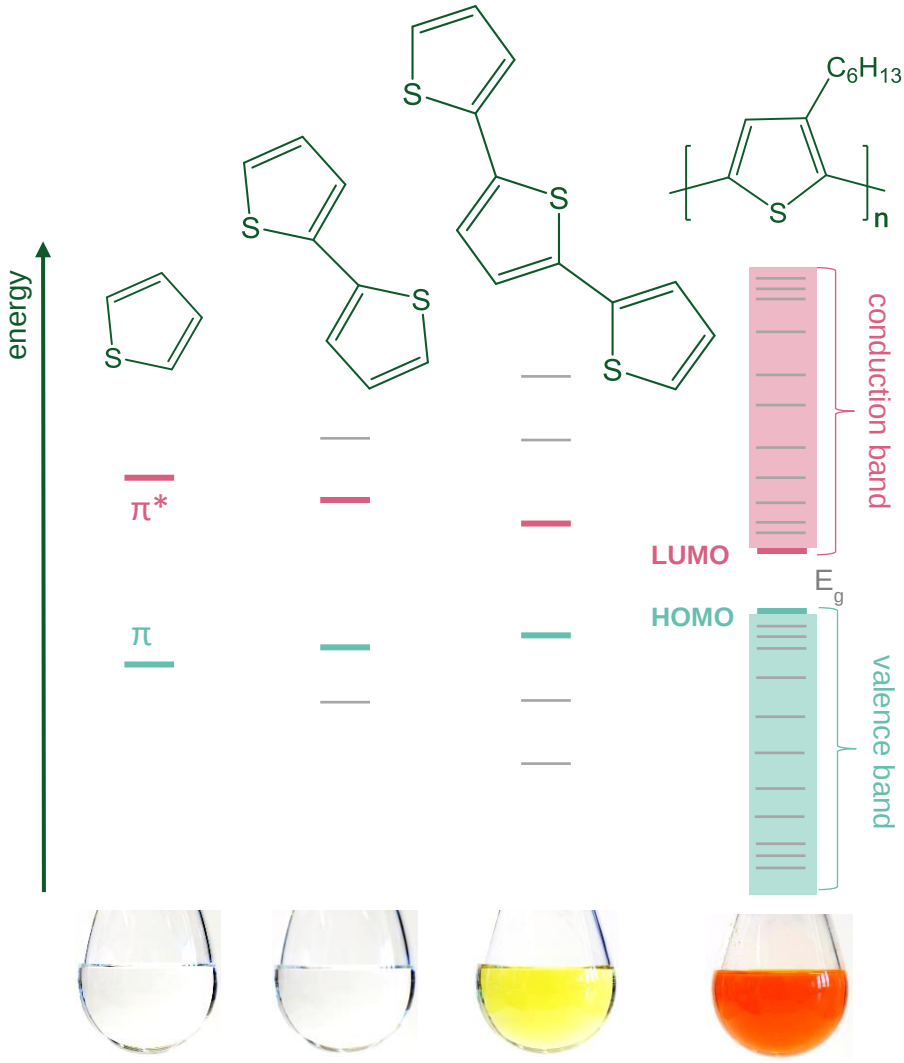

Figure 1.2. Evolution of the HOMO and LUMO levels as well as E_g, with increasing number of thiophene repeat units; the images of 5 g L^{-1} solutions of P3HT in chloroform illustrate the narrowing of E_g, which leads to a red-shift in absorption for P3HT. Crystallisation will lead to a further decrease in E_g due to electron delocalisation across adjacent chain segments. Adapted from reference [18]. Published by The Royal Society of Chemistry 2016.

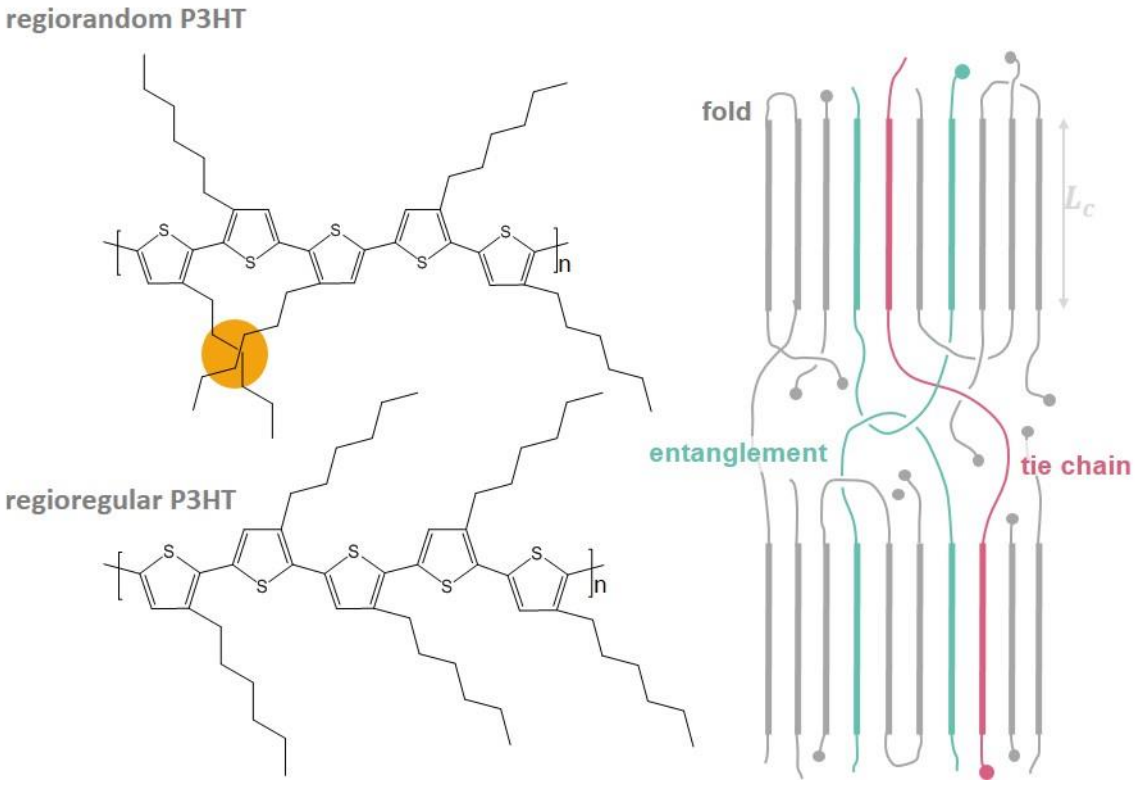

Figure 1.3. Left: Illustration of regiorandom and regioregular P3HT, coloured circle indicates the steric repulsion of the side chains. Right: Illustration of polymer entanglements and tie chains in a semicrystalline polymer. Adapted from reference [18]. Published by The Royal Society of Chemistry 2016.

The solid state nanostructure of P3HT determines both its mechanical and electronic properties (cf. section 1.4). The extent to which P3HT is able to crystallise and the type of solid state nanostructure that develops during solidification depend on three principal factors: (1) the regioregularity (RR),[32] (2) the molecular weight,[30, 32-36] and (3) the processing route.[36-39]

The regioregularity of P3HT varies because the repeating unit 3-hexylthiophene is asymmetric, which gives rise to different types of coupling during synthesis. Dimers of adjacent repeat units can form three distinct regioisomers: head-head (HH), head-tail (HT) and tail-tail (TT). Depending on the fraction of regioisomers and the coupling between them (HH-TH, HH-TT, TT-HT and HT-HT) the polymer will have a certain regioregularity (Figure 1.3). In a fully regioregular P3HT all couplings are HT-HT, which allows full conjugation resulting in a more planar backbone.[40] Instead, regio-irregularities result in steric repulsion of the side chains, which leads to twisting of the backbone. The ability of the backbone to become more planar affects the extent to which the polymer can crystallise and, hence, the optoelectronic properties of the material (cf. section 1.4.1).

The impact of the molecular weight and the selected processing method strongly influence each other and will be discussed in tandem. P3HT can be processed both from melt and solution. In both cases the molecular weight determines the viscosity and hence the conditions that must be chosen to impart processability. Above a molecular weight of about 25 kg mol^{-1} P3HT chains entangle in the melt, which leads to a drastic increase in viscosity.[32-34, 36]

When processed from the melt, short-chain material tends to form chain extended crystals. Instead, higher molecular weights give rise to a nanostructure comprised of crystalline lamellae, connected by ties chains, which are embedded in an amorphous matrix[41] (Figure 1.3).

When P3HT is processed from organic solvents, relatively low concentrations of about 1 - 20 g L^{-1} are typically chosen in order to reduce the degree of chain entanglement, and to ensure complete solubility, i.e. to avoid aggregation. Single crystals of P3HT grown from solution are rare, due to entanglements of polymer chains, and have been reported only by Rahimi *et al.*[42] There are however processing schemes that allow formation of highly ordered P3HT in the form of so-called nanofibrils, i.e. quasi 1D structures with a width of 10 - 20 nm and a length of 100s of nanometres to micrometres with π-stacking along their long axis. Common recipes for the growth of nanofibrils are the "whisker method",[43-44] "mixed solvent method"[45-46] and "sonification method".[47] There are several common techniques for the deposition of P3HT from solution, typically with the aim to form sub-micrometre thin films, including spin coating, drop casting, dip coating and doctor blading. These processes are fast and crystallisation occurs during drying of the solvent, which gives rise to a non-equilibrium crystallisation process. This typically leads to a material with a degree of order in between that of nanofibrils and melt processed P3HT. The choice of processing solvent will strongly affect the resulting solid state order of the polymer, with high boiling point solvents such as chlorinated benzenes giving rise to a higher degree of order than e.g. chloroform (CF) because they give the polymer more time to crystallise during evaporation of the solvent.[37-38, 48-50]

Several processing and post-processing techniques are commonly applied to increase the degree of order of P3HT. Those include the use of nucleating agents,[51] epitaxial crystallisation,[52] friction-transferred films,[53] high temperature rubbing,[54-56] strain alignment using a carrier substrate[57] and control of nucleation density by vapour annealing, which can lead to micrometre-large spherulites.[58] For bulk processing of P3HT cf. section 4.

1.3 Doping of Conjugated Polymers

Conjugated polymers are semiconductors, i.e. they do not contain free charges in their undoped form and therefore do not display any appreciable electrical conductivity. Free charges can be added through doping, typically by using acid/base dopants,[59-62] redox dopants[63-64] or Lewis acid/base dopants.[65-68] In case of redox dopants, which is employed in this thesis, doping involves the transfer of an electron between the backbone of the polymer and a small-molecular dopant, where oxidation of the backbone leads to p-doping and reduction to n-doping (Figure 1.4). It is important to note that, in contrast to inorganic semiconductors, the volume fraction of dopants needed to create a highly conducting material can exceed 10s of percent. Therefore, a doped conjugated polymer should be considered as a new material comprising of the polymer plus a sizable amount of small-molecular additive. Hence, doping is likely to affect the structural order of the polymer, which may reduce the charge carrier mobility and in turn lower the electrical conductivity (cf. section 1.4).

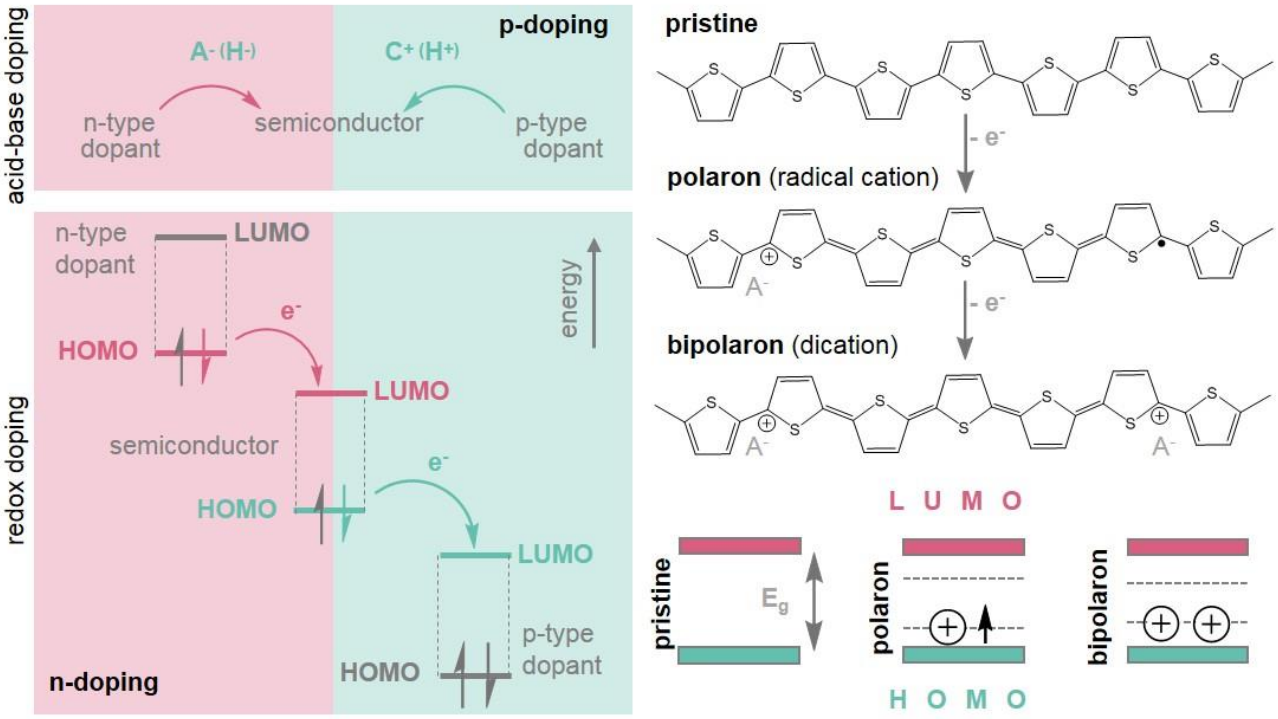

Figure 1.4. Left: Basic principle of acid–base doping; and redox doping; Right: Schematic for p-doping of polythiophenes. Electron transfer to the undoped polymer leads to the formation of a polaron and finally a bipolaron state;[69] counter ions ensure charge neutrality; below the corresponding band structure evolution. Adapted from reference [18]. Published by The Royal Society of Chemistry 2016.

The focus in this thesis will be on redox p-doping with molecular electron acceptors. There are two common fundamental interaction mechanisms of the dopant and the semiconducting matrix: ion pair formation through integer charge transfer (ICT) and ground state charge transfer complex (CTC) formation because of fractional charge transfer, which both result in a modified density of states (DOS). The density of state function describes the number of accessible states in a system and is essential when determining carrier concentrations and energy distributions of carriers within a semiconductor (a mathematical description of various occupied states, averaged over space and time domains). Whether an ICT or CTC is formed depends on the overlap between the molecular orbitals of the dopant and the semiconductor,[70-73] the distribution of charges in the semiconductor[74-76] and the strength of the dopant.[64, 77]

For ICT formation the electron affinity (EA) of the p-dopant must be equal or higher than the ionization energy (IE) of the polymer, as a result of which one electron is transferred from the polymer to the dopant (Figure 1.5). The transfer of an electron results in a dopant anion and a polymer cation, an ion pair. In some cases complete charge transfer has been observed even though the EA of the acceptor was below the IE of the donor, which was explained with electrostatic interactions between donor and acceptor.[78-80]

For CTC formation the frontier orbitals of the polymer and dopant hybridise and form a new set of occupied orbitals (Figure 1.5). Salzmann *et al.* have proposed that for p-type doping, the IE of the CTC is higher and its EA lower than the IE of the polymer, which creates a filled level below the conduction band of the polymer.[64]

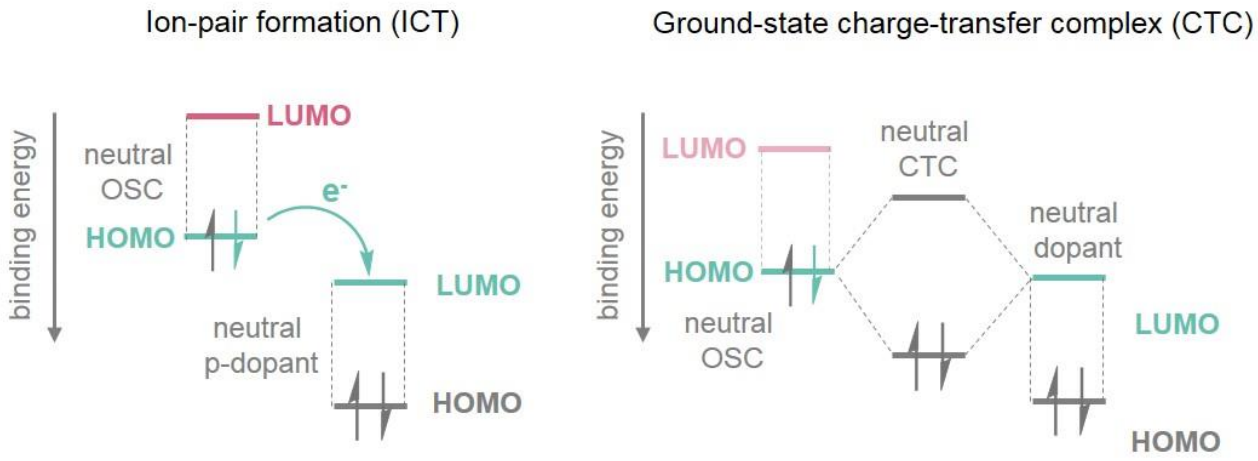

Figure 1.5. Schematic drawing of the formation of a charge transfer complex (ICT) (left) and ion pair (CTC) (right); both cases for p-type doping. Adapted from reference [64]. Published by American Chemical Society 2016.

The electrical conductivity of films with the same degree of doping, i.e. the same number of generated charges, can vary and is usually explained by differences in the solid state order of the polymer (cf. section 1.4.1). The choice of doping scheme is an important parameter and has an influence on ionization efficiency and on the resulting solid state structure of the doped material (cf. section 1.3.2 and 1.4). Two common doping schemes are well described in literature: (1) co-processing and (2) sequential doping. Co-processing of polymer and dopant is simple and only requires one processing step. The polymer and dopant are both dissolved in a common solvent, followed by evaporation of the solvent during spin coating, blade coating etc. One major drawback of co-processing is the risk of precipitation of the materials already in the processing solvent, caused by the formation of less soluble polymer-dopant complexes through charge transfer, which complicates film formation.[81-82] This can be circumvented by reducing the polymer concentration and heating of the processing solution. Sequential doping on the other hand is a two-step process where the polymer is first processed alone from solution or melt, which allows controlled solidification. Subsequently, the solid polymer (e.g. a solution cast thin film or a stretched tape) is doped through exposure to dopant vapour[79, 83-85] or through contact with a dopant dissolved in an orthogonal solvent.[81, 86] One limitation of sequential doping is the need for the dopant to diffuse through the polymer, which means that doping of bulk structures likely takes a considerable amount of time.[87]

1.3.1 Common Redox-type P-type Dopants

Early examples of redox doping involved the use of iodine vapour (I_2) or by doping with iron(III) chloride ($FeCl_3$) solutions. Iodine was for example used in the study by Shirakawa *et al.* in 1977 as mentioned earlier in section 1, as well as for doping of stretch-aligned PAc, which reached an electrical conductivity of about 10^5 S cm^{-1}.[88] However, small dopants such as iodine results in materials with poor stability of the doped state due to rapid diffusion and sublimation of the dopant.[89] In my work I have chosen to work with 2,3,5,6-tetrafluoro-7,7,8,8-tetracyanoquinodimethane (F4TCNQ) and molybdenum tris[1-(trifluoroacetyl)-2-(trifluoromethyl)ethane-1,2-dithiolene] ($Mo(tfd\text{-}COCF_3)_3$) (Figure 2.7).

F4TCNQ has been widely studied as a dopant for P3HT and hence the doping mechanism as well as the effect of different processing techniques are well established. A major drawback of F4TCNQ is its high vapour pressure, which means that it slowly sublimes, albeit less rapidly than iodine, leading to doped materials that are suitable for fundamental studies in a laboratory but would slowly lose their electrical properties when used for longer times (cf. section 2.4).

Doping of P3HT with the molybdenum complex $Mo(tfd\text{-}COCF_3)_3$, which for some time has been used as an oxidant in synthetic organometallic chemistry,[90] is less studied. $Mo(tfd\text{-}COCF_3)_3$ has a higher molecular weight compared to F4TCNQ (858.46 and 276.15 g mol^{-1} respectively), meaning that it likely diffuses less rapidly. Qi *et al.* reported an increased thermal stability of N,N'-di-[1-naphthyl)-N,N'-diphenyl]-1,1'-biphenyl-4'4'-diamine (α-NPD) doped with $Mo(tfd)_3$ at 110 °C compared to the same material doped with F4TCNQ, which was explained with the absence of diffusion of the former as indicated by Rutherford backscattering.[91]

1.3.2 Doping Efficiency

The term *doping efficiency* is often used in the literature but with different meaning. Here, I distinguish between two processes, (1) the ionization of the polymer-dopant pair, and (2) dissociation of polarons from the counterion. Upon addition of dopant molecules to a polymer the dopant first needs to ionize. During the ionization step, an electron is transferred from the donor (for p-type doping, the donor is the polymer) to the acceptor (for p-type doping, the acceptor is the dopant). The maximum ionization efficiency would be 100% in case of ICT and if all dopant molecules added to the material formed an ion pair with the semiconductor host. For doping of P3HT with F4TCNQ the ionization efficiency is typically on the order of 20 to 70 %,[92-93] limited because of aggregation of dopant molecules. Further, F4TCNQ has an EA ~ 5.2 eV, and therefore is able to undergo ICT with crystalline but not disordered P3HT, which has an IE of 5.0 eV and 5.25 eV, respectively (IE values measured with cyclic voltammetry (CV) by Ko *et al.*).[94] Hence, dopant molecules that reside in amorphous domains do not generate a hole charge on the polymer, reducing the ionization efficiency.

While P3HT and F4TCNQ typically undergo ICT, the resulting cation (hole polaron) and anion remain Coulombically bound to each other. Charge carriers that are created by ion pair formation must dissociate to become *free* charge carriers to contribute to the electrical conductivity. Dissociation of charges requires a large separation distance, which becomes more difficult with increasing dopant concentration since removal of the cation from its parent anion likely means that the cation is captured within the Coulomb radius of another nearby anion. Voss *et al*. recently reported trapped polarons (non-dissociated charges) for P3HT using ultrafast transient absorption spectroscopy.[95] The dissociation efficiency decreases with higher doping levels, and in case of P3HT and F4TCNQ has a value of about 5 %, as estimated by Pingel and Neher.[96]

Schwartz *et al.* recently investigated how the donor-acceptor distance affects charge dissociation.[97] The authors used a large dopant complex comprising of a dodecaborane (DDB)

core functionalised with 3,5-bis(trifluoromethyl)benzyloxy substituents, DDB-F_{72} (EA ~ 5.7 eV). DDB-F_{72} has a diameter of ~ 2 nm and is too large to enter the crystalline regions of P3HT and is therefore only present in the amorphous part of P3HT. Spatial separation of the anion charge, which is located on the DDB core, and the hole polaron on the polymer leads to highly delocalised and *mobile* charge carriers even in a poorly crystalline material. Further, Graham *et al.* investigated the effect of dopant size on the electrical properties of a variety of polymers with different IE's and solid state nanostructures (crystalline vs amorphous). The authors used Mo(tfd) derivatives that differed in size and EA and concluded that large dopants with a high EA and good miscibility with the polymer would provide a route for highly efficient doping. A larger dopant size was proposed to aid polaron delocalisation due to decreased Coulomb interaction between the hole polaron and dopant anion.[98]

1.4 Interplay of Solid State Order and Molecular Doping

P3HT is, as mentioned, semicrystalline, where crystalline lamellae of planar, π-stacked chain segments are separated by amorphous domains. P3HT has two crystal polymorphs, the more common form I (non-interdigitated side chains) and form II (interdigitated side chains) (Figure 1.6).

Thin films deposited from solution can display a preferential texture with regard to the orientation of crystals relative to the substrate. The texture can be (1) edge on and (2) face on, where in case of the former the π-stacking direction is oriented perpendicular to the substrate normal, whereas the latter is characterised by π-stacking along the substrate normal (Figure 1.6). In a study by Kline *et al*. the orientation of crystallites was altered through surface treatment of the substrate rendering a two to three orders of magnitude increase in the mobility by HMDS or OTS-treated surfaces and was attributed to an increase of in-plane π-stacking of the crystallites.[99] P3HT has an orthorhombic unit cell; the lamellar stacking distance of neat P3HT has a d_{100} spacing of ~ 1.6 nm, while the π-stacking distance is d_{010} ~ 0.38 nm. Upon doping with F4TCNQ the unit cell of P3HT changes dimensions to d_{100} ~ 1.9 nm and d_{010} ~ 0.36 nm.[70, 81-82]

Depending on the doping scheme (co-processing or sequential) and the degree of doping (dopant concentration) different explanations for resulting crystal structure have been proposed. Duong *et al*. argued that the dopant resides in the amorphous parts of P3HT in the low doping regime (molar fraction ~ 0.01), while in the intermittent regime (molar fraction ~ 0.03) a mixed crystal phase forms and at high concentrations (molar fraction >0.03) a new crystalline phase is formed where the P3HT and F4TCNQ form dopant:polymer co-crystallites.[82]

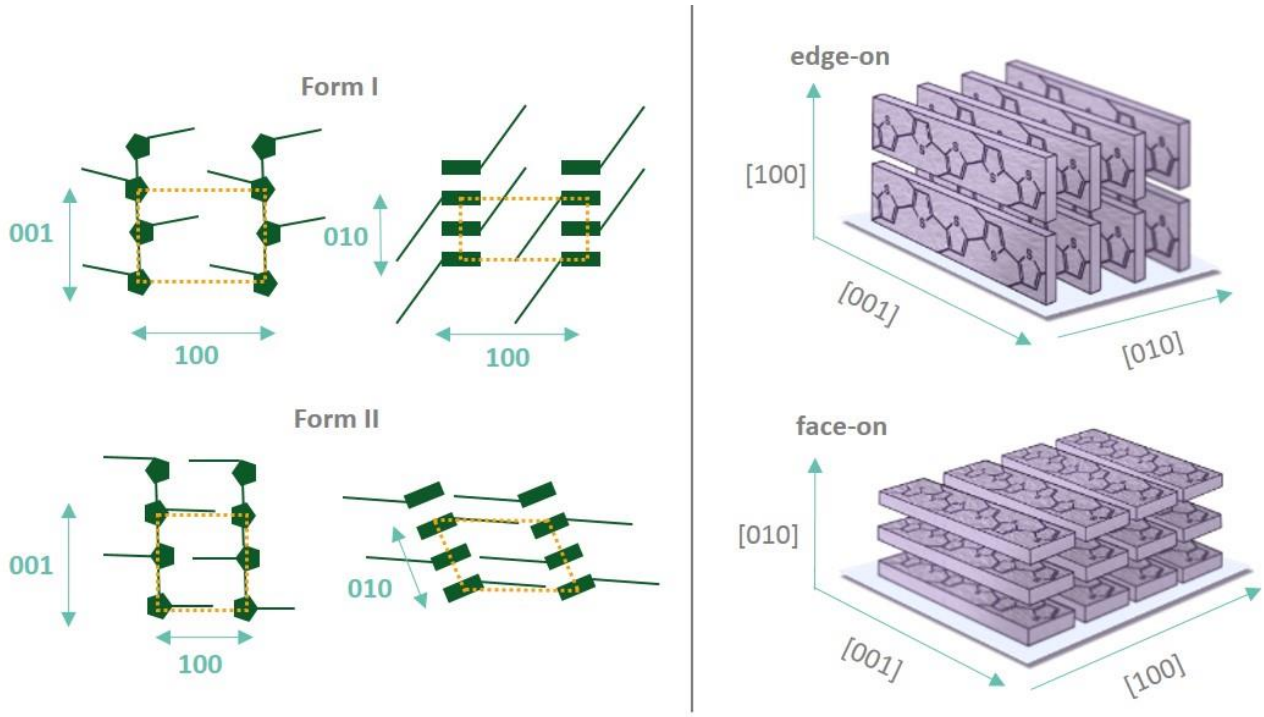

Figure 1.6. Left: Schematic of crystalline form (I) and (II) of P3HT adapted from reference [102] published by American Chemical Society 1996. Right: schematic of crystalline texture of form (I) oriented; edge-on (top) and face-on (bottom) with respect to the substrate.

Subsequently, several other studies of F4TCNQ doped P3HT also reported intercalation of F4TCNQ within the crystallites of P3HT.[70, 81, 86, 100-101]

The observed decrease in the π-stacking distance has been reported by many groups and has been described such as the sidechain geometry promotes closer stacking, orientation effects that alter the distance between the thiophene rings,[79, 85, 103] as well as delocalisation of the polaron across the backbone, which could slightly pull together the backbone in the π-stacking direction.[103-104]

Most studies that deal with doping of P3HT with F4TCNQ agree that the solid state structure of P3HT is of importance for the electrical properties of the doped material. Co-processing of the dopant and polymer usually results in a relatively disordered material because dopant:polymer complexes form already in solution and lead to a lower crystallinity and no texture. For sequentially doped P3HT, where the polymer film is formed first and then doped in a second step; the crystallinity is largely preserved upon sequential doping. As reported by Hamidi-Sakr *et al.* where they investigated the crystalline structure of P3HT upon sequential doing with F4TCNQ, the crystalline structure was largely preserved and the major effect was seen in the periodicity along the side-chains which increased from 16.6 Å to 17.4 - 17.8 Å.[56] Although P3HT

doped with F4TCNQ has been intensely studied, the exact makeup of the doped material with regard to dopant location and crystalline texture remains under debate.

1.4.1 The Effect of Solid State Structure on Charge Transport

A more disordered P3HT results in a lower electrical conductivity for the same concentration of dopant compared to a more ordered material. This is attributed to the different charge mobilities of amorphous and crystalline material. For example, Sirringhaus *et al.* used field effect transistors (FETs) to measure the charge mobility of P3HT as a function of regioregularity and found that for 81% regioregularity the mobility was only 2 x 10^{-4} cm^2 V^{-1} s^{-1} whilst increasing the regioregularity to 96% resulted in charge carrier mobilities of 0.05 - 0.1 cm^2 V^{-1} s^{-1}. π-stacking gives rise to substantial wavefunction overlap allowing 2-dimensional delocalisation of charges within ordered domains, which enhances the mobility of charges.[105] Instead, structural defects such as conformational changes that lead to twisting of the backbone, which is prevalent in disordered, amorphous domains, but also defects in ordered domains (stacking faults and dislocations) will result in loss of conjugation and therefore less mobile charge carriers.[106] More recent studies such as the work by Salleo *et al.* argue that tie chains enhance the connectivity between crystallites and hence benefit charge transport.[107] For low molecular weight material, instead, the nanostructure is comprised of chain extended crystals and each grain boundary represents a defect that impedes charge transport. As a result, the field effect mobility of P3HT strongly increases with chain length up to a molecular weight of about 20 kg mol^{-1}, above which tie chains are present. At the same time, the high viscosity of high molecular-weight material due to chain entanglements impacts the crystallisation kinetics, leading to a more disordered material and hence a somewhat lower charge mobility.[30] Here, it is important to point out that mobility values measured with FETs should not be used to quantitatively describe charge transport in molecularly doped systems since dopant ions represent Coulomb scattering centres that reduce the charge mobility.[96, 108]

The electrical properties of doped P3HT will ultimately depend on several factors including the ionization efficiency, dissociation efficiency and the solid-state nanostructure of the polymer.

1.4.2 Conjugated Polymers as Thermoelectric Materials

When an electrical conductor or semiconductor experiences a temperature gradient because it is placed in contact with a heat source or sink, charge carriers will move from the hot end to the cold end causing an electric potential which can be used to drive a current. This so-called Seebeck effect was discovered by Thomas J. Seebeck in 1821. A decade later in 1834 Jean Peltier

discovered that if an electric current flows through a junction between two semiconductors or conductors heat is generated or removed. This effect is called the Peltier effect. Thermoelectric materials can therefore be used to construct devices both for converting heat to electricity and for cooling/heating applications.

To compare different thermoelectric materials the dimensionless figure of merit $ZT = \alpha^2\sigma T/k$ can be used, where α is the Seebeck coefficient, σ is the electrical conductivity, T is the absolute temperature and k is the thermal conductivity. The ZT should be high and thermoelectric materials should therefore ideally have a large Seebeck coefficient, a high electrical conductivity, and a low thermal conductivity. Benchmark inorganic materials such as Bi_2Te_3 have a ZT of about 1 at room temperature.[109]

The thermal conductivity k describes the ability of a material to transfer heat. Both phonons and electrons contribute to heat transport, and the total thermal conductivity is the sum of their contributions $k = k_{phonon} + k_{electron}$. The electronic part is related to the electrical conductivity by the Wiedemann-Franz law $k_{electron} = L\sigma T$, where L is the Lorenz number, a proportionality constant that for e.g. metals has the value $L = 2.44 \times 10^{-8}$ W Ω K^{-2}. Liu *et al*. have shown that the relationship also holds for poly(3,4-ethylenedioxythiophene) polystyrene sulfonate (PEDOT:PSS).[110] Materials with a low electrical conductivity will have a minor electronic contribution and the thermal conductivity is largely given by the phonon contribution. A phonon is a quantified lattice vibrational energy that transfers heat through lattice vibration, unless it is scattered by defects, impurities and grain boundaries. As polymeric materials are rich in defects their intrinsic thermal conductivity is low, with k_{phonon} ranging from 0.1 to 0.5 W $m^{-1}K^{-1}$.[18] For conducting polymers this means that the electronic contribution is minor until their electrical conductivity approaches 100 S cm^{-1}, at which point $k_{electron}$ and k_{phonon} become comparable. Since many organic materials display a lower electrical conductivity, their ZT is often replaced by the power factor $PF = \alpha^2\sigma$ when evaluating their thermoelectric performance. Here it should be noted that k_{phonon} is considerably larger for oriented polymers leading to values of up to 20 W m^{-1} K^{-1} in case of highly oriented polymer fibres.[111]

The Seebeck coefficient can be regarded as the average entropy per charge carrier and describes the difference in potential ΔV that arises when a material experiences a temperature gradient ΔT according to $\alpha(T) = -dV/dT$. For small changes in temperature, $\alpha(T)$ is more or less constant and $\alpha = -(\Delta V/\Delta T)$. The sign of α denotes the type of charge carriers, $\alpha < 0$ indicates that the carriers are electrons (n-type materials) and $\alpha > 0$ when the carriers are holes (p-type materials).

The electrical conductivity σ is given by $\sigma = N\mu q$ where N, μ and q are the number, mobility and charge of the carriers. To increase the electrical conductivity one could either increase the mobility of the charge carriers by modifying the nanostructure (cf. section 1.4.1), or by adding charge carriers, i.e. through doping or by making the doping process more efficient (cf. section 1.3.2).

Doping of the semiconductor will increase the electrical conductivity but simultaneously decrease the Seebeck coefficient. Table 1 compares the thermoelectric parameters of some common p-type conducting isotropic polymers as well as selected inorganic materials (for anisotropic P3HT see Table 3).

Table 1: Selected literature values for the thermoelectric properties of some common p-type materials measured at a temperature *T*; electrical conductivity σ, Seebeck coefficient α, thermal conductivity *k*, figure of merit *ZT* and power factor *PF*.

Material	**T** (°C)	**σ** (S cm^{-1})	**α** (μV K^{-1})	***k*** (W m^{-1} K^{-1})	**ZT$_{max}$** (-)	**PF$_{max}$** (μW m^{-1} K^{-2})	**Ref.**
P3HT:$FeCl_3$	RT	45	122	-	-	56	112
PBTTT:FTS	RT	1000	33	-	-	110	113
PBTTT:F4TCNQ	RT	670	42	-	-	120	79
PEDOT:Tos+TDAE	RT	70	215	0.4	0.25	324	114
PEDOT:PSS	20	880	72	0.2	0.42	5	115
Bi_2Te_3	117	625	225	0.8	1.50	32	109
SnSe	650	100	350	0.4	2.60	10	116

1.4.3 Design and Efficiency

A thermoelectric element (Figure 1.7) consists of two legs that are composed of a p-type and an n-type material, respectively. One thermoelectric element can only produce a small thermovoltage, in the range of millivolts, which is insufficient to drive any electronic device. Therefore, thermoelectric elements are connected thermally in parallel and electrically in series to increase the overall output voltage, which is the sum of the contributions from each element. Just as for all heat engines the efficiency is limited by the Carnot efficiency $\eta_{carnot} = (T_{hot} + T_{cold})/T_{hot}$.

The maximum power conversion efficiency η_{max} of a thermoelectric leg is given by:

$$\eta_{max} = \eta_{carnot} \frac{\sqrt{1+ZT^*}-1}{\sqrt{1+ZT^*}+T_{cold}/T_{hot}} \quad (1)$$

Where $T^* = (T_{hot} + T_{cold})/2$

The second term in equation 1 balances internal losses due to Joule heating and heat conduction. Calculated maximum power conversion efficiencies with a ZT of 0.1, 0.5 and 1 at 300K are presented in Figure 1.7.[18]

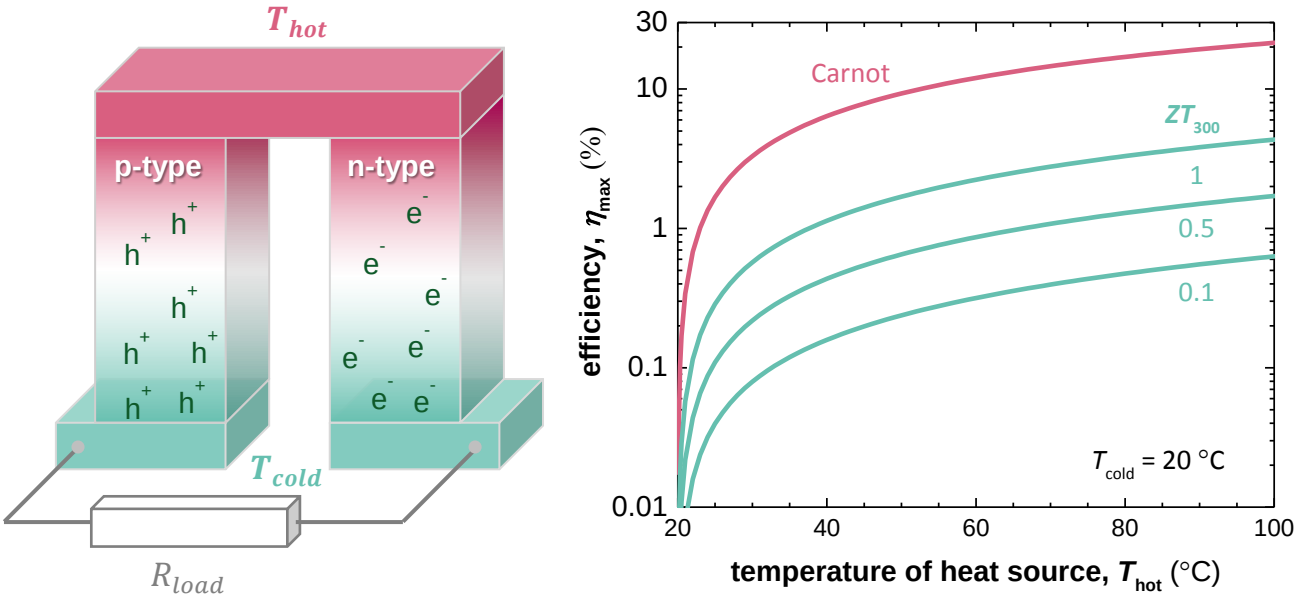

Figure 1.7. Left: Schematic of a thermoelectric element, which comprises one p- and one n-type leg that experience a temperature gradient leading to charge accumulation at the cold ends. Right: The Carnot efficiency (pink) and maximum efficiency of a thermoelectric leg (green) with increasing heat source temperature (the heat sink is kept at T_{cold} = 20 °C) for materials with a ZT of 0.1, 0.5 and 1. Adapted from reference [18]. Published by The Royal Society of Chemistry 2016.

1.5 Aims of This Thesis

In this thesis, the conjugated polymer P3HT is used as a model system to elucidate structure-property relationships relevant for organic thermoelectric materials. This thesis will investigate the following research questions:

- How does the solid state order of the polymer affect the electrical conductivity and Seebeck coefficient of sequentially p-doped P3HT?
- How does doping alter the solid state structure of P3HT?
- How does uniaxial alignment of the polymer in thin films and bulk samples impact the electrical conductivity and the Seebeck coefficient?

2. ISOTROPIC THIN FILMS OF P3HT

As described in the introduction there are multiple ways to control the solid state order of P3HT, which in turn will determine the resulting electronic properties. I wanted to investigate methods for introducing order in P3HT and study how this affects the electrical conductivity and the Seebeck coefficient. I started my PhD studies by investigating spin coated thin films. To produce films with different degrees of solid state order I varied the molecular weight, regioregularity and processing solvent.

2.1 Solid State Structure Modification of Thin Films of P3HT

In order to investigate the effect of the solid state order on the electrical conductivity of P3HT thin films I decided to first establish the impact of the polymer's regioregularity and molecular weight on the electrical conductivity of vapour doped P3HT.

When I planned the study, I wanted to use sequential doping to preserve the solid state structure of my formed P3HT films. I chose vapour doping as a tool to preserve the obtained solid state structure because at the time two promising studies on vapour doping of PBTTT with F4TCNQ had just been published.[83, 117] The setup that I designed consisted of a simple glass crucible containing ~ 20 mg of F4TCNQ where the P3HT film was suspended on top (Figure 2.1). To determine the sublimation temperature of F4TCNQ I performed thermogravimetric analysis (TGA). I observed a steady increase of the sublimation rate above 160°C, reaching a sublimation plateau above ~ 190°C (Figure 2.1). To further tailor the vapour doping parameters, I varied the temperature (150 - 220°C), doping time (from a few seconds to one hour), the heat sink and the material of the crucible (glass, stainless steel and Teflon) as well as the film thickness of P3HT. The best performing (most stable) experimental conditions, as judged by electrical conductivity measurements, were found when using a temperature of 180°C, three minutes doping time and a steel plate as a heat sink on top of the glass slide that carried the spin coated P3HT film. The heat sink maintained the sample temperature at ~ 40°C for doping times up to 10 min. For the mentioned conditions it was possible to dope films with a thickness of up to 120 nm (cf. paper I, Supporting Information Figure S1).

I found that a regioregularity of >84% was required to successfully dope P3HT with F4TCNQ, in terms of attained electrical conductivity. Regiorandom P3HT (28% regioregularity) only resulted in a conductivity of 0.01 S cm^{-1} whereas P3HT with a regioregularity of 84 % displayed a conductivity of 2 S cm^{-1}. This increase in electrical conductivity can be attributed to the lower

IE of P3HT with higher regioregularity. Regiorandom P3HT exhibits an IE ~ 5.25 eV, which is higher than the EA ~ 5.2 eV of F4TCNQ, making the electron transfer unfavourable, although some ordered regions in regiorandom P3HT still undergo charge transfer (cf. paper I: Supporting Information Figure S5 and section 1.4.1). Instead, regioregular P3HT has an IE ~ 5 eV, meaning that doping with F4TCNQ is energetically favoured, leading to a higher number of charges and hence a higher conductivity. In addition, the semicrystalline nature of regioregular P3HT leads to a higher charge carrier mobility, which likely also benefits the electrical conductivity. By using a molybdenum dithiolene complex type of dopant I could further increase the electrical conductivity of regiorandom P3HT to a value of 0.09 S cm^{-1} (cf. Figure 2.2).

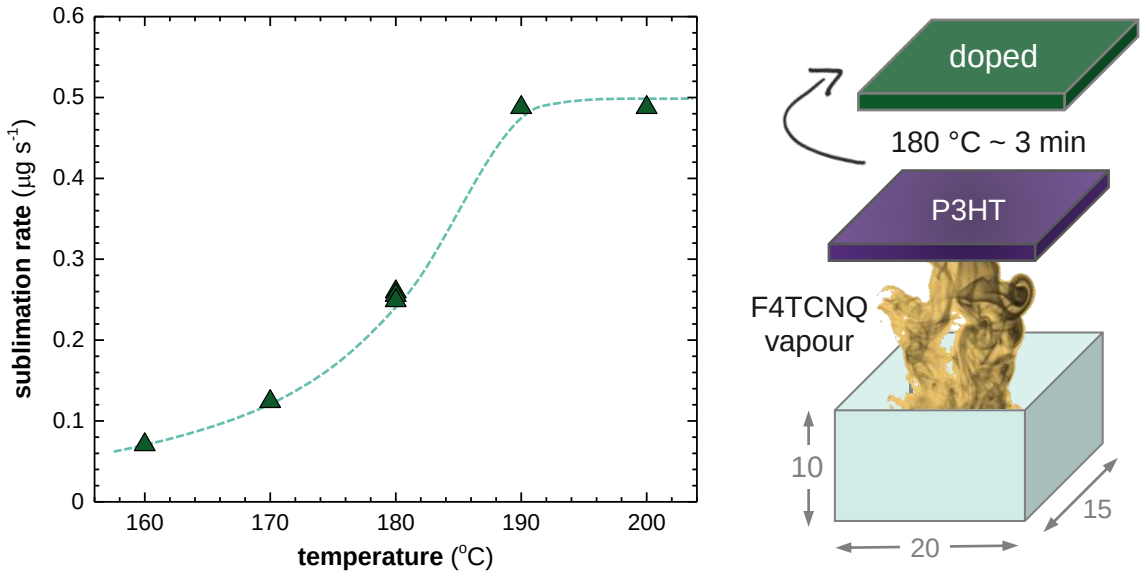

Figure 2.1. Left: F4TCNQ sublimation rate as a function of temperature calculated from the weight loss recorded during isothermal TGA measurements. Right: Schematic of home-built vapour doping chamber with the dimensions 20 × 15 × 10 mm.

Several studies that were published during the same time as paper I supported our findings. For example Scholes *et al.* studied the effect of crystallisation of P3HT by tailoring the processing solvent and regioregularity. A high regioregularity and casting from *o*-dichlorobenzene (oDCB) increased the conductivity to 12 S cm^{-1} compared to 2 S cm^{-1} measured for a film cast from CF.[103] Lim *et al*. studied the effect of regioregularity and found that the conductivity increases from 0.01 to 13 S cm^{-1} by varying the regioregularity from 0 to 100%.[85, 118] The authors assigned the improved charge transport to better connectivity of ordered domains as indicated by Resonant Soft X-ray Scattering (RSoXS).

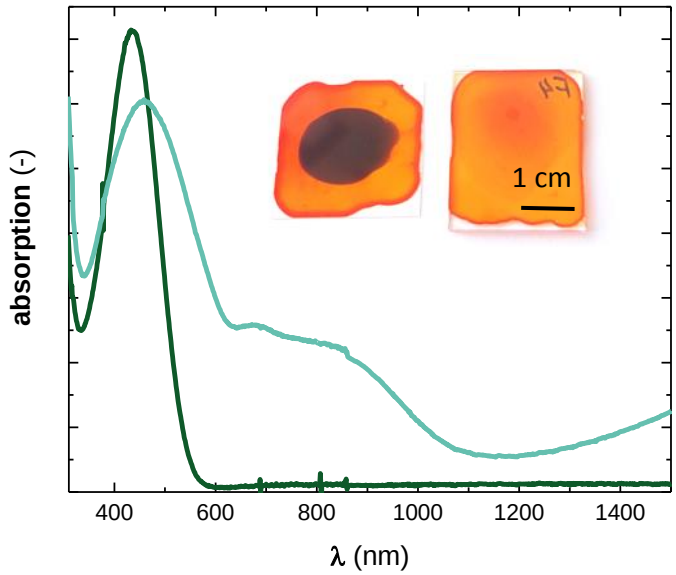

Figure 2.2. Representative UV-vis spectra of drop cast regiorandom (regioregularity 28%) P3HT (dark green) doped with Mo(tfd-$COCF_3$)$_3$ (light green); measured conductivity of 0.09 S cm^{-1}, inset pictures of regiorandom P3HT doped with Mo(tfd-$COCF_3$)$_3$ (left) and F4TCNQ (right).

Koch *et al*. summarised how for FETs the molecular weight strongly affects the charge carrier mobility, which increases from ~ 1 x 10^{-6} to ~ 1 x 10^{-2} up to a M_W of ~ 20 kg mol^{-1}, but then levels off at higher molecular weights. The authors concluded that charge transport was enhanced in non-entangled, extended-crystal architectures generally obtained for materials with an M_n just below the entanglement molecular weight of ~25 kg mol^{-1}, unless solidification occurred under specialised conditions, for example under high pressure or strain.[30]

I proceeded to study two series of materials that varied in molecular weight: (1) 95-97% regioregular P3HT with a M_W of 19 to 106 kg mol^{-1}, and (2) 84-88% regioregular P3HT with a M_W of 11 to 73 kg mol^{-1}. Both series included material below and above the entanglement molecular weight. I found that, within the experimental error of my measurements, the molecular weight did not have a pronounced effect on the electrical conductivity (Figure 2.3). Using UV-vis spectroscopy I noticed that the higher molecular weight P3HT (>50 kg mol^{-1}) with a regioregularity of 95-97% was less ordered compared to the lower molecular weight batches (Figure 2.3, cf. section 2.2). By changing solvent from a mixture of chlorobenzene (CB) and oDCB to p-xylene I could induce a higher degree of solid state order even for the high molecular weight batches and simultaneously observed an increase in the electrical conductivity from ~ 2 to ~ 8 S cm^{-1} (Figure 2.3). Therefore I suggest that for heavily doped P3HT the molecular weight plays a role regarding the formed solid state structure, which affects the transport properties and

likely also the dopant uptake. Reducing the amount of entanglements (by tailoring the processing scheme) will produce films with higher electrical conductivity.

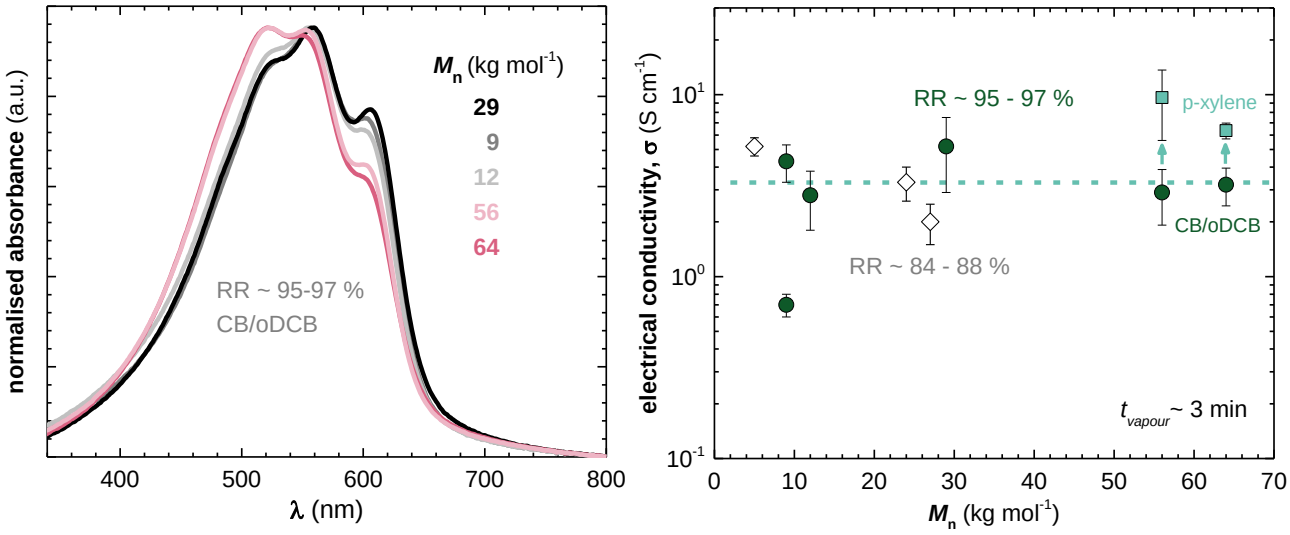

Figure 2.3. Left: Representative UV−vis absorption spectra of highly regioregular (95−97%) P3HT thin films as a function of molecular weight (spin-coated from CB/oDCB; film thickness ~ 45−95 nm. Right: Resulting electrical conductivity σ (t_{vapour} ~ 3 min) as a function of P3HT molecular weight: regioregularity of (◇) 84−88% and (●) 95− 97%; a change in processing solvent to p-xylene (■) increases the solid state order and hence electrical conductivity of high molecular weight P3HT.

I chose to further investigate the impact of the processing solvent on the solid state order and hence the electrical conductivity of spin coated films. In particular, I used seven different organic solvents to induce different degrees of P3HT aggregation. Solvents were chosen for their difference in boiling points and their ability to dissolve 10 g L^{-1} of P3HT at 60°C, with the exception of cyclohexanone (CHN), which required a temperature of 100°C to fully dissolve P3HT. The solvent properties are presented in Table 2.

Table 2: Chemical structures, boiling points and logP (octanol:water)[119]/ relative polarity (H_2O = 1)[120] of the solvents used in paper I and paper II

Solvent (abbreviation)	**Chemical structure**	**Boiling point** (°C)	**logP /relative polarity**
Cyclohexanone (CHN)	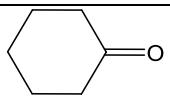	156	0.8 / 0.28
Chloroform (CF)	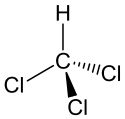	61	2.0 / 0.26
Chlorobenzene (CB)	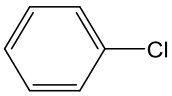	131	2.8 / 0.19
Toluene (Tol)	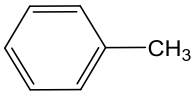	111	2.7 / 0.10
o-dichlorobenzene (oDCB)	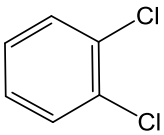	180	3.4 / -
1,2,4-trichlorobenzene (TCB)	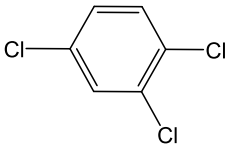	214	4 / -
p-xylene	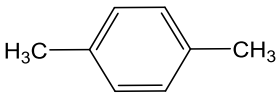	138	3.2 / 0.07

2.2 Characterisation of Solid State Order and Change Upon Doping

From UV-vis spectra of the formed films I could calculate the free exciton bandwidth, *W*, after the work by Spano *et al*.,[121-123] which correlates with the conjugation length of P3HT and in turn with the degree of order. The absorption spectra of P3HT consist of two parts: (I) a lower energy part that arises from crystalline domains (aggregates), and (II) a high energy part that arises from weakly interacting chains in amorphous domains (Figure 2.5). By using equation (1) in paper I, I could calculate *W*. Due to disappearance of the P3HT absorption upon doping it is not possible to calculate *W* after doping, and therefore no comparison of *W* before and after doping could be made.

To investigate the solid state order before and after doping I used Gracing-Incidence Wide-Angle X-ray Scattering (GIWAXS). GIWAXS allows to study the crystalline texture with respect to the substrate, the change of the lamellar stacking distance (d_{100}) and π-stacking distance (d_{010})

upon doping. No change in crystal orientation was observed and all thin films spin coated from the different solvents exhibited preferential edge-on orientation before and after doping (Figure 2.4).

Changes in d_{100} and d_{010} were consistent with previous reports dealing with F4TCNQ doped P3HT;[70, 81-82] an increase of the lamellar stacking distance d_{100} from ~ 1.6 to ~ 1.9 nm and a decrease of the π-stacking distance d_{010} from ~ 0.38 to 0.36 nm was found upon doping. Interesting to note is that both shifts are gradual, which implies that there is no sudden phase change at a certain doping concentration (Figure 2.4). This observation is in agreement with work by Hamidi-Sakr *et al.* who used transmission electron microscopy (TEM) to investigate the impact of sequential doping on the solid state structure of P3HT.[56] In accordance with this study I suggest that F4TCNQ does not intercalate in the π-stacking direction but is incorporated between the side chains and thus alters the lamellar stacking distance.

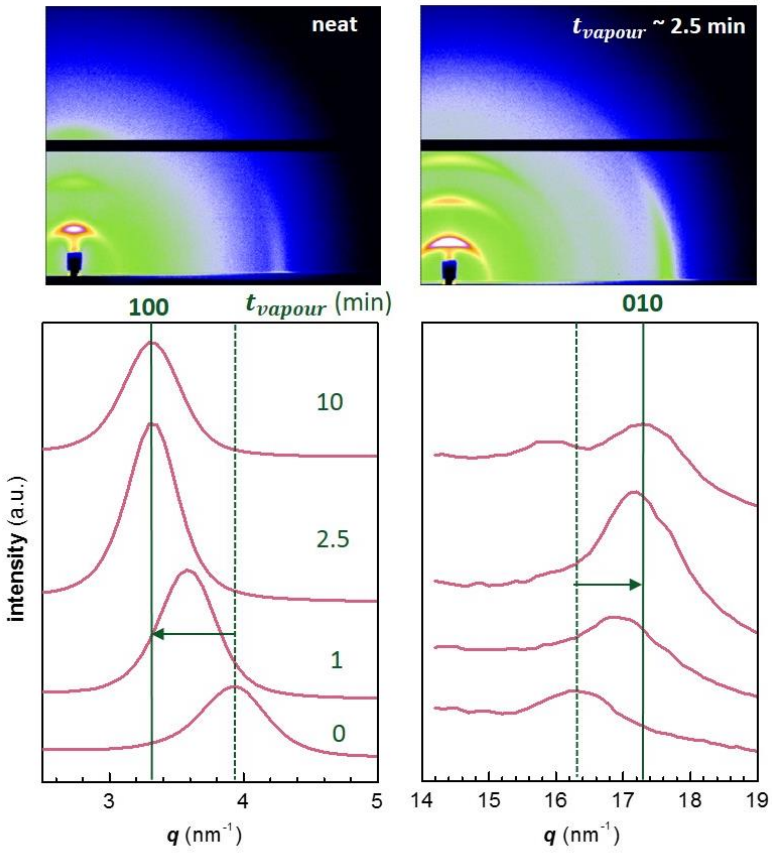

Figure 2.4. Top: GIWAXS images of neat P3HT (left) and F4TCNQ vapour doped P3HT (right), indicating preferential edge-on orientation of ordered domains. Bottom: Diffractograms obtained by integration of GIWAXS images along the azimuthal axis for t_{vapour} ~ 0, 1, 2.5, and 10 min for the d_{100} and d_{010} diffraction peak respectively, data are shifted in y-direction for clarity.

2.3 Thermoelectric Properties of Isotropic Thin Films

The electrical conductivity and Seebeck coefficient were measured for all films. Increasing the solid state order enhanced the electrical conductivity from ~ 0.8 S cm^{-1} for films spin-coated from CF (films spin-coated from CHN had a lower conductivity but because of a different surface topology (cf. paper I, Supporting Information Figure S6) samples prepared from CHN are excluded from the thesis) to ~ 13 S cm^{-1} for the higher ordered films spin-coated from p-xylene (Figure 2.5). The electrical conductivity depends on both the number and the mobility of charge carriers. We therefore went on to estimate the charge carrier concentration.

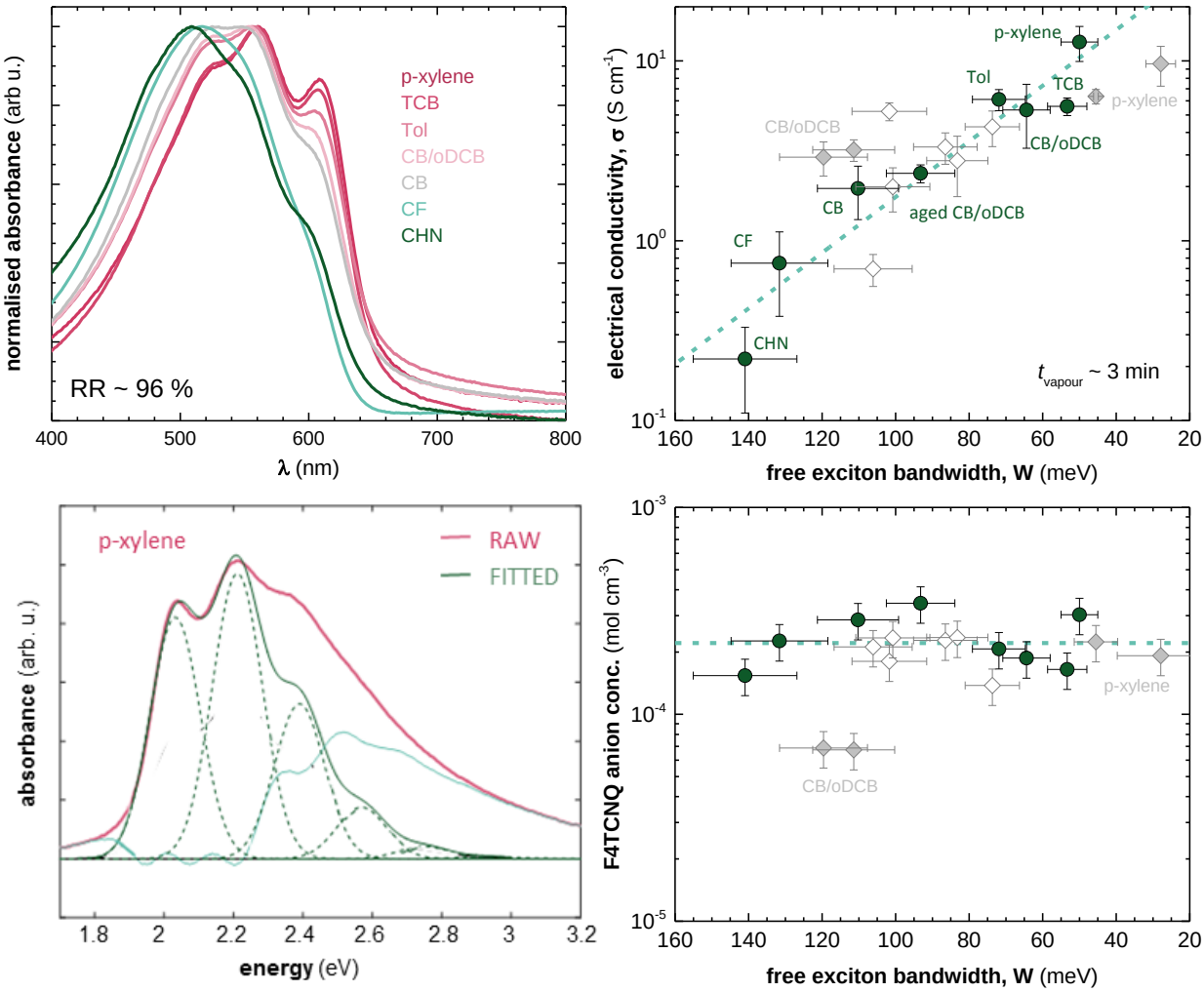

Figure 2.5. Top: Representative UV−vis absorption spectra of P3HT thin films spin coated from various solvents at 60 °C (except cyclohexanone, which required a temperature of 100 °C to dissolve P3HT) (left), electrical conductivity as a function of *W*. (right) Bottom: Representative UV-vis absorption spectrum of P3HT spin-coated from p-xylene (pink), fitted according to ref [121-123] (green) curve represents the best fit. (left), F4TCNQ anion concentration that corresponds to the electrical conductivities shown in the graph above (right).

We decided to use UV-vis spectroscopy to estimate the charge carrier concentration according to a procedure first proposed by Wang *et al.*,[93] which in turn will allow us to investigate if the observed changes in electrical conductivity should be assigned to a higher number or to a higher mobility of charge carriers. We calculated the F4TCNQ anion concentration (measurements and analysis done by David Kiefer, Chalmers, cf. paper I and II and ref [93]) for samples doped for 3 min, spin coated from different solvents. Doping of P3HT with F4TCNQ occurs through ICT (cf. section 1.3). Therefore, we assumed that each F4TCNQ anion would correspond to one charge on the polymer. The number of anions did not vary significantly between the different samples and we extracted a value of ~ 2 x 10^{-4} mol cm^{-3} corresponding to 0.03 anions per repeating unit of P3HT (Figure 2.5). However, this method does not distinguish between bound and free charge carriers. I used the number of anions and calculated the average mobility for all charge carriers (cf. paper I, equation (2)). The average mobility increases with increasing solid state order from 0.05 to 0.5 $cm^2\ V^{-1}\ s^{-1}$. Due to the fact that in F4TCNQ-doped P3HT only a small fraction of the generated charges are free[96] our mobility estimate represents a lower bound.

The Seebeck coefficient varied between ~ 43 to ~ 63 μV K^{-1} (cf. paper II and Figure 6.1). The most ordered sample (spin coated from p-xylene) exhibited a Seebeck coefficient of 43 μV K^{-1} and the least ordered sample (spin coated from CF) a Seebeck coefficient of 51 μV K^{-1}. Similarly, in case of PEDOT:Tos the Seebeck coefficient slightly increases with the degree of crystalline order at constant dopant concentration,[124] which according to Fabiano *et al.* can be explained with a steeper density of states at the Fermi level, caused by the presence of states in the bandgap as a result of delocalisation in ordered domains.

As the Seebeck coefficient predominately probes mobile charge carriers, the change in their concentration would influence the measured thermovoltage. Since the carrier concentration did not vary between our samples it is likely that the same number of charges are generated per volume of amorphous and crystalline phase. Gao *et al*. have argued that both regiorandom and regioregular P3HT can interact with F4TCNQ when dissolved in a common solvent but free charges are only generated in regioregular P3HT,[125] which is able to adopt a planar conformation. For the investigated samples, both disordered (amorphous) and ordered (crystalline) domains are present for all samples. Doping of P3HT in crystalline domains is more likely to lead to a free charge because the polymer is already planarised, whilst doping of P3HT in the less ordered domains requires that the polymer chain adopts a more planar conformation upon doping. Such a change in conformation upon doping has been reported previously.

Chew *et al.* proposed that for sequentially doped P3HT the connectivity between domains is improved because doping leads to more extended P3HT crystallites.[126]

Another study by Yee *et al.* also reported increased structural order upon doping of regiorandom P3HT. Still, the conductivity remains low, due to a lower number of free charge carriers (less mobile charges).[127] For my samples I ascribe the reduction of the Seebeck coefficient in case of films spin coated from p-xylene to a larger amount of mobile charges, which seems to increase with the solid state order of P3HT.

As the power factor is directly proportional to the electrical conductivity, it can also be expected to correlate with the degree of solid state order. In my studied systems, the power factor increases with the solid state order from 0.2 μW m^{-1} K^{-2} for thin films spin coated from chloroform to 2.7 μW m^{-1} K^{-2} when p-xylene was used instead. (Pink stars, Figure 6.1). Glaudell *et al*. established, for a wide range of conjugated polymers, that the power factor and electrical conductivity tend to follow the same empirical trend, $\alpha^2\sigma \propto \sigma^{1/2}$.[117] All the samples in my solvent study follow this empirical trend except for the samples coated from CF (least ordered sample). I explain this deviation with a lower charge carrier mobility, which is caused by the poor connectivity of ordered domains as a result of the low crystallinity of thin films spin coated from CF.

2.4 Stability of dopants

After two months at ambient conditions I noticed that crystals were appearing on the surface of the thin films (Figure 2.6), indicating F4TCNQ-migration from the bulk to the surface. I therefore went on to systematically study the stability of F4TCNQ doped P3HT (M_n ~ 27 kg mol^{-1}, RR ~ 84%). I measured the electrical conductivity and UV-vis of the thin films over time (Figure 2.6) and could conclude that thin films are stable for up to ~ 9 days (during this period the change in electrical conductivity was within the measurement error of the freshly prepared sample).

The stability of F4TCNQ-doped P3HT at elevated temperatures is relatively poor, as previously reported,[128-129] because F4TCNQ tends to sublime when heated. I therefore screened different dopants where I measured the UV-vis spectra and electrical conductivity at different temperatures to select a dopant that would result in materials with temperature-stable thermoelectric properties. Among the tested dopants a molybdenum dithiolene complex, $Mo(tfd\text{-}COCF_3)_3$, was the best performing dopant. With this molecule, doped films were stable up to the same temperatures as F4TCNQ, but displayed a higher electrical conductivity (Figure 2.7). Therefore, I chose to include this dopant as well as F4TCNQ in the rest of my studies.

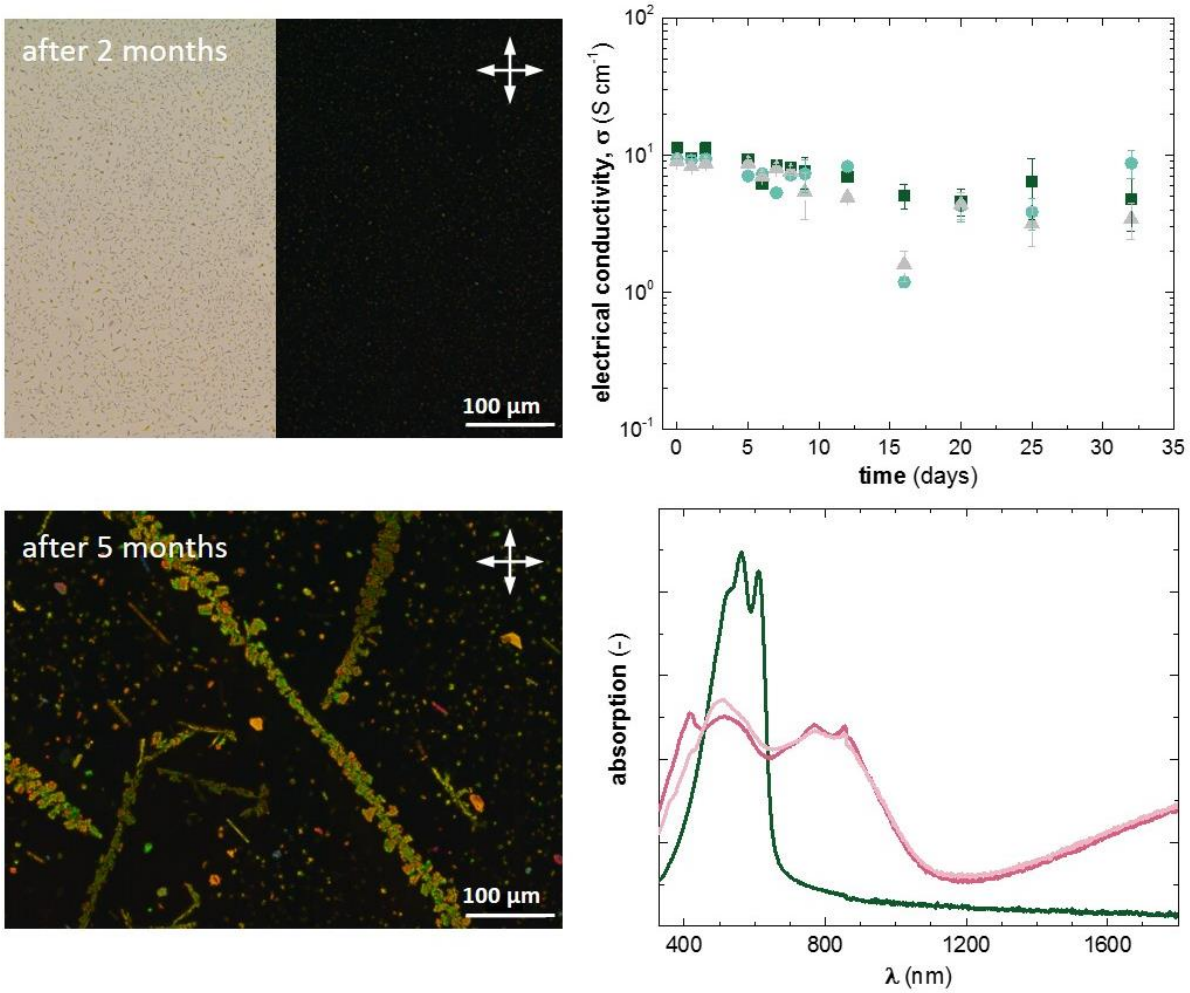

Figure 2.6. Left: Microscopy images of thin films of P3HT doped with F4TCNQ aged under ambient conditions for 2 (top) and 5 months (bottom) (arrows indicate polarised light). Right: Electrical conductivity as a function of aging for thin spin coated films of P3HT doped with F4TCNQ (top). Representative UV-vis absorption spectroscopy of P3HT doped with F4TCNQ measured immediately after doping (dark pink), measured one month after doping (light pink) (bottom).

Interestingly to note is that the Mo(tfd-$COCF_3$)$_3$ dopant has a tendency to only reside in the amorphous areas of P3HT (cf. section 3.2 and section 4.3), but still displays a high electrical conductivity. Mo(tfd-$COCF_3$)$_3$ has an EA of ~ 5.6 eV and is a stronger oxidant than F4TCNQ (EA ~ 5.2 eV) and 2,3-Dichloro-5,6-dicyano-1,4-benzoquinone (DDQ) (~ 4.6 eV)[78]. Therefore, Mo(tfd-$COCF_3$)$_3$ can be used to dope more disordered P3HT (Figure 2.2). P3HT thin films with different regioregularities (28, 84 and 96%, cf. paper I, equation (3) for definition of regioregularity) that were sequentially solution doped with Mo(tfd-$COCF_3$)$_3$ exhibit electrical conductivities of 0.09, 14 and 34 S cm^{-1} respectively. This can be compared with F4TCNQ doped films with conductivities of 0.01, 2 and 12 S cm^{-1} (for regioregularity of 28, 84 and 96%).

In addition to the high EA of the molybdenum dithiolene complex, its larger size may benefit polaron delocalisation and stabilisation as suggested by Liang *et al.*.[98]

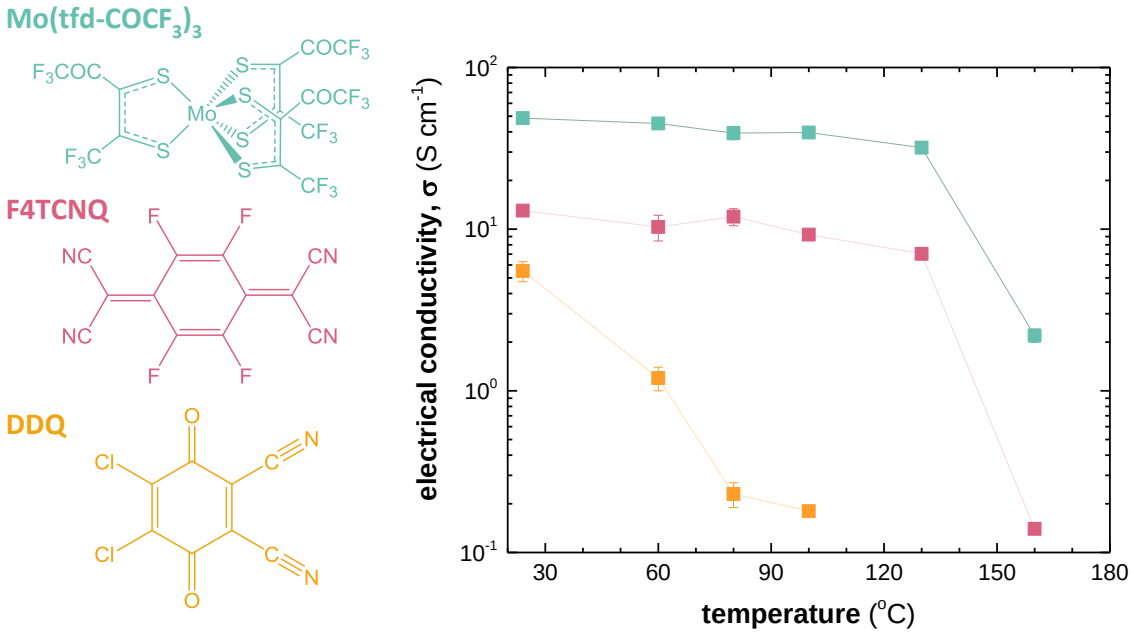

Figure 2.7. Left: Chemical structures of Mo(tfd-$COCF_3$)$_3$, F4TCNQ and DDQ. Right: Electrical conductivity as function of annealing temperature for thin (~70 nm) films of P3HT doped with Mo(tfd-$COCF_3$)$_3$ (green), F4TCNQ (pink) and DDQ (orange). Film were annealed at temperature *T* for 5 min and then the electrical conductivity was measured.

To test if the Mo(tfd-$COCF_3$)$_3$ dopant was affected by the amount/size of crystallites (i.e. the density of the material, cf. section 5.4) I performed an annealing study on thin films of P3HT. I spin coated (from p-xylene) thin films of P3HT (M_n ~ 64 kg mol^{-1}, RR ~ 95%) which I thermally annealed under nitrogen at 120°C for 30 min. Films were then sequentially doped by Mo(tfd-$COCF_3$)$_3$ (in AcN) and rinsed with AcN to remove the excess dopant from the surface. Electrical conductivity and Seebeck coefficient was measured, the neat film exhibited an electrical conductivity of 34 S cm^{-1} and a Seebeck coefficient of 64 µV K^{-1} whilst the annealed film exhibited a much lower electrical conductivity of 17 S cm^{-1} and a Seebeck coefficient of 87 µV K^{-1} (Figure 2.8). As the Mo(tfd-$COCF_3$)$_3$ dopant at the time was thought to reside in the amorphous areas of (rinsed) P3HT the reduction in electrical conductivity could stem from an reduced amount of amorphous domains in the annealed film resulting in less "free-space" for the dopant (cf. section 3.2 and 5.4).

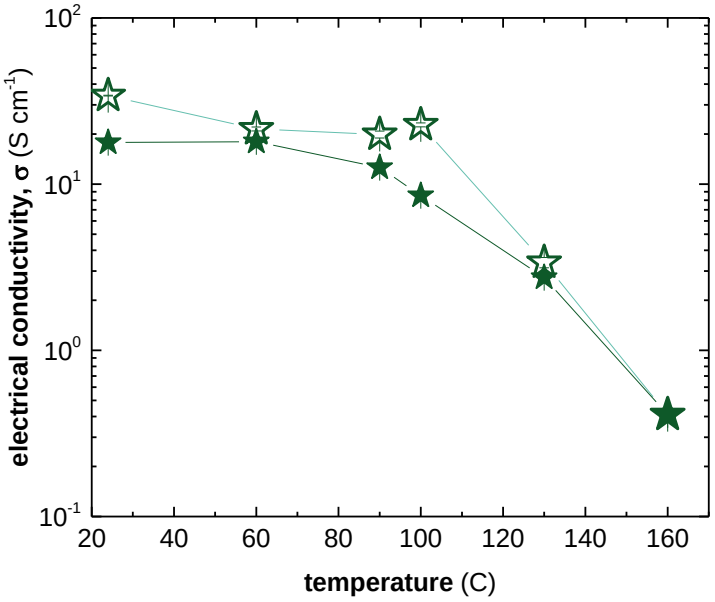

Figure 2.8. Electrical conductivity as a function of temperature for Mo(tfd-$COCF_3$)$_3$ doped thin films of P3HT, not-annealed film (open stars) pre-annealed films at 120°C for 30 min (closed stars).

3. ANISOTROPIC THIN FILMS OF P3HT

There are multiple ways of preparing highly ordered and anisotropic films of P3HT such as using nucleating agents,[51] epitaxial crystallisation,[52] friction-transferred films,[53] high temperature rubbing,[54-55, 130] strain alignment using a carrier substrate[57] and by controlling the nucleation density.[58] Sequential doping can be used to ensure that the nanostructure and orientation of P3HT films is not unduly disturbed[81, 85-86, 117] (cf. section 1.3).

Among conducting polymers, the highest conductivities (10^5 S cm^{-1}) and hence power factors (>1 mW m^{-1} K^{-2}) have been reported for oriented PAc and PBTTT.[88, 130-131] With regard to P3HT a number of studies have explored the impact of orientation on its thermoelectric properties (Table 3).[56, 130, 132-134] Hamidi *et al*. studied high temperature rubbing of P3HT, producing highly anisotropic films that were sequentially doped with F4TCNQ. The authors found a significant degree of anisotropy in both the electrical conductivity and the Seebeck coefficient ($\alpha_{II}/\alpha_L \sim 3$ and $\sigma_{II}/\sigma_L \sim 9$).[56] Qu *et al.* produced anisotropic films through epitaxial crystallisation and found an anisotropy in conductivity $\sigma_{II/L} \sim 3$ whilst there was no significant anisotropy in the Seebeck coefficient.[132] Both studies attribute the increased conductivity to an increased mobility of charge carriers along the direction of orientation and connectivity/percolation between crystalline domains.[56, 132]

Table 3: Anisotropy in electrical properties for aligned P3HT: electrical conductivity σ, Seebeck coefficient α, power factor *PF* (predicted from trend proposed by Glaudell *et al*.[117]) subscripts *II* and *L* refer to in-plane values measured parallel and perpendicular to the direction of orientation.

dopant	σ_{II} (S cm^{-1})	σ_L (S cm^{-1})	α_{II} (μV K^{-1})	α_L (μV K^{-1})	$PF_{predicted}$ (μW m^{-1} K^{-2})	$PF_{calculated}$ (μW m^{-1} K^{-2})	**Ref.**
$Fe(TFSI)_3$	250	90	39	38	~ 15	62	132
$FeCl_3$	570	48	5.4	2.3	~ 24	21	130
F4TCNQ	22	2	60	20	~ 5	8.5	56
Mo(tfd-$COCF_3)_3$	12.7	2	112	138	~ 3	16	135
Mo(tfd-$COCF_3)_3$	336	56	56	13	~ 18	105	*

***Manuscript in preparation. At the time this thesis was printed the film thickness was under investigation, absolute values and error bars are likely to change for the final draft of the manuscript.*

3.1 High Temperature Rubbing of P3HT

As the isotropic films described in section 2.3 displayed an increase in electrical conductivity and power factor with crystallinity, I decided to explore means to further increase the order of thin films of P3HT. During the time of my PhD the Brinkman group (University of Strasbourg, CNRS, France) had reported the thermoelectric properties of highly aligned films of P3HT doped with F4TCNQ, prepared using a high temperature rubbing technique.[55-56] Very recently, high temperature rubbing of thin films of P3HT followed by sequential doping with $FeCl_3$ was found to result in an electrical conductivity of 570 S cm^{-1} along the direction of orientation.[130] I was therefore interested in comparing how these highly aligned and crystalline films would behave if we doped them using the larger Mo(tfd-$COCF_3$)$_3$ dopant.

To investigate the anisotropy in the thermoelectric properties I worked together with Viktoriia Untilova from the Brinkman group. We used the high temperature rubbing technique that the group in Strasbourg has perfectioned.[54-55] (cf. experimental in paper III)

Rubbed films of P3HT (M_w ~ 44 kg mol^{-1}, PDI ~ 1.8, RR ~ 96%) were prepared by Viktoriia Untilova, and investigated using polarised light optical microscopy and polarised UV-Vis absorption spectroscopy. Strong birefringence and highly polarised absorption indicate that the films were highly oriented (Figure 3.1). The absorption of P3HT was considerably stronger parallel to the rubbing direction with a maximum dichroic ratio of 11.5 at 633 nm, which confirms uniaxial alignment of the polymer backbone.

3.2 Characterisation of Solid State Order and Change upon Doping

To preserve the crystalline order as much as possible we decided to use Mo(tfd-$COCF_3$)$_3$. At the time we thought that the dopant would only reside in the amorphous areas as described previously in section 2.4. We screened different solvents and solvent combinations (AcN, CF and a mixture of AcN/CF) to prepare solutions for sequential doping, and found that a 1:1 mixture of AcN/CF resulted in the highest electrical conductivities (~ 130 S cm^{-1} in the rubbing direction, *rinsed film*). Initially, we used a concentration of 2.5 g L^{-1} Mo(tfd-$COCF_3$)$_3$ in AcN/CF and we rinsed the doped films before performing electrical measurements. Polarised optical microscopy (Figure 3.1) and TEM (Figure 3.2) showed that the orientation and crystalline texture was largely preserved upon doping. Electron diffraction (ED) patterns revealed that both the d_{100} diffraction and the d_{010} diffraction were oriented along the meridian, indicating that the orientation of the conjugated backbone along the rubbing direction was preserved upon doping.

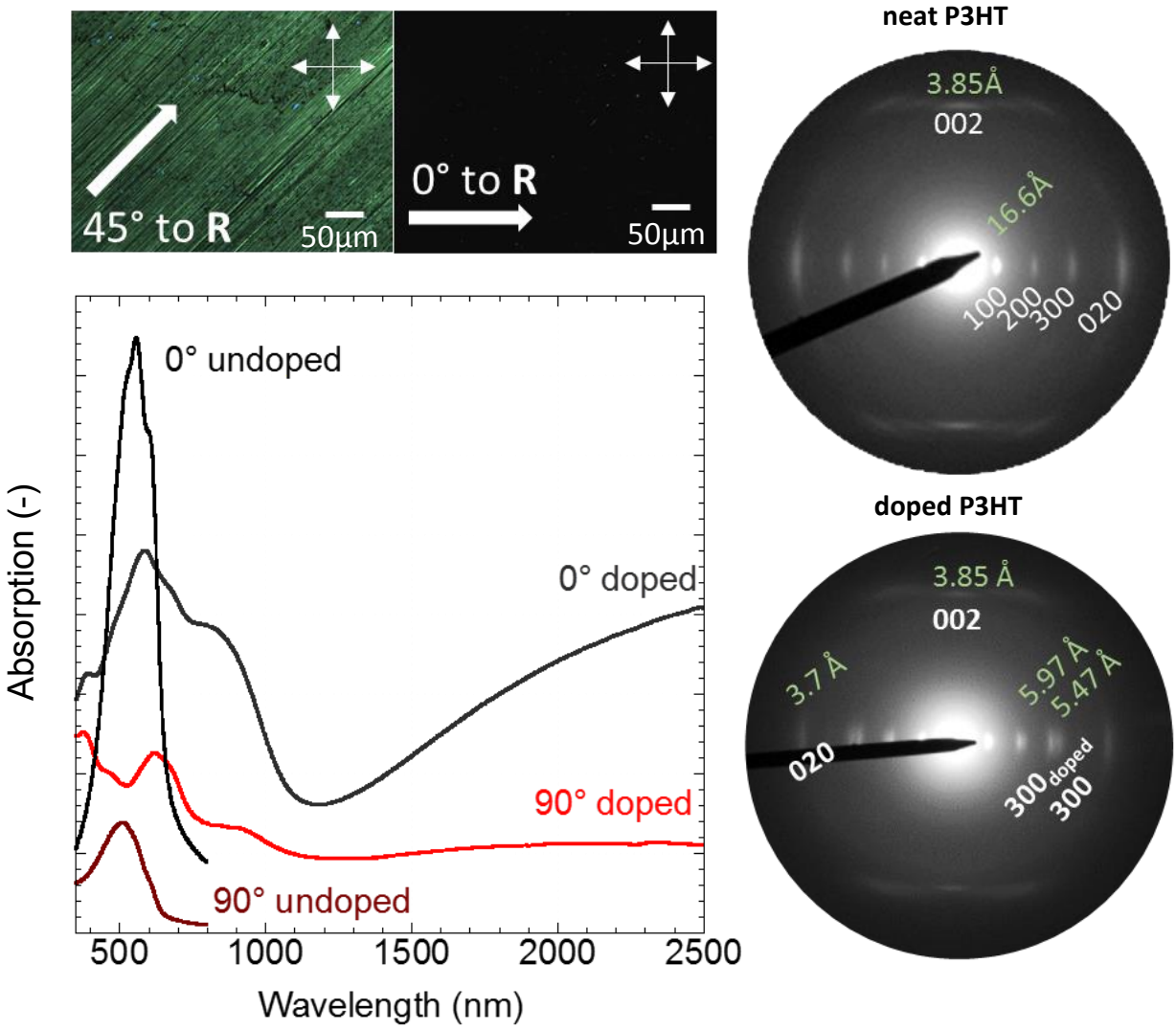

Figure 3.1. Top left: Polarised light optical microscopy images of rubbed P3HT films doped by Mo(tfd-$COCF_3$)$_3$. Polariser and analyser orientations are shown to be crossed. Bottom left: Representative UV-Vis absorption spectra of oriented P3HT films in their undoped and doped states in parallel (0°) and in perpendicular (90°) to the rubbing direction. Data is shifted in y-direction for clarity. Right: ED patterns of rubbed P3HT films before (top) and after doping (bottom) by Mo(tfd-$COCF_3$)$_3$.

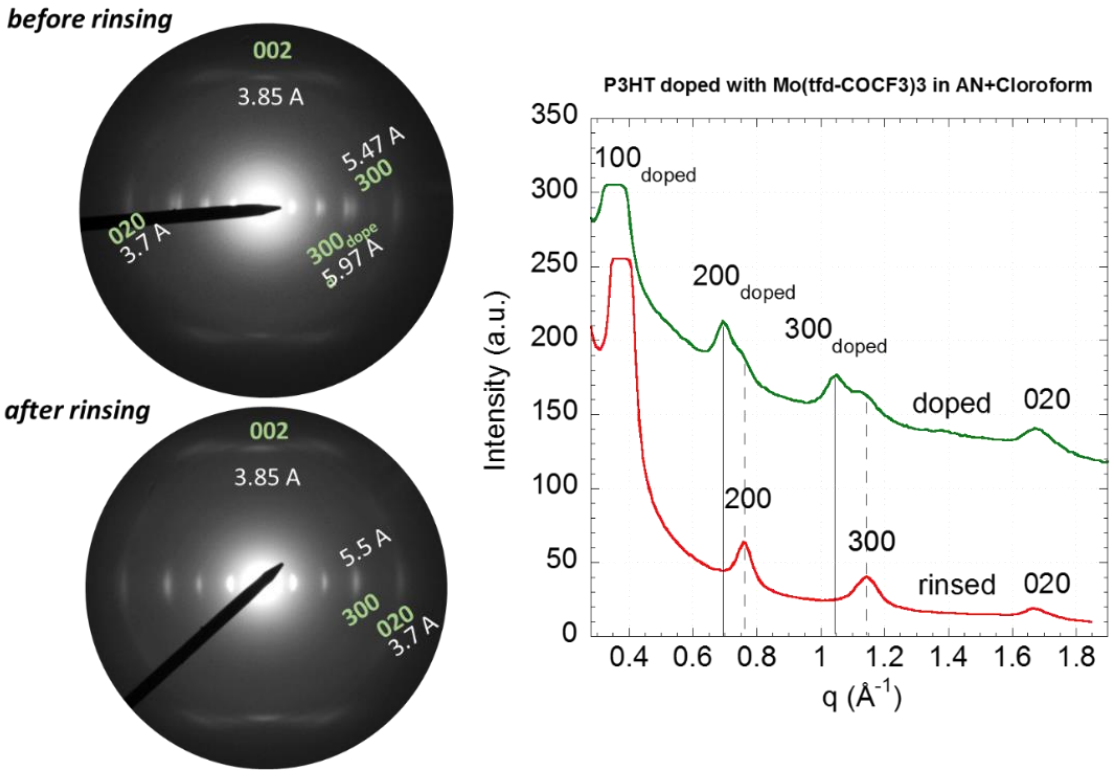

Figure 3.2. Left: ED patterns of rubbed and doped P3HT film before (top) and after rinsing (bottom) doped film with AcN. Left: Section profiles of ED patterns along the equator indicating doubling of the h00 reflections (green curve), upon rinsing ED pattern returns to its neat form (red curve). Data is shifted in y-direction for clarity.

3.3 Thermoelectric Properties of Rubbed P3HT

When we later out of curiosity measured the electrical conductivity of non-rinsed films we noticed a threefold increase in the electrical conductivity (~ 400 S cm^{-1} in the rubbing direction), which we assign to a higher charge carrier concentration. TEM images showed a markedly different nanostructure for *non*-rinsed films compared to the rinsed films. The section profile of ED patterns along the equator revealed a doubling of the 100 reflections, indicating a partially modified crystal structure of the doped but *non*-rinsed films (Figure 3.1 and 3.2). We therefore decided to investigate if the concentration of the doping solutions (0.1 - 7.5 g L^{-1}) had an effect on the crystal structure. We varied the concentration of the dopant solution, measured the electrical conductivity and Seebeck coefficient, and finally calculated the power factor of neat and rubbed films measured in this study (see Table 4 and Figure 3.3).

Table 4. Electrical conductivity σ, Seebeck coefficient α, power factor *PF*, number and mobility of charges, n and μ, for films with a thickness d, sequentially doped with an AcN/CF solution containing a concentration of c_{Mo} of Mo(tfd-$COCF_3$)$_3$; subscripts *II* and *L* refer to in-plane values measured parallel and perpendicular to the rubbing direction.

Rubbed P3HT films*

c_{Mo}	d	n	σ_{II}	σ_L	α_{II}	α_L	PF_{II}	PF_L	μ_{II}	μ_L
(g L^{-1})	(nm)	(10^{26} m^{-3})	(S cm^{-1})		(μV K^{-1})		(μW m^{-1} K^{-2})		(cm^2 V^{-1} s^{-1})	
1	67	5.0	336	56	56	13	105	1	4.2	0.7
2.5	83	4.2	417	82	47	17	92	2	6.2	1.2
7.5	89	3.5	407	30	43	6	75	0.1	7.3	0.5

Neat P3HT*

c_{Mo}	d	n	σ	α	PF	μ
(g L^{-1})	(nm)	(10^{26} m^{-3})	(S cm^{-1})	(μV K^{-1})	(μW m^{-1} K^{-2})	(cm^2 V^{-1} s^{-1})
0.1	91	0.5	0.6	139	1	0.1
1	86	2.7	174	44	34	4.0
7.5	95	2.6	154	35	19	3.7

**At the time this thesis was printed the film thickness was under investigation, absolute values and error bars are likely to change for the final draft of the manuscript.*

It was interesting to note that the highest electrical conductivity was obtained when we used a moderate dopant concentration (1 - 2.5 g L^{-1}). Using a concentration of 1 g L^{-1} resulted in the highest power factor for both neat and rubbed films (34 and 105 μW m^{-1} K^{-2}, respectively).

These results indicate that the rubbing induced orientation either enhances the charge carrier density or mobility of doped samples. To estimate the charge carrier concentration and to calculate the charge carrier mobility we performed spectroelectrochemistry (experiment and analysis was carried out by Dr. Anna I. Hofmann, Chalmers; cf. experimental paper III). For electrochemically doped P3HT, the polaron absorption at 780 nm increases linearly with the concentration of injected charges, which indicates that only one charge species is present, i.e. polarons. Therefore, we could use the absorption peak at 780 nm to construct a calibration curve that allowed us to estimate the charge carrier density of molecularly doped samples. For rubbed samples, the extracted values for *n* are likely an overestimate because the in-plane alignment of the polymer and hence of hole polarons can be expected to enhance the absorption when measured in transmission.

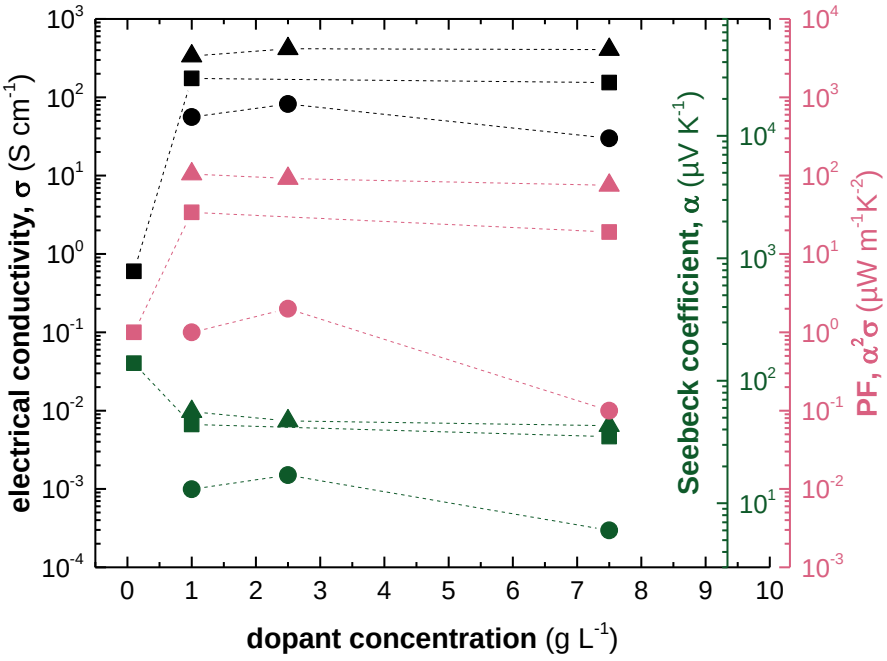

Figure 3.3. Electrical conductivity σ (black), Seebeck coefficient α (green) and power factor $\alpha^2\sigma$ (pink) as a function of dopant solution concentration for neat P3HT (squares), rubbed P3HT measured parallel to rubbing direction (tringles) and rubbed P3HT measured perpendicular to rubbing direction (circles).

We then calculated the charge carrier mobilities for rubbed films of P3HT doped with 1 g L^{-1} of Mo(tfd-$COCF_3$)$_3$ and found that μ_{II} ~ 4.2 cm^2 V^{-1} s^{-1} and μ_L ~ 0.7 S cm^{-1}. The calculated mobilities for the rubbed films measured in the direction of rubbing are similar or slightly higher than corresponding values of the isotropic samples (cf. Table 4), while μ_L is significantly lower.

The anisotropy in the electrical conductivity could be a result of different hopping rates and/or attempt frequencies parallel and perpendicular to the direction of orientation (cf. paper I and paper IV).

In agreement with previous studies[56, 130] the Seebeck coefficient also displays considerable anisotropy, e.g. α_{II}/α_L ~ 4 in case of P3HT doped with 1 g L^{-1} Mo(tfd-$COCF_3$)$_3$. A Seebeck coefficient of α_{II} ~ 56 μV K^{-1} and an electrical conductivity of 336 S cm^{-1} give rise to a maximum power factor of $\alpha_{II}^2\sigma_{II}$ ~ 105 μW m^{-1} K^{-2} along the rubbing direction. Our results confirm that alignment of P3HT can be used to further increase the power factor (cf. chapter 4).

At the start of our collaboration we noticed discrepancies in our respective measurements (made in Gothenburg and Strasbourg), which I assign to the different sample environments, i.e. at Chalmers we typically carry out measurements in air while in the lab in Strasbourg all measurements are done inside a glove box. We therefore measured the electrical conductivity of a film prior and after exposure to air. By exposing the film to ambient conditions the electrical conductivity was halved. These findings highlight the importance of environmentally stable dopants as will be further discussed in section 7.

I conclude that the use of a dopant with a high EA such as Mo(tfd-$COCF_3$)$_3$ in combination with structural anisotropy, is a powerful way of improving the thermoelectric properties of conjugated polymers such as P3HT.

4. BULK PROCESSING OF P3HT

The active layers of most organic opto-electronic devices are deposited from dilute solution and usually are about 100 nm to 1 µm thin. However, for some applications such as textile fibres or thermoelectric modules it is vital that the polymer is processed in bulk. Regardless, work on organic thermoelectric materials has mainly focused on thin layers on plastic substrates, which can be folded,[136] rolled up[137] or stacked,[138] or on coatings of fibres and yarns, which can be integrated into textiles.[139-140]

To create bulk structures the polymer should be processed from the melt or from a concentrated solution. Bulk processing of P3HT has previously been reported and techniques such as melt pressing,[30, 141] solid state pressing,[142] melt spinning,[133] and solution spinning[25, 134] have been employed. The chain length has a strong influence on the melt processability of P3HT, in particular for molecular weights above ~ 25 kg mol^{-1} because chain entanglements start to form, which significantly increases the melt viscosity of the material.[143-144] As a result, the molecular weight has a pronounced effect on the resulting nano- and microstructure. For instance, an increase in melt viscosity reduces the rate of crystallisation, and therefore leads to a reduced crystal thickness and lower crystallinity.[30, 35, 145] Polymers can be disentangled through dissolution, which is one reason why solution processed P3HT tends to have a higher crystallinity than melt processed P3HT. As mentioned previously in section 1.4 and section 2.3 π-stacking allows delocalisation of charges,[105-106] and hence a less ordered system such as melt processed P3HT will display a lower charge carrier mobility.

4.1 Anisotropic Bulk Films

A number of papers have studied the impact of orientation on the electrical properties of P3HT tapes and fibres (cf. section 3 and 5). The electrical conductivity for P3HT can be greatly enhanced by solid state tensile drawing, which leads to orientation of the polymer along the stretching direction. Since the polymer becomes intractable upon doping, it is necessary to carry out tensile drawing prior to the doping step (cf. sequential doping in section 1.4). Moulton *et al*. studied solution spun P3HT fibres that were sequentially doped with $FeCl_3$ and found that drawn fibres exhibited a 2 - 5 times higher electrical conductivity than undrawn fibres.[25, 134] The increased electrical conductivity of tensile drawn polymers is explained by the increased connectivity between polymer chains (both inter- and intra-chain i.e. increase in conjugation length and increase order in the π-stacking direction) upon drawing. As shown previously, molecular doping of drawn polymers tends to reduce the mechanical properties such as the

Young's modulus, which can be rationalised with the associated volume expansion and reduced polymer-polymer interactions upon introduction of the dopant.[146] For example, it was shown that the Young's modulus of tensile drawn PAc was reduced from 50 to 10 GPa upon doping with iodine.[146]

Increased order can also have an adverse effect on the electrical conductivity because it reduces the ability of the material to take up molecular dopants. The alignment of polymer chains leads to a denser material, which reduces the absolute amount of dopant molecules that can be incorporated in the bulk of the oriented polymer (cf. section 5). Further, dopant molecules are likely to diffuse less rapidly in a denser material, which likely reduces the rate of the doping process. Such effects likely play a minor role for small dopants such as iodine or $FeCl_3$, which have been used extensively in the past,[25, 88] but can be expected be more prominent for the larger dopants used in this thesis. On the other hand, smaller dopants can also leave the material more easily, which is the reason why the electrical properties of iodine doped conducting polymers are notoriously unstable.[89]

4.2 Tensile Drawn P3HT

I decided to shift my attention from thin films (paper I, II and III) to bulk samples (paper IV) to investigate material dimensions that are more relevant for thermoelectrics. As alignment has shown to enhance the electrical properties as described in section 3, I wanted to investigate stretch aligned films and study the thermoelectric and mechanical properties of neat and doped material. I chose to use a dynamic mechanical analyser to stretch P3HT tapes (Figure 4.1), which I prepared by drop casting from p-xylene. To be able to stretch the tapes, I chose to work with a high molecular weight P3HT (M_n ~ 91 kg mol^{-1}), because I anticipated that free-standing tapes of this material would be easier to handle. I chose to use a P3HT with a regioregularity of ~ 93%, guided by my observation that a regioregularity of at least 84% is needed to efficiently dope P3HT with F4TCNQ (c.f. section 2.1 and paper I).

To prepare freestanding tapes, I chose drop casting instead of melt pressing due to the availability of material (solution processing generally requires less material). Trials with different drop casting parameters such as substrate temperature, processing solvent and solution temperature were made to find a drop casting procedure that produced smooth and homogeneous films. The procedure that I chose for my experiments was to drop cast from p-xylene (20 - 25 g L^{-1}) on a hot substrate (90°C). When the solvent was evaporated too quickly it lead to buckling and ridges in the formed film. For tensile drawing such heterogeneous films would not be ideal as

inhomogeneities may cause the film to rupture prematurely. Therefore, films were slowly dried under a petri dish (1h). When dry, the films were peeled off from the glass substrate resulting in tapes with a thickness of 10 - 40 µm.

To set up a drawing procedure I tried different drawing temperatures (room temperature to 110°C) and strain rates (0.1 - 10 mm min^{-1}). At a temperature of 60°C and a draw rate of 0.5 mm min^{-1} I was able to draw the tapes to an elongation of 500% ($\lambda \sim 6$). Increased draw rates (>0.5 mm min^{-1}) and decreased drawing temperatures (<60°C) resulted in a higher fraction of tapes that fractured prematurely compared to tapes that were drawn at increased temperatures and slower draw rates. The glass transition temperature of P3HT is $T_g \sim 20$°C, and therefore I choose to draw the films at $T > T_g$. Increasing the temperature above 60°C did not make a noticeable difference in the speed and ease of drawing or the achievable degree of elongation.

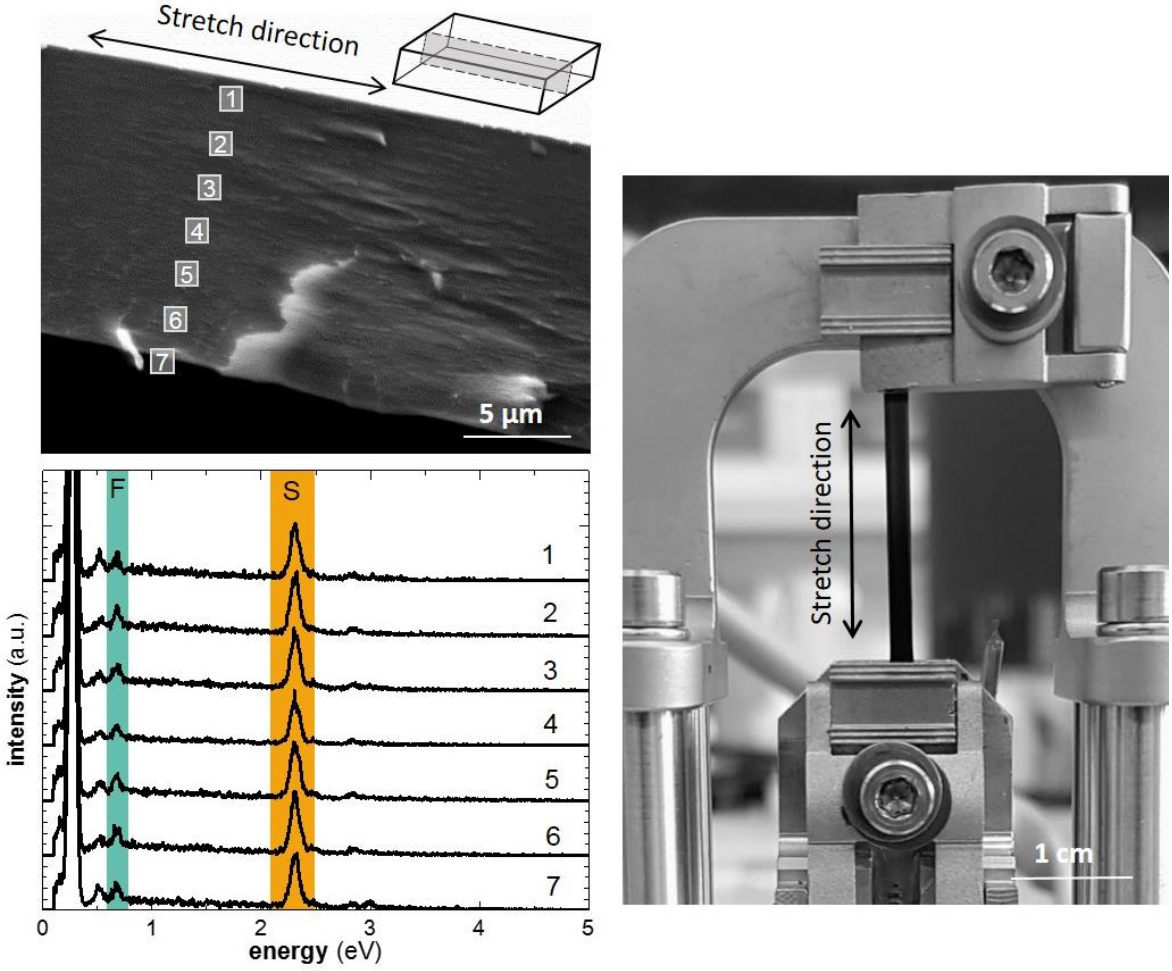

Figure 4.1. Top left: Scanning electron microscopy (SEM) image of the freeze-fractured surface used for EDX; inset: sketch of EDX sample, the freeze fractured surface is shown by the dashed line. Bottom left: EDX spectrogram of stretched P3HT sequentially doped with $Mo(tfd\text{-}COCF_3)_3$ for 72 h,; fluorine and sulphur peaks are coloured green and orange respectively, the S/F ratio varied between 0.3 to 0.5 across the tape. Right: Stretched film of P3HT, clamped in a DMA instrument.

4.2.1 Doping of Bulk Structures

I chose to further study tapes that had been stretched to 300% ($\lambda \sim 4$) elongation. I did not study samples with a higher elongation because of practical limitations; to achieve an elongation of more than 300% the sample had to be remounted in the dynamic mechanical analyser, which introduces an uncertainty in the final elongation as retraction of the tapes may occur during dismantling. I used sequential doping from solution as previous investigations had shown that vapour doping would not be suitable for such thick bulk samples (c.f. section 2.1). By immersing tapes in a solution of F4TCNQ or Mo(tfd-$COCF_3$)$_3$ in AcN with different concentrations of the dopant (2.5 - 15 g L^{-1}), different volumes of dopant solution (0.5 - 4 mL) and by varying the doping times (from minutes to days) I could establish that 2.5 g L^{-1} and 72 h of doping was sufficient to dope tapes with a thickness of 40 µm. After immersing the tapes in the dopant solution the tapes were rinsed with AcN as excess Mo(tfd-$COCF_3$)$_3$ was visible on the surface of the tape. Higher concentrations or longer times did not result in higher dopant uptake (c.f. paper IV). The uptake of F4TCNQ was 6 wt% and for Mo(tfd-$COCF_3$)$_3$ 30 wt% corresponding to 4 and 9 mol%, respectively. These values are in agreement with a study by Liang *et al*. who investigated regioregular P3HT doped with Mo(tfd)$_3$ or Mo(tfd-CO_2Me)$_3$ and found that the electrical conductivity plateaued above a dopant concentration of 5 - 10%, which they assigned to a saturation in the number of polarons.[98] Changing the volume of the dopant solution (0.5 - 4 mL) did not influence the dopant uptake, as all doping solutions contained a large excess of dopant compared to the size/weight of the P3HT film (a 0.5 mL solution containing 1.25 mg dopant corresponds to ~ 55wt% dopant when compared to a P3HT film with a weight of ~ 2.2 mg).

To examine the stability of Mo(tfd-$COCF_3$)$_3$ in AcN for prolonged times, stability experiments of the dopant solution were conducted. Different concentrations of Mo(tfd-$COCF_3$)$_3$ in AcN were prepared and UV-vis spectra of the (not degassed) solution were collected from 0h to 48h of aging in air (Figure 4.2). I could conclude that 5 - 10% of the dopant showed degradation after 48h for a solution containing 2.5 g L^{-1}. For lower concentrations of the dopant (0.03 mM) a pronounced degradation was noticed already after ~ 1h. Therefore, I chose to work with more concentrated solutions (2.5 - 5 g L^{-1}). For F4TCNQ solutions, instead, no change in the UV-vis absorption spectrum was observed after 4 days, which suggests a high degree of stability under ambient conditions.

Energy dispersive X-ray spectroscopy (EDX; carried out by Dr. Anja Lund, Chalmers) was used to probe concentration gradients of the dopant, which was done by comparing the relative size

between the sulphur and fluorine peak. Our analysis indicated a homogeneous distribution of the dopant across the tape (c.f. paper IV) suggesting that the dopant is able to enter the whole tape in 72h (Figure 4.1).

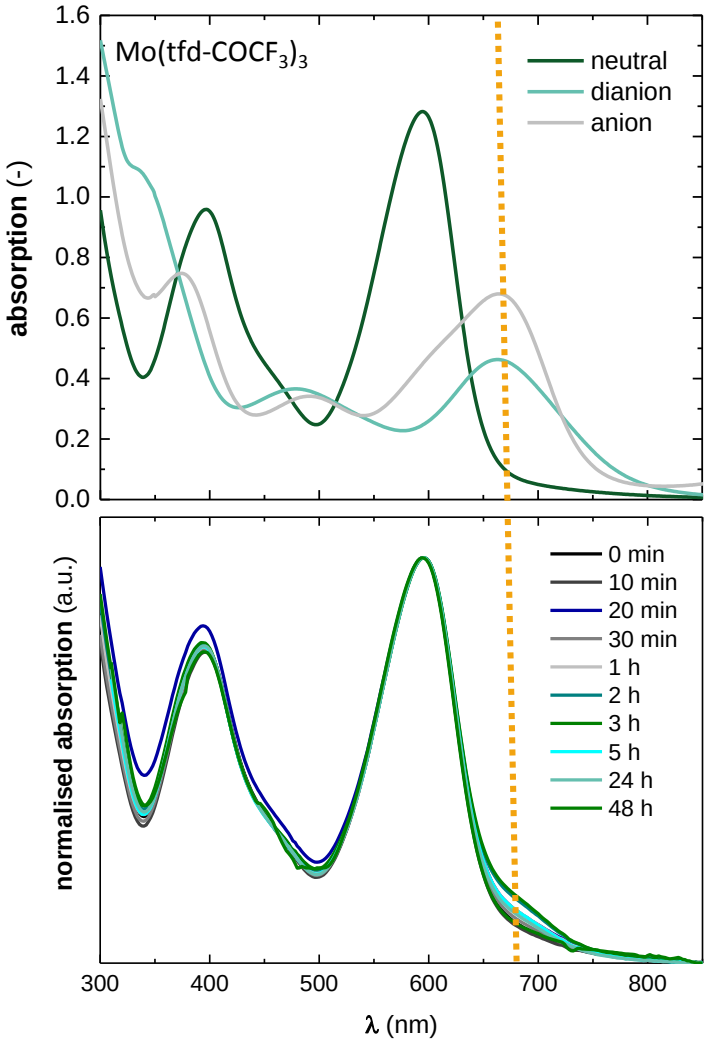

Figure 4.2. Top: Solution UV−vis absorption spectra of Mo(tfd-$COCF_3$)$_3$ in CF in its neutral, anion and dianion form, data from ref [147]. Bottom: representative normalised solution UV-vis spectra of Mo(tfd-$COCF_3$)$_3$ in AcN as a function of time in solution. Emergence of the shoulder at ~ 675nm indicates degradation involving conversion from its neutral form to its ionic species.

4.3 Characterisation of Solid State Order and Change upon Doping

Wide Angle X-ray Scattering (WAXS) was used to investigate the crystalline structure of undrawn and drawn tapes before and after doping. Drawn tapes showed considerable orientation of ordered domains compared with undrawn P3HT both before and after doping (Figure 4.3). The majority of tapes that I have studied were rinsed with AcN to remove excess dopant.

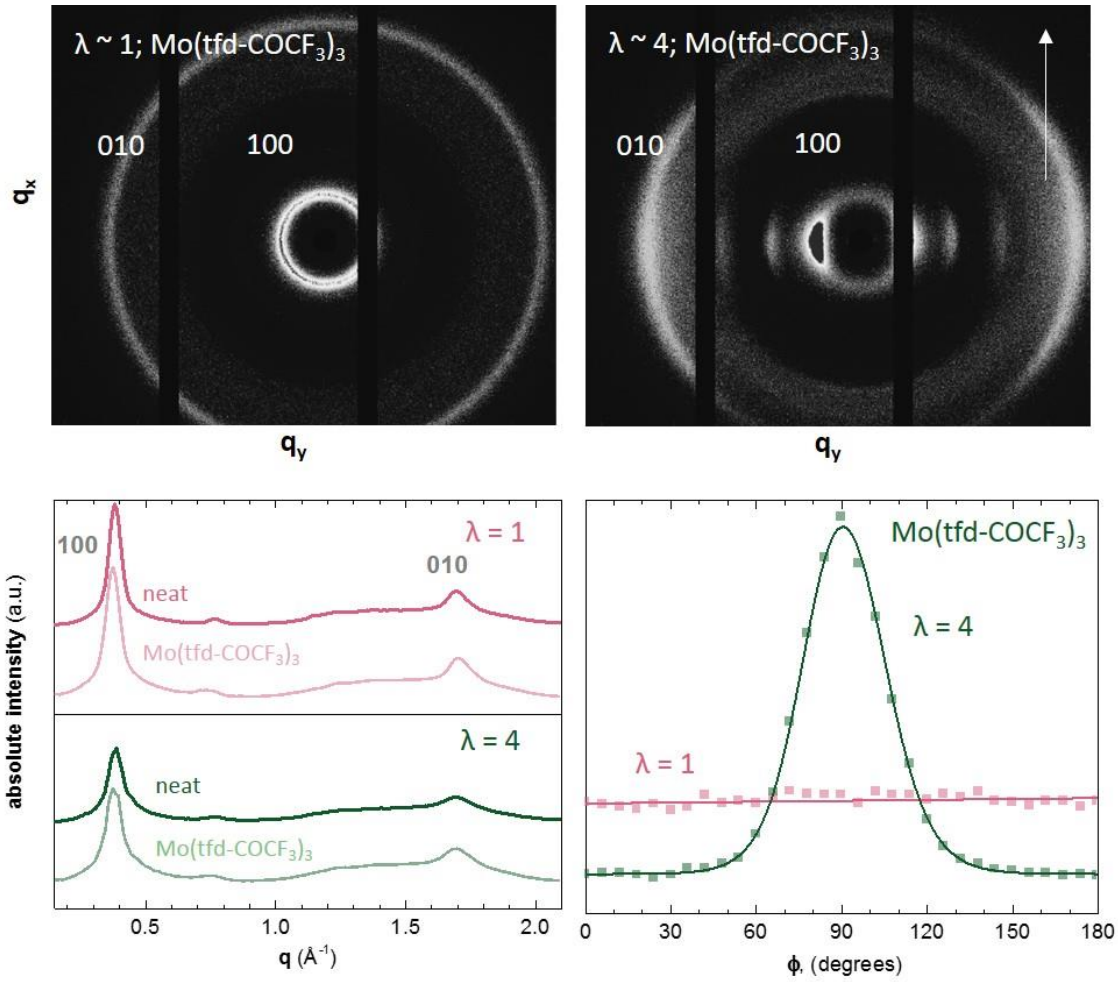

Figure 4.3. Top: WAXS patterns, of as-cast (λ ~ 1) (left) and tensile drawn P3HT (λ ~ 4; arrow indicates drawing direction) (right) sequentially doped with Mo(tfd-$COCF_3$)$_3$. Bottom: Diffractograms showing the radial intensity distribution for λ ~ 1 (pink) and λ ~ 4 (green), data is shifted in y-direction for clarity (left) and angular distribution of the prominent d_{100} diffraction (azimuth angle $\phi = 0, \pi$ is parallel to drawing direction) (right).

WAXS indicated that doping with Mo(tfd-$COCF_3$)$_3$ did not alter the crystalline structure, as evidenced by the invariant diffractions at d_{100} ~ 1.65 nm and d_{010} ~ 0.37 nm. Since neat and Mo(tfd-$COCF_3$)$_3$ doped P3HT feature the same diffraction pattern (Figure 4.3), it can be concluded that the dopant is predominately located in amorphous domains. Instead, for doping with F4TCNQ we obtained the previously reported shift of d_{100} to 1.85 nm and d_{010} to 0.36 nm, which arises due to intercalation of the dopant into crystalline domains (cf. section 1.4). In paper IV we explained the unaltered WAXS patterns of P3HT doped with the molybdenum dithiolene complex by the larger size of the dopant as compared to F4TCNQ, which prevents the dopant from entering the lamellar regions of P3HT crystallites. This interpretation was also provided by Liang *et al*. who made a corresponding observation for regioregular P3HT doped with Mo(tfd)$_3$ or Mo(tfd-CO_2Me)$_3$.[98]

However, our later work on thin rubbed films (c.f. section 3.3) challenged this hypothesis, because we were able to detect a distinct change in the WAXS pattern for doped but *not* rinsed films, i.e. films where excess dopant was not removed from the film surface.

I therefore decided to carry out WAXS on tensile drawn P3HT tapes doped with Mo(tfd-$COCF_3)_3$ that were *not* rinsed with AcN. I could notice that even for bulk films the diffraction pattern *can* change upon doping (Figure 4.4). The d-spacing corresponding to the lamellar repeat distance shifted to $d_{100} \sim 1.76$ nm, while the π-stacking distance changed to $d_{010} \sim 0.36$ nm, which is similar to P3HT doped with F4TCNQ. My hypothesis is that upon rinsing a large amount of Mo(tfd-$COCF_3)_3$ is removed from the surface of the tape, which acted as a reservoir of excess dopant. The removal of excess dopant alters the equilibrium distribution of the dopant inside the polymer. Dopant molecules are pushed out of crystalline domains into amorphous areas, leaving behind dopant free P3HT crystallites, and hence the diffraction pattern of neat polymer is recovered.

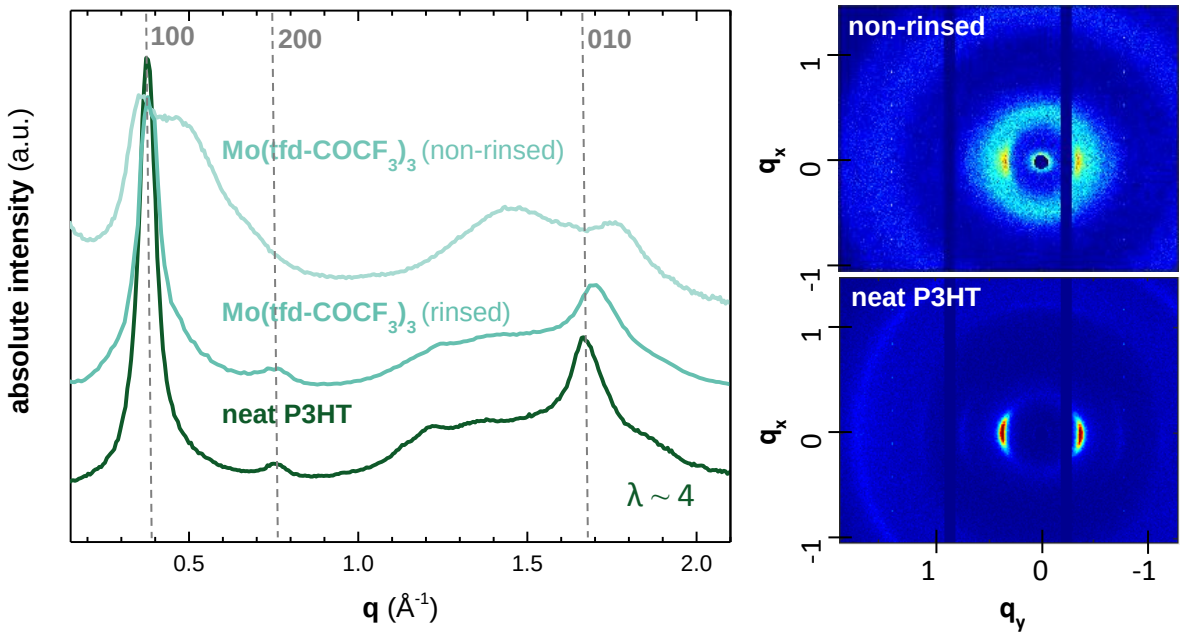

Figure 4.4. Left: Diffractograms showing the radial intensity distribution for tensile drawn (λ ~ 4) P3HT (dark green), sequentially doped with Mo(tfd-COCF3)3 (light green) before and after rinsing with AcN, data is shifted in y-direction for clarity. Right: WAXS patterns of neat and non-rinsed P3HT from the left graph, the broad scattering and existence of a double peak for the non-rinsed sample might indicate that we have two crystal populations, either from P3HT altered crystallites or from crystallised dopant on the surface. Rinsed WAXS pattern are presented in Figure 4.3.

4.4 Thermoelectric Properties of Tensile Drawn P3HT

Tensile drawn tapes doped with Mo(tfd-$COCF_3$)$_3$ (and rinsed with AcN) exhibited a higher electrical conductivity than films doped with F4TCNQ. Note that for these rinsed tapes the molybdenum dithiolene complex was only located in amorphous domains. Mo(tfd-$COCF_3$)$_3$ (EA ~ 5.6) is a stronger oxidant than F4TCNQ (EA ~ 5.2 eV), which allows Mo(tfd-$COCF_3$)$_3$ to dope disordered P3HT (cf. section 2.1) and may explain why we observe a higher electrical conductivity for Mo(tfd-$COCF_3$)$_3$ doped tapes.

The electrical conductivity of tapes doped with Mo(tfd-$COCF_3$)$_3$ considerably increased upon tensile drawing. While neat tapes show a value of only 0.3 S cm^{-1}, for stretched tapes we measure a conductivity of 12.7 S cm^{-1} along the direction of stretching, leading to an anisotropy of $\sigma_{II}/\sigma_L \sim 8$. To investigate if the increase in electrical conductivity could be due to an increase in the amount or size of crystallites upon drawing at elevated temperatures (due to thermal annealing and alignment), I performed differential scanning calorimetry (DSC). Figure 4.5 shows DSC thermograms for stretched and as-cast P3HT, which indicate no change in peak melting temperature (T_m ~ 238°C) and only a slight change in the enthalpy of fusion (ΔH ~ 17 and 21 J g^{-1}). I could therefore conclude that stretching of P3HT at 60°C only slightly increases the crystallinity but has a pronounced effect on the orientation of crystallites (cf. Figure 4.3 WAXS spectra).

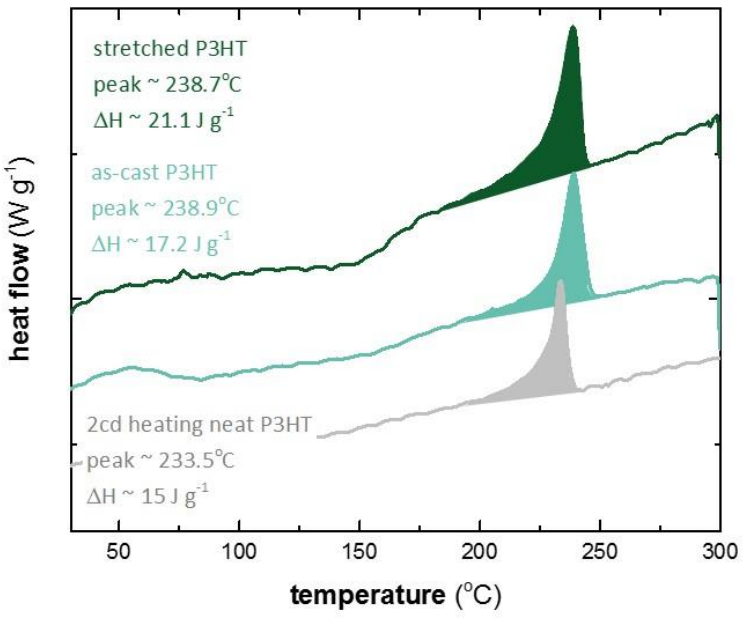

Figure 4.5. DSC heating thermograms of stretched, as-cast and neat P3HT, ΔH values obtained by integration (shaded area) 21, 17, and 15 J g^{-1} respectively. Data are shifted in y-direction for clarity.

The Seebeck coefficient of tapes doped with Mo(tfd-$COCF_3$)$_3$ only slightly changed upon stretching from 138 to 112 µV K^{-1}, and did not develop any anisotropy ($\alpha_{II}/\alpha_L \sim 0.8$), indicating that the alignment of polymer chains either increases the charge carrier mobility or that the stretched tapes had a higher dopant uptake (note that we rule out the latter in section 4.2.1). Tensile drawn tapes doped with Mo(tfd-$COCF_3$)$_3$ displayed a power factor of 16 µW m^{-1}K^{-2}, which is five times larger than the value predicted by the empirical trend that p-doped organic semiconductors tend to follow; $\alpha^2\sigma \propto \sigma^{1/2}$ (Figure 4.6).[117]

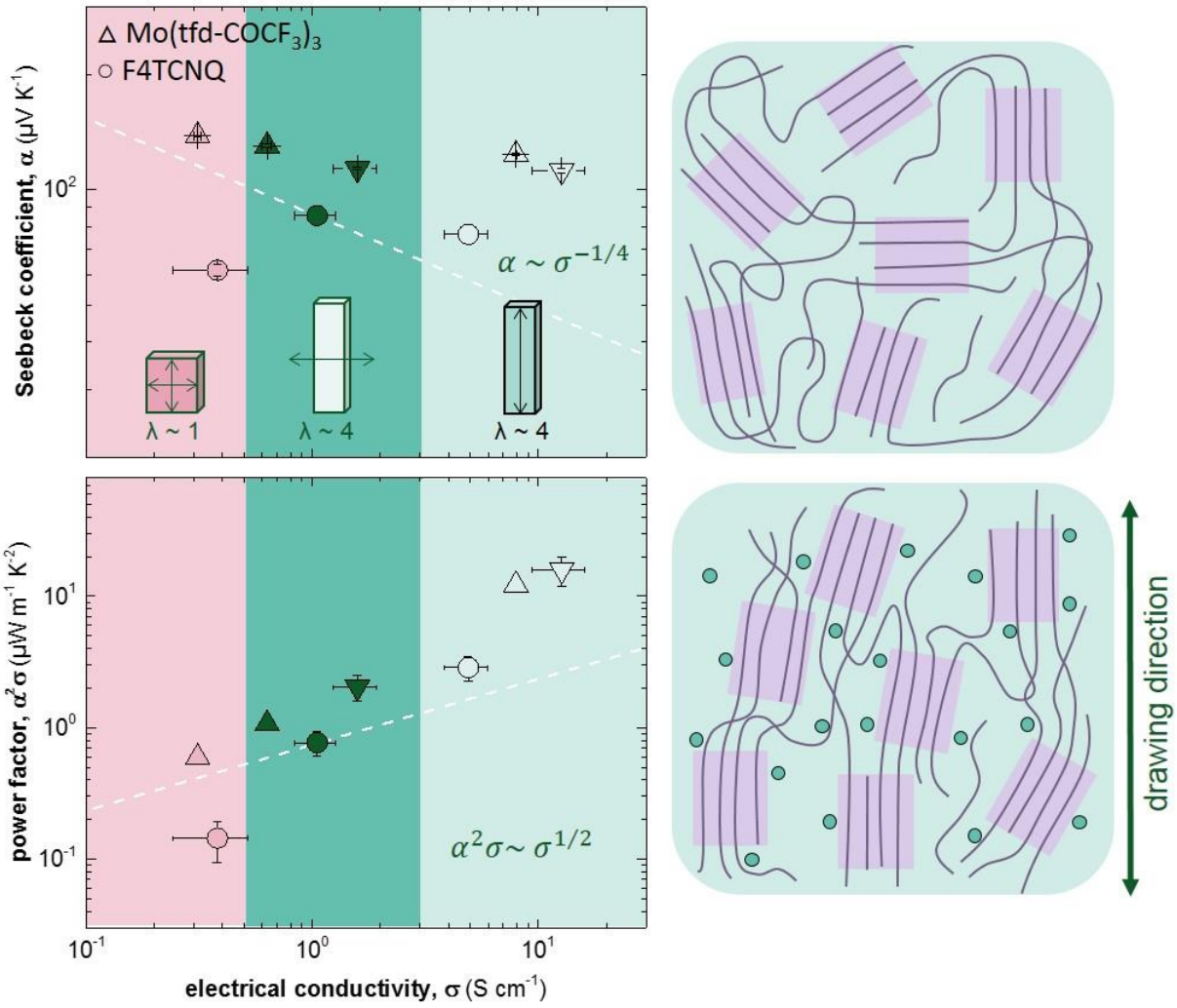

Figure 4.6. Left: Seebeck coefficient (top) and power factor (bottom) as a function of electrical conductivity for P3HT doped with Mo(tfd-$COCF_3$)$_3$ (triangles) and F4TCNQ (circles) for isotropic (pink), transverse (green) and parallel (light green) to stretching direction; triangles pointing up indicate 48 h doping; pointing down indicate 72 h doping; dashed lines show the empirical trends $\alpha \sim \sigma^{-1/4}$ and $\alpha^2\sigma \sim \sigma^{1/2}$. Right: Schematic of the nanostructure of neat (top) and tensile drawn (bottom) P3HT illustrating crystals (purple) within an amorphous matrix (light green) and the dopant Mo(tfd-$COCF_3$)$_3$ (green circles)

4.5 Mechanical Properties of Doped P3HT Tapes

As discussed before, doping can have a pronounced effect on the mechanical properties of a conjugated polymer.[92, 146, 148] I wanted to investigate how the doping affected the mechanical properties of tensile drawn P3HT tapes. We measured the storage and loss modulus of neat and doped tapes using variable-temperature dynamic mechanical analysis (DMA) from -100 to 50°C. Both, neat tapes and samples doped with Mo(tfd-$COCF_3$)$_3$ displayed a similar T_g ~ 20°C, whilst doping with F4TCNQ increased the T_g to ~ 40°C. Evidently, tapes doped with F4TCNQ are more brittle at room temperature than tapes doped with Mo(tfd-$COCF_3$)$_3$. The storage modulus of non-stretched films only slightly decreased upon doping. Instead, for the stretched tapes doped with either F4TCNQ or Mo(tfd-$COCF_3$)$_3$ the storage modulus strongly decreased when measured perpendicular to the drawing direction (Table 5). I explain this observation with a plasticising effect through presence of the dopant and reduced cohesion between adjacent polymer chains in the amorphous domains (elastic deformation as measured with DMA only occurs in the amorphous domains).

Table 5. Draw ratio λ, glass transition temperature T_g, storage modulus, electrical conductivity σ and Seebeck coefficient α for P3HT tapes.

doping	**Draw ratio** (λ)	**Tg** (°C)	**direction of measurement**	**storage modulus @ 0 °C** (GPa)	***σ*** (S cm^{-1})	***α*** (μV K^{-1})
-	1	23	isotropic	0.6	-	-
-	4	20	L	0.1	-	-
-	4	21	II	1.1	-	-
Mo	1	21	isotropic	0.5	0.3 ± 0.1	138 ± 1
Mo	4	20	L	0.1	1.6 ± 0.4	113 ± 1
Mo	4	17	II	0.4	12.7 ± 3.3	112 ± 1
F4TCNQ	1	38	isotropic	0.4*	0.4 ± 0.1	61 ± 1
F4TCNQ	4	-	L	0.03*	1.0 ± 0.2	85 ± 1
F4TCNQ	4	42	II	0.9*	4.9 ± 1.0	76 ± 1

**for DMA measurements of F4TCNQ doped tapes average values for 3 measurements are given*

As discussed above, thin films display a considerably higher electrical conductivity than bulk samples (Table 5, Figure 6.1). My first thought was that the bulk tapes where not fully doped but since EDX measurements show a homogeneous distribution of dopant across the tape and a dopant uptake of 9 mol% in case of Mo(tfd-$COCF_3)_3$, I argue that these samples have reached the solubility limit of the dopant in the bulk of the polymer. I can identify two possible reasons for the higher conductivity of thin films: (1) thin films display a higher crystallinity and anisotropy compared to bulk samples, which is however not corroborated by WAXS and DSC measurements, and (2) thin films allow a more strongly doped surface layer where additional dopant does not need to diffuse into the polymer to dope a significant fraction of the active material.

5. P3HT FIBRES

The field of textile electronics aims to develop clothing with electronic functionality. To realise devices that are truly pliable, breathable and wearable we need to move away from rigid substrates such as glass, silicon and plastic foils. Conducting fibres could be used to weave/knit fabrics for future electronic textiles. So far, work on electrically conducting fibres has explored a range of different materials such as conjugated polymers,[149-152] carbon nanomaterials and composites,[153-157] blends of conjugated and insulating polymers[62, 158-160] or by using existing natural or synthetic fibres (such as cotton, silk, nylon) which are coated with a conducting coating.[161-164] The electrical conductivity and mechanical properties of fibres depend on the materials used to produce them and by the method they are produced. By carefully selecting both the material and the processing scheme the Young's modulus and electrical conductivity can be varied by many orders of magnitude. For instance, Moulton and Smith have shown that reducing the side chain length of poly(3-alkylthiophene) from dodecyl to hexyl, where the later yields P3HT, leads to an increase of the modulus from 1 to 4 GPa and enhances the conductivity from 80 to 160 S cm^{-1}.[25] An Ashby plot comparing electrical conductivity and Young's modulus is shown in Figure 5.1.[146]

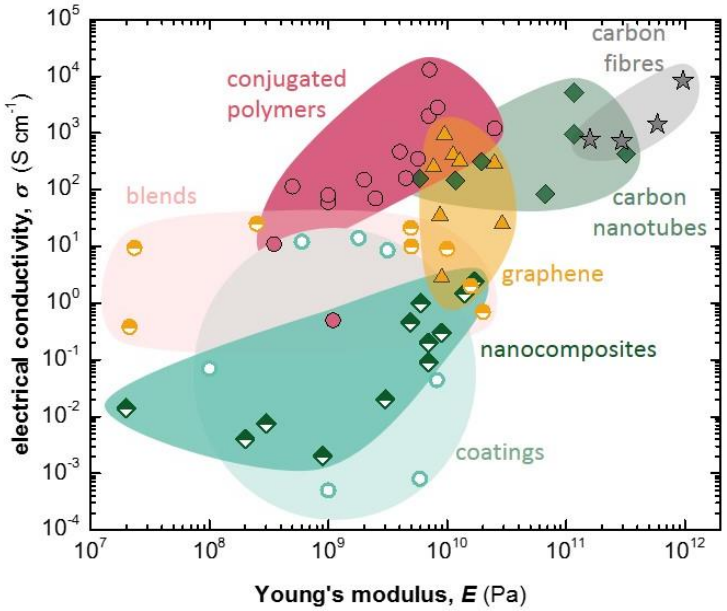

Figure 5.1: Ashby plot of the electrical conductivity versus Young's modulus of fibres based on carbon fibres (grey stars), carbon nanotubes (green diamonds), graphene (yellow triangles), conjugated polymers (pink circles), blends of conjugated and insulating polymers (orange/white circles), nanocomposites of carbon black, carbon nanotubes or graphene embedded in an insulating polymer matrix (green/white diamonds), and coatings of textile fibres with conjugated polymers, carbon nanotubes or graphene (green/white circles). References are found in [146] graph is adapted from reference [146]. Published by Materials Science and Engineering: R: Reports. 2018

Fibres intended for e-textiles need to have an adequate mechanical strength and a high electrical conductivity. During the fibre spinning process the polymer chains align. For conjugated polymers this results in an increased coherence length (beneficial for intra-chain transport) and enhanced π-stacking (beneficial for inter-chain charge transport). Early work by Moulton and Smith has shown that the electrical conductivity of wet spun, $FeCl_3$-doped poly(3-alkylthiophene) fibres could be increased by 3-5 orders of magnitude upon drawing of the fibre.[25] Fanous *et.al* reported that melt spun, $FeCl_3$-doped P3HT fibres can display a conductivity of ~ 350 S cm^{-1}.[133]

I wanted to follow up on earlier work and therefore explored both wet and melt spinning of P3HT fibres, with the goal to create model systems for studies involving redox dopants such as F4TCNQ. The experiments were carried out by Emmy Järsvall who I supervised during her Master thesis work. I expected that fibre spinning would be a good method to further increase the solid state order, allowing me to further enhance the electrical conductivity of P3HT. We chose to work with a P3HT grade with a M_n ~ 91 kg mol^{-1}, which is high for this polymer, and a regioregularity of ~ 93%. Moreover, we were able to purchase 25 g of the same batch, since melt spinning with our compounder requires 5 g of material per extrusion.

5.1 Wet Spinning of P3HT

We first tried wet spinning of P3HT using a Pump 11 Elite syringe pump from Harvard Apparatus. A 50 g L^{-1} solution of P3HT dissolved in p-xylene was heated to 80°C, transferred to a syringe and finally injected through a needle (diameter 0.4 mm) into a coagulation bath of methanol at room temperature (~ 21°C). The thus created fibre was collected on a winder without further drawing. To characterise the cross section and local order of the fibre we used SEM and optical microscopy. The wet spun fibres exhibited a sheet like structure with a width of ~ 300 µm and a thickness of ~ 20 µm. Using polarised light microscopy we noticed that the polymer chains in the fibres were not oriented (Figure 5.2). Cold drawing of the wet spun fibres was difficult and for the majority of the fibres not possible due to premature fracture upon applying a tensile force, likely because the diameter of wet spun fibres varied along their length. We therefore decided to carry out melt spinning to produce highly anisotropic P3HT fibres with a circular cross section.

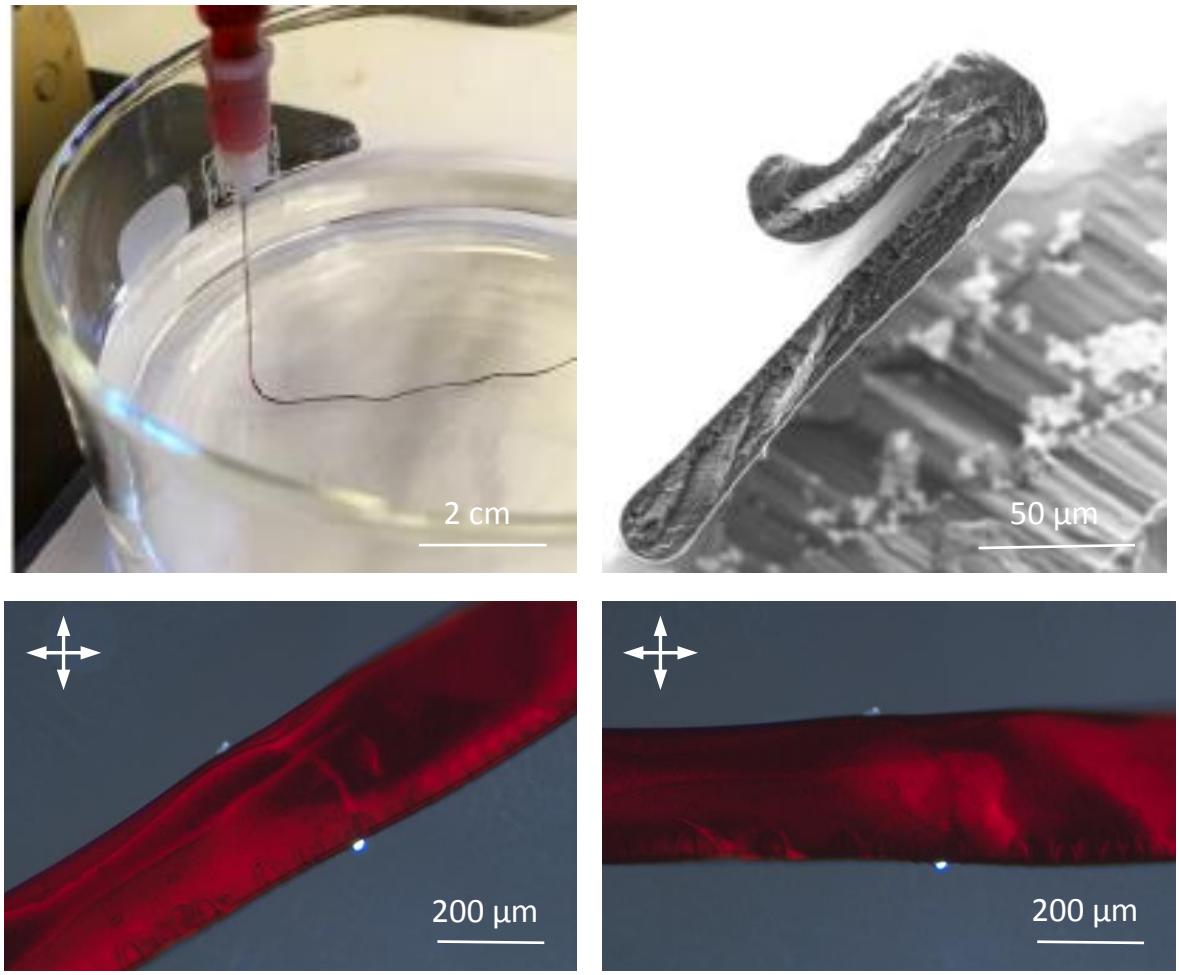

Figure 5.2. Top: Wet spinning process where an 80 °C hot solution of P3HT was injected into a precipitation bath of methanol (left), SEM image of the cross-section of a wet spun fibre (right). Bottom: Polarised light optical microscopy images of wet spun fibre. Polariser and analyser orientations are shown to be crossed. 45° (left) and 0° (right) when the fibre direction is set parallel to the polarisation of the incident light.

5.2 Melt Spinning of P3HT

Melt spinning was performed using a Xplore micro compounder with a nozzle diameter of 0.15 mm. Spinning was conducted under nitrogen at a temperature of 300°C. The temperature was chosen after performing DSC of the neat material, which indicated a melting temperature of ~ 250°C (Figure 5.3). We attempted extrusion at lower temperatures (270 - 290°C) but found 300°C to be optimal. In particular, at 300°C the outflow of material was sufficiently high, which was needed to collect a continuous filament. We chose to work with an extrusion pressure of 460 - 480 N, winder velocity of 5 m min^{-1} and a torque of 20 N. The resulting melt spun fibre was ~ 50 m long (Figure 5.4). Using SEM we noticed a circular cross-section with a diameter varying between 50 - 150 µm. Light microscopy was used to investigate the surface structure of the fibre,

which did not show any indication of shark skin (Figure 5.4). Upon increasing the extrusion pressure melt instabilities may form as the melt exits the die resulting in shark skin formation (or other extrudate instabilities). At the same time the extrusion pressure must be high enough for the melt to exit the die. To investigate the anisotropy we used polarised light microscopy. The melt spun fibres were indeed highly anisotropic (Figure 5.4).

Since drawing of P3HT fibres has previously been found to enhance the electrical conductivity[25, 133] we wanted to perform solid state drawing of our fibres. The fibres were drawn by hand using a hotplate at a temperature of 110 °C, which lies between the T_g and T_m of P3HT. Fibres were elongated to a maximum of 300%.

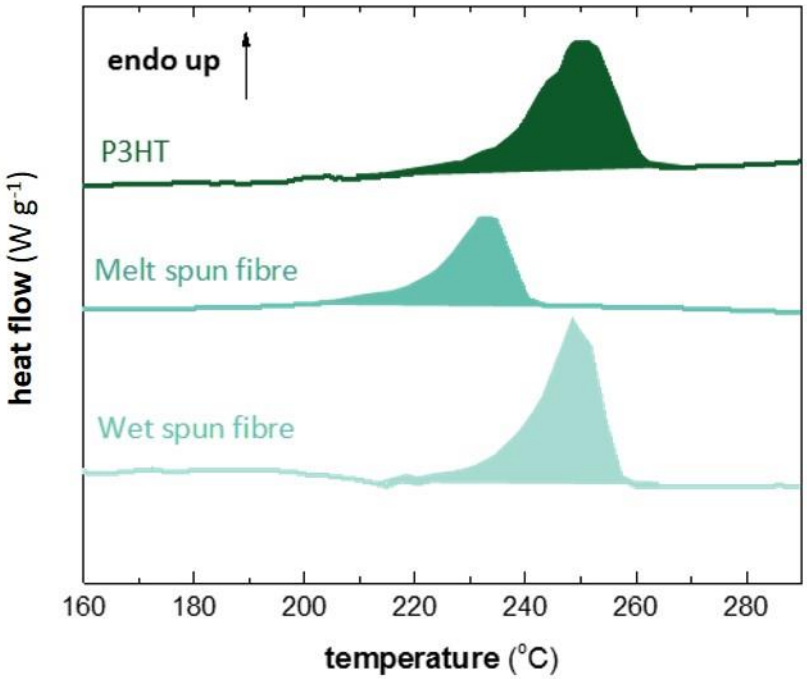

Figure 5.3. DSC heating thermograms of neat P3HT, melt spun fibre and wet spun fibre (T_m ~ 250, 233 and 249°C respectively), ΔH obtained by integration of shaded area 27, 17, and 24 J g^{-1} respectively. Data is shifted in y-direction for clarity.

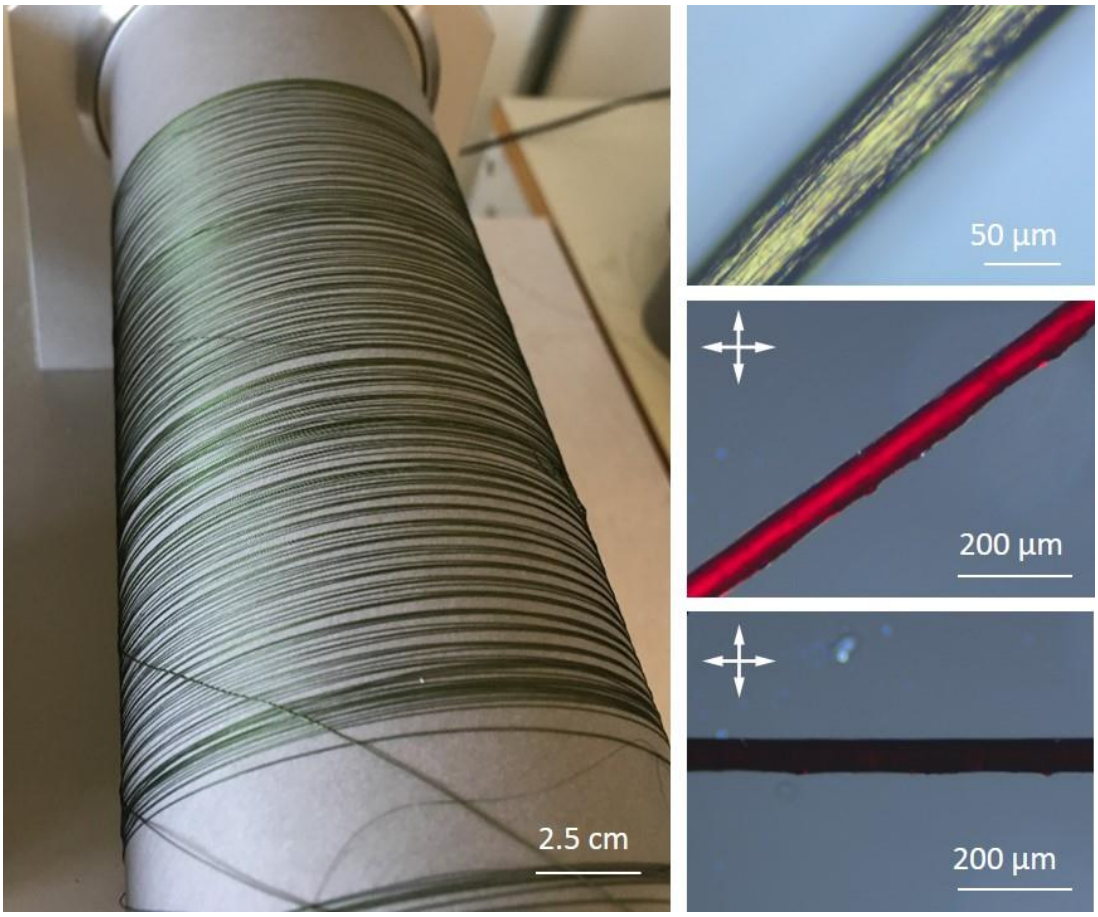

Figure 5.4. Left: Photograph of melt spun fibre Right: Optical light microscope (reflective light) image of the fibre surface (top), polarised light microscopy image of a melt spun fibre 45° (middle) and 0° (bottom), fibre spinning direction is set parallel to the polarisation of the incident light.

5.3 Doping of fibres

To dope the fibres we used sequential doping. We immersed pieces of fibres into solutions of CF, AcN or CF/AcN and one of two dopants, F4TCNQ or Mo(tfd-$COCF_3$)$_3$. A large spread in the resulting electrical conductivities (~ 0.001 to ~ 5 S cm^{-1}) was obtained for the different fibres (melt and wet spun) and solvents/solvent combinations (Figure 5.5). We noticed that the choice of solvent influenced the resulting electrical conductivity, where the fibres doped in CF showed the highest electrical conductivity. However, the use of CF resulted in a green precipitate in the vial indicating that P3HT was leaching out from the fibre.

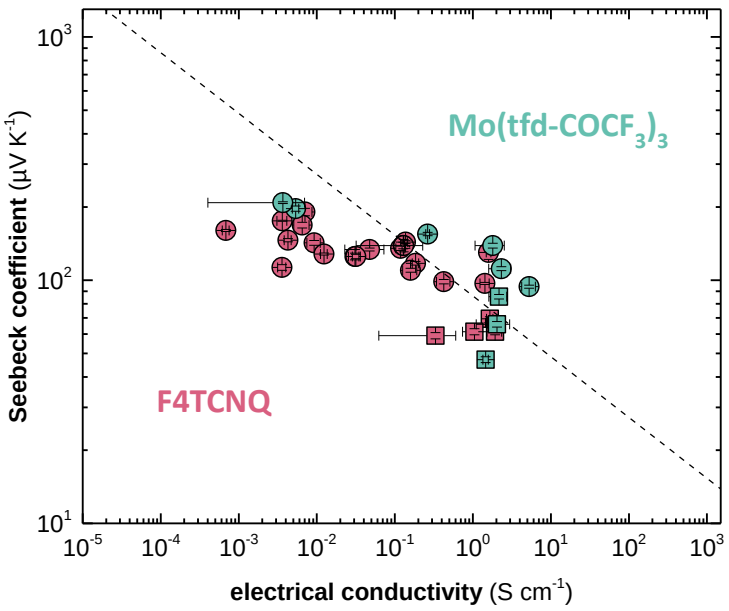

Figure 5.5. Seebeck coefficient as a function of electrical conductivity of melt spun fibres (circles) and wet spun fibres (squares).

5.4 Thermoelectric properties of P3HT fibres

Wet spinning resulted in fibres with an electrical conductivity of up to 2 S cm^{-1} and a Seebeck coefficient of ~ 85 μV K^{-1} obtained with Mo(tfd-$COCF_3$)$_3$, in CF. For the melt spun fibres the stretched fibre (λ ~ 2) displayed the highest electrical conductivity with a value of ~ 5 S cm^{-1} as well as a Seebeck coefficient of ~ 95 μV K^{-1} obtained with Mo(tfd-$COCF_3$)$_3$ in CF.

To investigate the reason for the spread in conductivity values we performed EDX (carried out by Dr. Anja Lund, Chalmers) and WAXS to study the uptake of dopant into the fibres. Since Mo(tfd-$COCF_3$)$_3$ is only present in the amorphous domains we could not draw any conclusions from the WAXS data for Mo(tfd-$COCF_3$)$_3$ doped fibres (c.f. Figure 5.6). Fibres doped for 48h with F4TCNQ in AcN displayed two diffraction peaks at 0.38 and 0.34 $Å^{-1}$, one corresponding to neat P3HT crystals and one to crystals containing the dopant. This observation can be explained with a core-shell structure, meaning that the fibres have an outer doped layer that surrounds a core of undoped P3HT. Fibres doped for 72h only display a single diffraction at 0.34 $Å^{-1}$, which indicates that the polymer is fully doped (Figure 5.6).

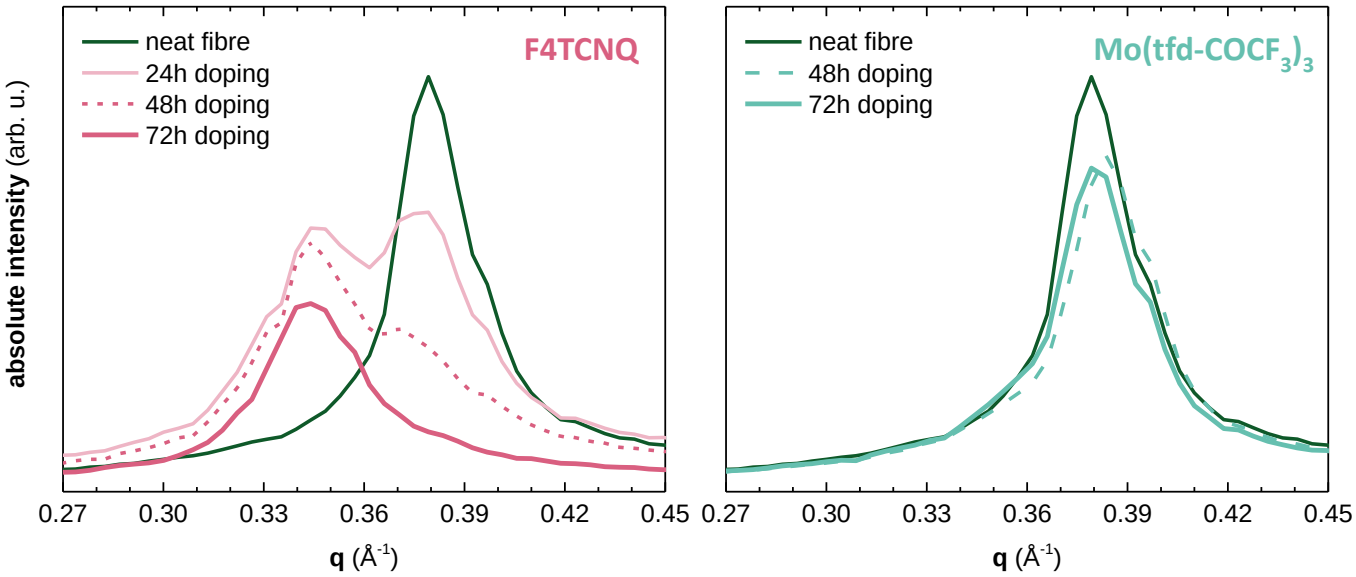

Figure 5.6: Diffractograms showing the radial intensity distribution for P3HT fibre (dark green), sequentially doped with F4TCNQ (pink) and Mo(tfd-$COCF_3$)$_3$ (light green)

Evidently, the doping time (and hence also the fibre diameter) had a strong influence on the extent to which the dopant was able to enter the fibres. However, the highest conductivity was obtained for a fibre doped for 48h (~ 5 S cm^{-1}). Fibres doped for 7 days (regardless of solvent) only exhibited an electrical conductivity of 0.01 to 0.3 S cm^{-1}, indicating that prolonged doping times are detrimental for the electrical conductivity of the fibre.

EDX allowed us to compare the fluorine to sulphur ratio of melt- and wet spun fibres, which scales with the dopant concentration since only the dopants contain fluorine. Values of ~ 0.05 and ~ 0.35 for melt- and wet spun fibres doped for 48h, respectively, indicate that the later are able to take up considerably more dopant (for stretched tapes the fluorine to sulphur ratio was 0.3 to 0.5). Further, our EDX measurements confirm that the fibres are evenly doped, as evidenced by a constant fluorine to sulphur ratio across the fibre cross section (Figure 5.7). I propose that the slower uptake for the melt spun fibres is due to a higher density of the fibre as the polymer chains are aligned upon melt spinning, which increases local order (π-stacking) in the amorphous areas.

We performed DSC scans to compare the crystallinity of fibres and tapes. My hypothesis was that if the crystallinity was increased for the fibres compared to the tapes, the lower electrical conductivity could be the result of limited diffusion of the dopant through crystalline areas of the fibre.

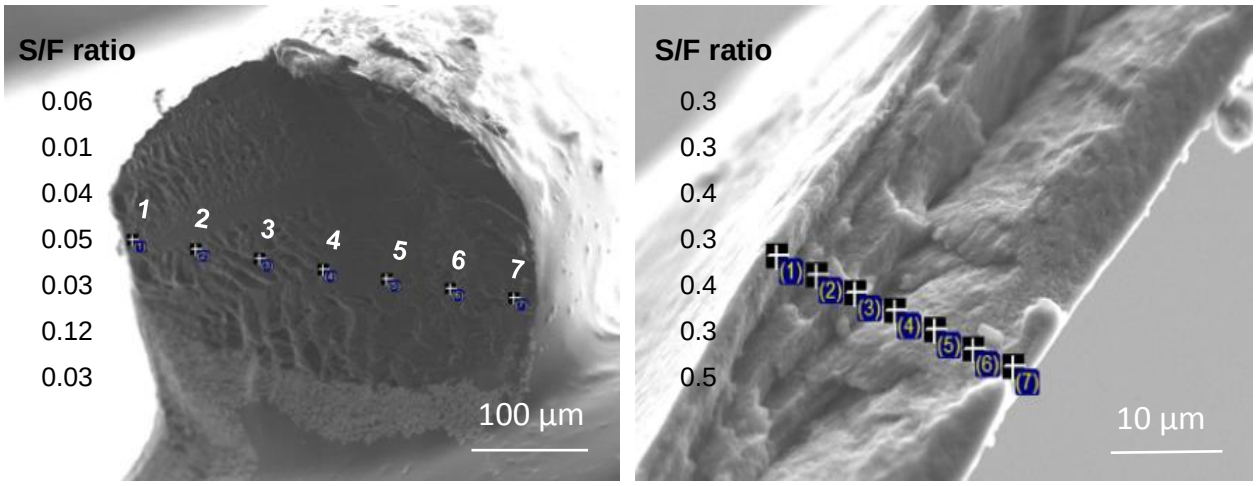

Figure 5.7. SEM images of the freeze-fractured surface used for EDX of a melt spun fibre (left) and a wet spun fibre (right). Values listed in the image is the sulphur to fluorine ratio (S/F ratio) for points marked in the SEM images.

The melting temperature of wet spun fibres, melt spun fibres and tapes was 249, 233 and 238°C, respectively and the heat of enthalpy 24, 17 and 21 J g^{-1} (Figure 5.3). Indicating that the wet spun fibres are more crystalline compared to melt spun fibres and drop cast stretched tapes. This is not surprising as polymers processed from solutions are less entangled than polymers processed from melt, resulting in an increased crystallinity. Instead, melt spun fibres are quenched as the filament exits the die (300°C to ~ 21°C on exiting the die), which leaves the polymer less time to crystallise and hence results in a lower degree of crystallinity for the melt spun fibres. The wet spun fibres did indeed have the lowest electrical conductivity reaching only ~ 2 S cm^{-1}. Therefore I propose that the crystallinity and density of the material affects the diffusion of dopant when sequentially doped in solution. We also tried doping the fibres using iodine vapour but without success, maximum conductivity for the iodine doped fibres was 0.01 S cm^{-1}.

In summary, we successfully produced P3HT fibres using wet and melt spinning. While wet spinning resulted in fibres with an irregular cross section, melt spinning produced circular and highly ordered fibres. However, we found that it was difficult to dope the melt spun fibres because of a considerably lower uptake of molecular dopants (F4TCNQ and $Mo(tfd\text{-}COCF_3)_3$) as compared to less ordered wet spun fibres or solution-cast and stretched tapes (c.f. section 4.2.1). I explain the difficulty in doping melt spun fibres with a higher density of the material, which would hinder the ingression of dopants into the fibre and hence lead to a material that is able to take up less dopant.

6. CONCLUSIONS

In this work I have demonstrated that the solid state structure for P3HT strongly influences the electrical conductivity of sequentially doped P3HT, both for thin films and bulk structures. Uniaxial alignment of both thin and bulk films of P3HT can be used to produces thermoelectric materials where the power factor exceeds the predicted trend $\alpha^2\sigma \propto \sigma^{1/2}$[117] (Figure 6.1).

I started my PhD studying isotropic spin coated films. I varied the solid state order by using a range of different processing solvents with different boiling points. To preserve the obtained nanostructure I used sequential doping with F4TCNQ from the vapour phase. The electrical conductivity was increased by two orders of magnitude as the solid state order of P3HT was increased. The increase in electrical conductivity was attributed to an increase in the mobility of the charge carriers. The molecular weight of P3HT, which I varied from 5 to 64 kg mol^{-1}, did not strongly affect the electrical conductivity for thin spin coated films of P3HT. For strongly doped P3HT, charge transport did not appear to suffer from an absence of connectivity between crystalline domains (through tie chains). The power factor of thin films of spin coated isotropic P3HT films could be increased from 0.2 to ~ 2.7 μW m^{-1} K^{-2} (Figure 6.1, pink stars). This was achieved by selecting processing protocols that lead to a for charge transport beneficial nanostructure, i.e. a nanostructure that gives rise to a high charge carrier mobility.

In further experiments, I collaborated with the Brinkmann group in Strasbourg where we used a high temperature rubbing technique to produce highly aligned and anisotropic thin films of P3HT. These rubbed films were sequentially doped from solution using the larger p-type dopant $Mo(tfd\text{-}COCF_3)_3$. Initial studies had shown that this larger dopant only resides in the amorphous areas of the P3HT film. I later discovered that the dopant (depending on the concentration) could however also be located in the crystal areas of P3HT, as ED patterns of samples prepared by high temperature rubbing and doped (*non*-rinsed) with $Mo(tfd\text{-}COCF_3)_3$ did show a doubling of the d_{100} peak, indicating a partially altered crystal structure of P3HT. By rinsing the doped film and thus removing excess dopant from the surface the crystal structure reverted back to the neat form of P3HT. Evidently, the same doped sample can show either the crystal structure of neat P3HT or an altered crystal structure, depending on the concentration of the dopant.

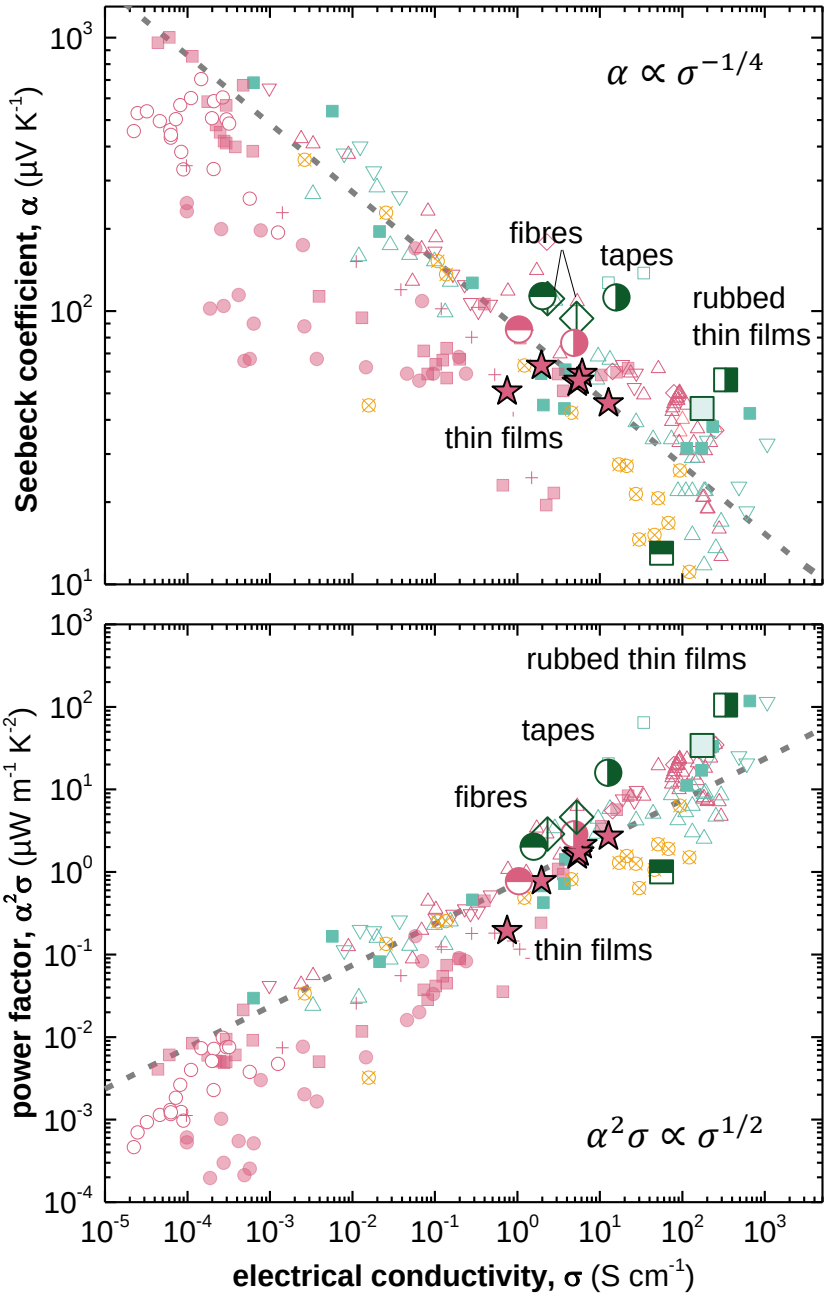

Figure 6.1. Seebeck coefficient (top) and power factor (bottom) as a function of electrical conductivity measured in my work (pink stars – paper I and paper II; green and pink circles – paper IV; diamonds – P3HT fibres; green squares – rubbed films (paper III), and extracted from literature: P3HT doped with F4TCNQ (filled pink squares), $NOPF_6$ (pink crosses), FTS or TFSI (open pink triangles), or $FeCl_3$ (open pink diamonds); P3HT/PEO doped with F4TCNQ (filled pink circles); P3HT/P3HTT doped with F4TCNQ (open pink circles); PBTTT doped with F4TCNQ (filled light green squares), FTS or TFSI (open light green triangles), or F2TCNQ (open light green squares); and p($g_4$2T-T) doped with F4TCNQ or DDQ (yellow open crossed circles); see paper II for original references.

The thermoelectric properties of the rubbed films were best when a moderate concentration of the dopant (1 g L^{-1}) was used, resulting in an electrical conductivity of ~ 330 S cm^{-1} and a Seebeck coefficient of 56 μV K^{-1}, measured parallel to the rubbing direction, which gave rise to a power factor of ~ 105 μW m^{-1} K^{-1} (Figure 6.1, green squares). In contrast to the previous study (paper I and paper II) the mobility of the rubbed films was not markedly increased compared to isotropic films (for 1 g L^{-1} dopant concentration the mobility was 4.0 versus 4.2 cm^2 V^{-1} s^{-1}). Our results conclude that uniaxial alignment of P3HT can be a tool to further increase the power factor of P3HT.

Furthermore, I wanted to study bulk structures of P3HT and see if I could increase the thermoelectric properties by increasing the solid state order. For bulk processed P3HT I demonstrated that tensile drawing creates an opportunity to further enhance the thermoelectric power factor when doped with large acceptors such as $Mo(tfdCOCF_3)_3$. The electrical conductivity increases along the drawing direction, whereas the Seebeck coefficient is essentially unaffected, leading to a power factor of up to ~ 16 μW m^{-1} K^{-2} (Figure 6.1, green and pink half-filled circles). Doping of oriented bulk samples of P3HT did not affect the T_g ~ 20 °C and the storage modulus at room temperature was maintained for isotropic samples and samples measured along the direction of stretching. This shows that tensile drawing is a promising tool for the fabrication of flexible thermoelectric materials.

We also successfully produced P3HT fibres using wet and melt spinning. Melt spinning produced circular and highly ordered fibres with a power factor of ~ 4.6 μW m^{-1} K^{-2}. However, it was found to be difficult to dope the melt spun fibres. I propose that the difficulty in doping could be due to the more dense material, hindering dopant diffusion. Although an increased crystallinity was not pronounced as investigated by DSC, polymer chains likely order through local π-stacking but that these locally ordered parts are not extended crystals.

My work indicates that efforts to improve the thermoelectric power factor of conjugated polymer based materials should primarily focus on enhancing the electrical conductivity. This can be effectively done by increasing the solid state order as demonstrated in this thesis. The solid state order of the polymer can be altered by tailoring the polymer, choosing the right processing conditions and by post-processing treatments such as high temperature rubbing or tensile drawing.

7. OUTLOOK

In my thesis I have established that the solid state order of P3HT strongly influences the electrical conductivity and the thermoelectric power factor. Increasing the order leads to a better performing material both for thin and bulk films. The molecular weight of P3HT did not seem to affect the electrical conductivity for highly doped samples, which opens up the possibility to tune the mechanical properties without affecting the electrical properties.

To further enhance the power factor of polymeric materials it would be interesting to study doped high-mobility polymers (such as indacenodithiophene (IDT) or diketopyrrolopyrrole (DPP) containing polymers). Alignment of these polymers would allow us to investigate if the same structure-property relationships that I have observed for P3HT are applicable to other materials.

To further enhance the electrical properties of P3HT fibres investigated in my work, it would be interesting to blend the P3HT with either a commodity polymer, less regioregular P3HT or to use a higher molecular weight P3HT. This could possibly reduce the density of the fibre and could enhance the uptake of the dopant leading to an increase in the electrical conductivity.

One limitation of my studies is the absence of thermal conductivity measurements. For thermoelectric applications the figure of merit needs to be optimised, which means that the thermal conductivity must be minimised. It is well known that increasing the solid state order will increase the thermal conductivity (cf. section 1.4.2);[110-111, 138] for diamonds (single crystal carbon material) the thermal conductivity is in the range of ~ 2000 W m^{-1} K^{-1} at 300 K,[165] and even for polyethylene the thermal conductivity can reach ~ 13 W m^{-1} K^{-1} at RT.[111] Xu *et al.* demonstrated that bottom-up oxidative chemical vapour deposition (oCVD) of P3HT can lead to a thermal conductivity of 2.2 W m^{-1} K^{-1} near room temperature. The authors attribute the increase in thermal conductivity to the increased solid state order of oCVD deposited P3HT.[166] Reported values of the thermal conductivity of isotropic P3HT vary from ~ 0.18[167-168] to ~ 0.33 W m^{-1} K^{-1}.[87, 92] It is therefore important to investigate the thermal conductivity for my aligned samples, which would allow to compare the ZT of isotropic and stretched P3HT.

Another aspect that I have not covered in my thesis to a larger extent is the choice of dopant. The p-type dopants used in my studies are not viable for practical use due to poor environmental stability and because they are highly toxic. What also needs to be considered is the diffusion-limited transport of the dopant through bulk materials, which results in impractically long doping times (days). To be able to co-process the dopant and the polymer would be beneficial, because it would decrease the processing time. Kiefer *et al.* has shown that the introduction of polar side

chains instead of aliphatic side chains eases co-processing.[169] It would be interesting to further study if the same structure-property relationships that I have discussed in my thesis hold for this type of polar polythiophenes.

To avoid aggregation upon interaction between the dopant and polymer previous work has suggested light or heat activated doping with photoacid or thermal acid generators (PAGs or TAGs).[170] Other possible solutions could be to use polymers that are grafted with donor/acceptor units as found in the literature of OSCs.[171-172] Using polymers as dopant molecules would reduce the diffusion rate due to the size of the molecule, similar as the widely used conducting polymer:polyanion complex PEDOT:PSS where the counterion-carrying PSS is a macromolecule.

BIBLIOGRAPHY

1. Shirakawa, H.; Louis, E. J.; MacDiarmid, A. G.; Chiang, C. K.; Heeger, A. J., *J. Chem. Soc., Chem. Commun.* **1977,** (16), 578-580.
2. NobelPrize.org Pressmeddelande: Nobelpriset i kemi år 2000. https://www.nobelprize.org/prizes/chemistry/2000/8943-pressmeddelande-nobelpriset-i-kemi-ar-2000/ (accessed 191001).
3. Xu, R.-P.; Li, Y.-Q.; Tang, J.-X., *J. Mater. Chem. C* **2016,** *4* (39), 9116-9142.
4. AlSalhi, M. S.; Alam, J.; Dass, L. A.; Raja, M., *Int. J. Mol. Sci.* **2011,** *12* (3), 2036-2054.
5. Sekine, C.; Tsubata, Y.; Yamada, T.; Kitano, M.; Doi, S., *Sci. Technol. Adv. Mater.* **2014,** *15* (3), 034203.
6. Di Carlo Rasi, D. and Janssen, R. A. J., *Adv. Mater.* **2019,** *31* (10), 1806499.
7. Gurney, R. S.; Lidzey, D. G.; Wang, T., *Rep. Prog. Phys.* **2019,** *82* (3), 036601.
8. Xue, R.; Zhang, J.; Li, Y.; Li, Y., *Small* **2018,** *14* (41), 1801793.
9. Lee, Y. H.; Kweon, O. Y.; Kim, H.; Yoo, J. H.; Han, S. G.; Oh, J. H., *J. Mater. Chem. C* **2018,** *6* (32), 8569-8612.
10. Sekitani, T.; Zschieschang, U.; Klauk, H.; Someya, T., *Nat. Mater.* **2010,** *9* (12), 1015-1022.
11. Sirringhaus, H., *Adv. Mater.* **2014,** *26* (9), 1319-1335.
12. Muench, S.; Wild, A.; Friebe, C.; Häupler, B.; Janoschka, T.; Schubert, U. S., *Chem. Rev.* **2016,** *116* (16), 9438-9484.
13. Mike, J. F. and Lutkenhaus, J. L., *J. Polym. Sci., Part B: Polym. Phys.* **2013,** *51* (7), 468-480.
14. Rivnay, J.; Owens, R. M.; Malliaras, G. G., *Chem. Mater.* **2014,** *26* (1), 679-685.
15. Simon, D. T.; Gabrielsson, E. O.; Tybrandt, K.; Berggren, M., *Chem. Rev.* **2016,** *116* (21), 13009-13041.
16. Wallace, G. G.; Moulton, S. E.; Clark, G. M., *Science* **2009,** *324* (5924), 185-186.
17. Otero, T. F.; Martinez, J. G.; Arias-Pardilla, J., *Electrochim. Acta* **2012,** *84*, 112-128.
18. Kroon, R.; Mengistie, D. A.; Kiefer, D.; Hynynen, J.; Ryan, J. D.; Yu, L.; Müller, C., *Chem. Soc. Rev.* **2016,** *45* (22), 6147-6164.
19. Russ, B.; Glaudell, A.; Urban, J. J.; Chabinyc, M. L.; Segalman, R. A., *Nat. Rev. Mater.* **2016,** *1* (10), 16050.
20. Chen, Y.; Zhao, Y.; Liang, Z., *Energy Environ. Sci.* **2015,** *8* (2), 401-422.
21. Gayner, C. and Kar, K. K., *Prog. Mater. Sci.* **2016,** *83*, 330-382.
22. Ma, Y.; Kang, Z.; Zheng, Q., *J. Mater. Chem. A* **2017,** *5* (5), 1860-1872.
23. Kroon, R.; Lenes, M.; Hummelen, J. C.; Blom, P. W. M.; de Boer, B., *Polym. Rev.* **2008,** *48* (3), 531-582.
24. Motamedi, F.; Ihn, K. J.; Ni, Z.; Srdanov, G.; Wudl, F.; Smith, P., *Polymer* **1992,** *33* (5), 1102-1104.

25. Moulton, J. and Smith, P., *Polymer* **1992,** *33* (11), 2340-2347.
26. McCullough, R. D., *Adv. Mater.* **1998,** *10* (2), 93-116.
27. Takakazu, Y.; Ken-ichi, S.; Akio, Y., *Bull. Chem. Soc. Jpn.* **1983,** *56* (5), 1497-1502.
28. Elsenbaumer, R. L.; Jen, K. Y.; Oboodi, R., *Synth. Met.* **1986,** *15* (2), 169-174.
29. Jen, K.-Y.; Miller, G. G.; Elsenbaumer, R. L., *J. Chem. Soc., Chem. Commun.* **1986,** (17), 1346-1347.
30. Koch, F. P. V.; Rivnay, J.; Foster, S.; Müller, C.; Downing, J. M.; Buchaca-Domingo, E.; Westacott, P.; Yu, L.; Yuan, M.; Baklar, M.; Fei, Z.; Luscombe, C.; McLachlan, M. A.; Heeney, M.; Rumbles, G.; Silva, C.; Salleo, A.; Nelson, J.; Smith, P.; Stingelin, N., *Prog. Polym. Sci.* **2013,** *38* (12), 1978-1989.
31. Müller, C., *Chem. Mater.* **2015,** *27* (8), 2740-2754.
32. Kline, R. J.; McGehee, M. D.; Kadnikova, E. N.; Liu, J.; Fréchet, J. M. J.; Toney, M. F., *Macromolecules* **2005,** *38* (8), 3312-3319.
33. Wu, Z.; Petzold, A.; Henze, T.; Thurn-Albrecht, T.; Lohwasser, R. H.; Sommer, M.; Thelakkat, M., *Macromolecules* **2010,** *43* (10), 4646-4653.
34. Zen, A.; Pflaum, J.; Hirschmann, S.; Zhuang, W.; Jaiser, F.; Asawapirom, U.; Rabe, J. P.; Scherf, U.; Neher, D., *Adv. Funct. Mater.* **2004,** *14* (8), 757-764.
35. Zen, A.; Saphiannikova, M.; Neher, D.; Grenzer, J.; Grigorian, S.; Pietsch, U.; Asawapirom, U.; Janietz, S.; Scherf, U.; Lieberwirth, I.; Wegner, G., *Macromolecules* **2006,** *39* (6), 2162-2171.
36. Verilhac, J.-M.; LeBlevennec, G.; Djurado, D.; Rieutord, F.; Chouiki, M.; Travers, J.-P.; Pron, A., *Synth. Met.* **2006,** *156* (11), 815-823.
37. Yang, H.; Shin, T. J.; Yang, L.; Cho, K.; Ryu, C. Y.; Bao, Z., *Adv. Funct. Mater.* **2005,** *15* (4), 671-676.
38. Yang, H.; LeFevre, S. W.; Ryu, C. Y.; Bao, Z., *Appl. Phys. Lett.* **2007,** *90* (17), 172116.
39. Dang, M. T.; Hirsch, L.; Wantz, G.; Wuest, J. D., *Chem. Rev.* **2013,** *113* (5), 3734-3765.
40. Ludwigs, S., Springer-Verlag: Berlin Heidelberg, 2014; pp 41-42.
41. Ludwigs, S., Springer-Verlag: Berlin Heidelberg, 2014; pp 97-103.
42. Rahimi, K.; Botiz, I.; Stingelin, N.; Kayunkid, N.; Sommer, M.; Koch, F. P. V.; Nguyen, H.; Coulembier, O.; Dubois, P.; Brinkmann, M.; Reiter, G., *Angew. Chem. Int. Ed.* **2012,** *51* (44), 11131-11135.
43. Ihn, K. J.; Moulton, J.; Smith, P., *J. Polym. Sci., Part B: Polym. Phys.* **1993,** *31* (6), 735-742.
44. Berson, S.; De Bettignies, R.; Bailly, S.; Guillerez, S., *Adv. Funct. Mater.* **2007,** *17* (8), 1377-1384.
45. Sun, S.; Salim, T.; Wong, L. H.; Foo, Y. L.; Boey, F.; Lam, Y. M., *J. Mater. Chem.* **2011,** *21* (2), 377-386.
46. Kiriy, N.; Jähne, E.; Adler, H.-J.; Schneider, M.; Kiriy, A.; Gorodyska, G.; Minko, S.; Jehnichen, D.; Simon, P.; Fokin, A. A.; Stamm, M., *Nano Lett.* **2003,** *3* (6), 707-712.

47. Kim, B.-G.; Kim, M.-S.; Kim, J., *ACS Nano* **2010,** *4* (4), 2160-2166.
48. Chang, J.-F.; Sun, B.; Breiby, D. W.; Nielsen, M. M.; Sölling, T. I.; Giles, M.; McCulloch, I.; Sirringhaus, H., *Chem. Mater.* **2004,** *16* (23), 4772-4776.
49. Bao, Z.; Dodabalapur, A.; Lovinger, A. J., *Appl. Phys. Lett.* **1996,** *69* (26), 4108-4110.
50. Wang, G.; Swensen, J.; Moses, D.; Heeger, A. J., *J. Appl. Phys.* **2003,** *93* (10), 6137-6141.
51. Treat, N. D.; Nekuda Malik, J. A.; Reid, O.; Yu, L.; Shuttle, C. G.; Rumbles, G.; Hawker, C. J.; Chabinyc, M. L.; Smith, P.; Stingelin, N., *Nat. Mater.* **2013,** *12*, 628.
52. Brinkmann, M.; Wittmann, J.-C., *Adv. Mater.* **2006,** *18* (7), 860-863.
53. Nagamatsu, S.; Takashima, W.; Kaneto, K.; Yoshida, Y.; Tanigaki, N.; Yase, K.; Omote, K., *Macromolecules* **2003,** *36* (14), 5252-5257.
54. Hartmann, L.; Tremel, K.; Uttiya, S.; Crossland, E.; Ludwigs, S.; Kayunkid, N.; Vergnat, C.; Brinkmann, M., *Adv. Funct. Mater.* **2011,** *21* (21), 4047-4057.
55. Biniek, L.; Leclerc, N.; Heiser, T.; Bechara, R.; Brinkmann, M., *Macromolecules* **2013,** *46* (10), 4014-4023.
56. Hamidi-Sakr, A.; Biniek, L.; Bantignies, J.-L.; Maurin, D.; Herrmann, L.; Leclerc, N.; Lévêque, P.; Vijayakumar, V.; Zimmermann, N.; Brinkmann, M., *Adv. Funct. Mater.* **2017,** *27* (25), 1700173.
57. O'Connor, B.; Kline, R. J.; Conrad, B. R.; Richter, L. J.; Gundlach, D.; Toney, M. F.; DeLongchamp, D. M., *Adv. Funct. Mater.* **2011,** *21* (19), 3697-3705.
58. Crossland, E. J. W.; Tremel, K.; Fischer, F.; Rahimi, K.; Reiter, G.; Steiner, U.; Ludwigs, S., *Adv. Mater.* **2012,** *24* (6), 839-844.
59. Han, C. C.; Elsenbaumer, R. L., *Synth. Met.* **1989,** *30* (1), 123-131.
60. Heeger, A. J., *Synth. Met.* **2001,** *125* (1), 23-42.
61. Epstein, A. J.; Ginder, J. M.; Zuo, F.; Woo, H. S.; Tanner, D. B.; Richter, A. F.; Angelopoulos, M.; Huang, W. S.; MacDiarmid, A. G., *Synth. Met.* **1987,** *21* (1), 63-70.
62. Cao, Y.; Smith, P.; Heeger, A. J., *Synth. Met.* **1992,** *48* (1), 91-97.
63. Jacobs, I. E. and Moulé, A. J., *Adv. Mater.* **2017,** *29* (42), 1703063.
64. Salzmann, I.; Heimel, G.; Oehzelt, M.; Winkler, S.; Koch, N., *Acc. Chem. Res.* **2016,** *49* (3), 370-378.
65. Welch, G. C.; Coffin, R.; Peet, J.; Bazan, G. C., *J. Am. Chem. Soc.* **2009,** *131* (31), 10802-10803.
66. Pingel, P.; Arvind, M.; Kölln, L.; Steyrleuthner, R.; Kraffert, F.; Behrends, J.; Janietz, S.; Neher, D., *Adv. Electron. Mater.* **2016,** *2* (10), 1600204.
67. Han, Y.; Barnes, G.; Lin, Y.-H.; Martin, J.; Al-Hashimi, M.; AlQaradawi, S. Y.; Anthopoulos, T. D.; Heeney, M., *Chem. Mater.* **2016,** *28* (21), 8016-8024.

68. Yurash, B.; Cao, D. X.; Brus, V. V.; Leifert, D.; Wang, M.; Dixon, A.; Seifrid, M.; Mansour, A. E.; Lungwitz, D.; Liu, T.; Santiago, P. J.; Graham, K. R.; Koch, N.; Bazan, G. C.; Nguyen, T.-Q., *Nat. Mater.* **2019**.
69. Bredas, J. L.; Street, G. B., *Acc. Chem. Res.* **1985,** *18* (10), 309-315.
70. Méndez, H.; Heimel, G.; Winkler, S.; Frisch, J.; Opitz, A.; Sauer, K.; Wegner, B.; Oehzelt, M.; Röthel, C.; Duhm, S.; Többens, D.; Koch, N.; Salzmann, I., *Nat. Commun.* **2015,** *6*, 8560.
71. Jacobs, I. E.; Cendra, C.; Harrelson, T. F.; Bedolla Valdez, Z. I.; Faller, R.; Salleo, A.; Moulé, A. J., *Mater. Horiz.* **2018,** *5* (4), 655-660.
72. Salzmann, I.; Heimel, G.; Duhm, S.; Oehzelt, M.; Pingel, P.; George, B. M.; Schnegg, A.; Lips, K.; Blum, R.-P.; Vollmer, A.; Koch, N., *Phys. Rev. Lett.* **2012,** *108* (3), 035502.
73. Li, J.; Duchemin, I.; Roscioni, O. M.; Friederich, P.; Anderson, M.; Da Como, E.; Kociok-Köhn, G.; Wenzel, W.; Zannoni, C.; Beljonne, D.; Blase, X.; D'Avino, G., *Mater. Horiz.* **2019,** *6* (1), 107-114.
74. Ghani, F.; Opitz, A.; Pingel, P.; Heimel, G.; Salzmann, I.; Frisch, J.; Neher, D.; Tsami, A.; Scherf, U.; Koch, N., *J. Polym. Sci., Part B: Polym. Phys.* **2015,** *53* (1), 58-63.
75. Di Nuzzo, D.; Fontanesi, C.; Jones, R.; Allard, S.; Dumsch, I.; Scherf, U.; von Hauff, E.; Schumacher, S.; Da Como, E., *Nat. Commun.* **2015,** *6* (1), 6460.
76. Pingel, P.; Zhu, L.; Park, K. S.; Vogel, J.-O.; Janietz, S.; Kim, E.-G.; Rabe, J. P.; Brédas, J.-L.; Koch, N., *J. Phys. Chem. Lett.* **2010,** *1* (13), 2037-2041.
77. Méndez, H.; Heimel, G.; Opitz, A.; Sauer, K.; Barkowski, P.; Oehzelt, M.; Soeda, J.; Okamoto, T.; Takeya, J.; Arlin, J.-B.; Balandier, J.-Y.; Geerts, Y.; Koch, N.; Salzmann, I., *Angew. Chem. Int. Ed.* **2013,** *52* (30), 7751-7755.
78. Li, J.; Zhang, G.; Holm, D. M.; Jacobs, I. E.; Yin, B.; Stroeve, P.; Mascal, M.; Moulé, A. J., *Chem. Mater.* **2015,** *27* (16), 5765-5774.
79. Patel, S. N.; Glaudell, A. M.; Peterson, K. A.; Thomas, E. M.; O'Hara, K. A.; Lim, E.; Chabinyc, M. L., *Sci. Adv.* **2017,** *3* (6).
80. Mityashin, A.; Olivier, Y.; Van Regemorter, T.; Rolin, C.; Verlaak, S.; Martinelli, N. G.; Beljonne, D.; Cornil, J.; Genoe, J.; Heremans, P., *Adv. Mater.* **2012,** *24* (12), 1535-1539.
81. Scholes, D. T.; Hawks, S. A.; Yee, P. Y.; Wu, H.; Lindemuth, J. R.; Tolbert, S. H.; Schwartz, B. J., *J. Phys. Chem. Lett.* **2015,** *6* (23), 4786-4793.
82. Duong, D. T.; Wang, C.; Antono, E.; Toney, M. F.; Salleo, A., *Org. Electron.* **2013,** *14* (5), 1330-1336.
83. Kang, K.; Watanabe, S.; Broch, K.; Sepe, A.; Brown, A.; Nasrallah, I.; Nikolka, M.; Fei, Z.; Heeney, M.; Matsumoto, D.; Marumoto, K.; Tanaka, H.; Kuroda, S.-i.; Sirringhaus, H., *Nat. Mater.* **2016,** *15*, 896.
84. Hynynen, J.; Kiefer, D.; Yu, L.; Kroon, R.; Munir, R.; Amassian, A.; Kemerink, M.; Müller, C., *Macromolecules* **2017,** *50* (20), 8140-8148.

85. Lim, E.; Peterson, K. A.; Su, G. M.; Chabinyc, M. L., *Chem. Mater.* **2018,** *30* (3), 998-1010.
86. Jacobs, I. E.; Aasen, E. W.; Oliveira, J. L.; Fonseca, T. N.; Roehling, J. D.; Li, J.; Zhang, G.; Augustine, M. P.; Mascal, M.; Moulé, A. J., *J. Mater. Chem. C* **2016,** *4* (16), 3454-3466.
87. Kroon, R.; Ryan, J. D.; Kiefer, D.; Yu, L.; Hynynen, J.; Olsson, E.; Müller, C., *Adv. Funct. Mater.* **2017,** *27* (47), 1704183.
88. Nogami, Y.; Kaneko, H.; Ishiguro, T.; Takahashi, A.; Tsukamoto, J.; Hosoito, N., *Solid State Commun.* **1990,** *76* (5), 583-586.
89. Rolland, M.; Lefrant, S.; Aldissi, M.; Bernier, P.; Rzepka, E.; Schue, F., *J. Electron. Mater.* **1981,** *10* (4), 619-630.
90. Connelly, N. G. and Geiger, W. E., *Chem. Rev.* **1996,** *96* (2), 877-910.
91. Qi, Y.; Sajoto, T.; Kröger, M.; Kandabarow, A. M.; Park, W.; Barlow, S.; Kim, E.-G.; Wielunski, L.; Feldman, L. C.; Bartynski, R. A.; Brédas, J.-L.; Marder, S. R.; Kahn, A., *Chem. Mater.* **2010,** *22* (2), 524-531.
92. Kiefer, D.; Yu, L.; Fransson, E.; Gómez, A.; Primetzhofer, D.; Amassian, A.; Campoy-Quiles, M.; Müller, C., *Adv. Sci.* **2017,** *4* (1), 1600203.
93. Wang, C.; Duong, D. T.; Vandewal, K.; Rivnay, J.; Salleo, A., *Phys. Rev. B* **2015,** *91* (8), 085205.
94. Ko, S.; Hoke, E. T.; Pandey, L.; Hong, S.; Mondal, R.; Risko, C.; Yi, Y.; Noriega, R.; McGehee, M. D.; Brédas, J.-L.; Salleo, A.; Bao, Z., *J. Am. Chem. Soc.* **2012,** *134* (11), 5222-5232.
95. Voss, M. G.; Scholes, D. T.; Challa, J. R.; Schwartz, B. J., *Faraday Discuss.* **2019,** *216* (0), 339-362.
96. Pingel, P. and Neher, D., *Phys. Rev. B* **2013,** *87* (11), 115209.
97. Aubry, T. J.; Axtell, J. C.; Basile, V. M.; Winchell, K. J.; Lindemuth, J. R.; Porter, T. M.; Liu, J.-Y.; Alexandrova, A. N.; Kubiak, C. P.; Tolbert, S. H.; Spokoyny, A. M.; Schwartz, B. J., *Adv. Mater.* **2019,** *31* (11), 1805647.
98. Liang, Z.; Zhang, Y.; Souri, M.; Luo, X.; Boehm, Alex M.; Li, R.; Zhang, Y.; Wang, T.; Kim, D.-Y.; Mei, J.; Marder, S. R.; Graham, K. R., *J. Mater. Chem. A* **2018,** *6* (34), 16495-16505.
99. Joseph Kline, R.; McGehee, M. D.; Toney, M. F., *Nat. Mater.* **2006,** *5* (3), 222-228.
100. Müller, L.; Nanova, D.; Glaser, T.; Beck, S.; Pucci, A.; Kast, A. K.; Schröder, R. R.; Mankel, E.; Pingel, P.; Neher, D.; Kowalsky, W.; Lovrincic, R., *Chem. Mater.* **2016,** *28* (12), 4432-4439.
101. Harrelson, T. F.; Cheng, Y. Q.; Li, J.; Jacobs, I. E.; Ramirez-Cuesta, A. J.; Faller, R.; Moulé, A. J., *Macromolecules* **2017,** *50* (6), 2424-2435.
102. Prosa, T. J.; Winokur, M. J.; McCullough, R. D., *Macromolecules* **1996,** *29* (10), 3654-3656.
103. Scholes, D. T.; Yee, P. Y.; Lindemuth, J. R.; Kang, H.; Onorato, J.; Ghosh, R.; Luscombe, C. K.; Spano, F. C.; Tolbert, S. H.; Schwartz, B. J., *Adv. Funct. Mater.* **2017,** *27* (44), 1702654.

104. Liu, W.; Müller, L.; Ma, S.; Barlow, S.; Marder, S. R.; Kowalsky, W.; Köhn, A.; Lovrincic, R., *J. Phys. Chem. C* **2018,** *122* (49), 27983-27990.
105. Sirringhaus, H.; Brown, P. J.; Friend, R. H.; Nielsen, M. M.; Bechgaard, K.; Langeveld-Voss, B. M. W.; Spiering, A. J. H.; Janssen, R. A. J.; Meijer, E. W.; Herwig, P.; de Leeuw, D. M., *Nature* **1999,** *401* (6754), 685-688.
106. Rivnay, J.; Noriega, R.; Kline, R. J.; Salleo, A.; Toney, M. F., *Phys. Rev. B* **2011,** *84* (4), 045203.
107. Noriega, R.; Rivnay, J.; Vandewal, K.; Koch, F. P. V.; Stingelin, N.; Smith, P.; Toney, M. F.; Salleo, A., *Nat. Mater.* **2013,** *12*, 1038.
108. Zuo, G.; Abdalla, H.; Kemerink, M., *Phys. Rev. B* **2016,** *93* (23), 235203.
109. Xie, W.; He, J.; Kang, H. J.; Tang, X.; Zhu, S.; Laver, M.; Wang, S.; Copley, J. R. D.; Brown, C. M.; Zhang, Q.; Tritt, T. M., *Nano Lett.* **2010,** *10* (9), 3283-3289.
110. Liu, J.; Wang, X.; Li, D.; Coates, N. E.; Segalman, R. A.; Cahill, D. G., *Macromolecules* **2015,** *48* (3), 585-591.
111. Wang, X.; Ho, V.; Segalman, R. A.; Cahill, D. G., *Macromolecules* **2013,** *46* (12), 4937-4943.
112. Jung, I. H.; Hong, C. T.; Lee, U.-H.; Kang, Y. H.; Jang, K.-S.; Cho, S. Y., *Sci. Rep.* **2017,** *7*, 44704.
113. Patel, S. N.; Glaudell, A. M.; Kiefer, D.; Chabinyc, M. L., *ACS Macro Lett.* **2016,** *5* (3), 268-272.
114. Bubnova, O.; Khan, Z. U.; Malti, A.; Braun, S.; Fahlman, M.; Berggren, M.; Crispin, X., *Nat. Mater.* **2011,** *10* (6), 429-433.
115. Kim, G. H.; Shao, L.; Zhang, K.; Pipe, K. P., *Nat. Mater.* **2013,** *12*, 719.
116. Zhao, L.-D.; Lo, S.-H.; Zhang, Y.; Sun, H.; Tan, G.; Uher, C.; Wolverton, C.; Dravid, V. P.; Kanatzidis, M. G., *Nature* **2014,** *508*, 373.
117. Glaudell, A. M.; Cochran, J. E.; Patel, S. N.; Chabinyc, M. L., *Adv. Energy Mater.* **2015,** *5* (4), 1401072.
118. Lim, E.; Glaudell, A. M.; Miller, R.; Chabinyc, M. L., *Adv. Electron. Mater.* **2019**, 1800915.
119. PubChem.
120. Reichhardt C. and Welton T., Wiley-VCH: 2010.
121. Clark, J.; Chang, J.-F.; Spano, F. C.; Friend, R. H.; Silva, C., *Appl. Phys. Lett.* **2009,** *94* (16), 163306.
122. Spano, F. C., *J. Chem. Phys.* **2005,** *122* (23), 234701.
123. Spano, F. C., *Chem. Phys.* **2006,** *325* (1), 22-35.
124. Fabiano S., P. I., Fleury G., Hadziioannou G. and Crispin X., Wiley: Weinheim, 2017; pp 37-52.
125. Gao, J.; Niles, E. T.; Grey, J. K., *J. Phys. Chem. Lett.* **2013,** *4* (17), 2953-2957.

126. Chew, A. R.; Ghosh, R.; Shang, Z.; Spano, F. C.; Salleo, A., *J. Phys. Chem. Lett.* **2017,** *8* (20), 4974-4980.
127. Yee, P. Y.; Scholes, D. T.; Schwartz, B. J.; Tolbert, S. H., *J. Phys. Chem. Lett.* **2019,** *10* (17), 4929-4934.
128. Li, J.; Rochester, C. W.; Jacobs, I. E.; Aasen, E. W.; Friedrich, S.; Stroeve, P.; Moulé, A. J., *Org. Electron.* **2016,** *33*, 23-31.
129. Duhm, S.; Salzmann, I.; Bröker, B.; Glowatzki, H.; Johnson, R. L.; Koch, N.,. *Appl. Phys. Lett.* **2009,** *95* (9), 093305.
130. Vijayakumar, V.; Zhong, Y.; Untilova, V.; Bahri, M.; Herrmann, L.; Biniek, L.; Leclerc, N.; Brinkmann, M., *Adv. Energy Mater.* **2019,** *9* (24), 1900266.
131. Park, Y. W.; Park, C.; Lee, Y. S.; Yoon, C. O.; Shirakawa, H.; Suezaki, Y.; Akagi, K., *Solid State Commun.* **1988,** *65* (2), 147-150.
132. Qu, S.; Yao, Q.; Wang, L.; Chen, Z.; Xu, K.; Zeng, H.; Shi, W.; Zhang, T.; Uher, C.; Chen, L., *NPG Asia Mater.* **2016,** *8* (7), e292-e292.
133. Fanous, J.; Schweizer, M.; Schawaller, D.; Buchmeiser, M. R., *Macromol. Mater. Eng.* **2012,** *297* (2), 123-127.
134. Moulton, J. and Smith, P., *Synth. Met.* **1991,** *40* (1), 13-22.
135. Hynynen, J.; Järsvall, E.; Kroon, R.; Zhang, Y.; Barlow, S.; Marder, S. R.; Kemerink, M.; Lund, A.; Müller, C., *ACS Macro Lett.* **2019,** *8* (1), 70-76.
136. Hewitt, C. A.; Kaiser, A. B.; Roth, S.; Craps, M.; Czerw, R.; Carroll, D. L., *Nano Lett.* **2012,** *12* (3), 1307-1310.
137. Søndergaard, R. R.; Hösel, M.; Espinosa, N.; Jørgensen, M.; Krebs, F. C., *Energ. Sci. Eng.* **2013,** *1* (2), 81-88.
138. Wei, Q.; Mukaida, M.; Kirihara, K.; Ishida, T., *ACS Macro Lett.* **2014,** *3* (9), 948-952.
139. Du, Y.; Cai, K.; Chen, S.; Wang, H.; Shen, S. Z.; Donelson, R.; Lin, T., *Sci. Rep.* **2015,** *5*, 6411.
140. Ryan, J. D.; Mengistie, D. A.; Gabrielsson, R.; Lund, A.; Müller, C., *ACS Appl. Mater. Interfaces* **2017,** *9* (10), 9045-9050.
141. Müller, C.; Zhigadlo, N. D.; Kumar, A.; Baklar, M. A.; Karpinski, J.; Smith, P.; Kreouzis, T.; Stingelin, N., *Macromolecules* **2011,** *44* (6), 1221-1225.
142. Baklar, M. A.; Koch, F.; Kumar, A.; Domingo, E. B.; Campoy-Quiles, M.; Feldman, K.; Yu, L.; Wobkenberg, P.; Ball, J.; Wilson, R. M.; McCulloch, I.; Kreouzis, T.; Heeney, M.; Anthopoulos, T.; Smith, P.; Stingelin, N., *Adv. Mater.* **2010,** *22* (35), 3942-3947.
143. Koppe, M.; Brabec, C. J.; Heiml, S.; Schausberger, A.; Duffy, W.; Heeney, M.; McCulloch, I., *Macromolecules* **2009,** *42* (13), 4661-4666.
144. Heffner, G. W. and Pearson, D. S., *Macromolecules* **1991,** *24* (23), 6295-6299.
145. Brinkmann, M. and Rannou, P., *Adv. Funct. Mater.* **2007,** *17* (1), 101-108.

146. Lund, A.; van der Velden, N. M.; Persson, N. K.; Hamedi, M. M.; Müller, C., *Mater. Sci. Eng. R Rep.* **2018,** *126*, 1-29.
147. Mohapatra, S. K.; Zhang, Y.; Sandhu, B.; Fonari, M. S.; Timofeeva, T. V.; Marder, S. R.; Barlow, S., Synthesis, *Polyhedron* **2016,** *116*, 88-95.
148. Root, S. E.; Savagatrup, S.; Printz, A. D.; Rodriquez, D.; Lipomi, D. J., *Chem. Rev.* **2017,** *117* (9), 6467-6499.
149. Cao, Y.; Smith, P.; Heeger, A. J., *Polymer* **1991,** *32* (7), 1210-1218.
150. Andreatta, A.; Cao, Y.; Chiang, J. C.; Heeger, A. J.; Smith, P., *Synth. Met.* **1988,** *26* (4), 383-389.
151. Zhou, J.; Li, E. Q.; Li, R.; Xu, X.; Ventura, I. A.; Moussawi, A.; Anjum, D. H.; Hedhili, M. N.; Smilgies, D.-M.; Lubineau, G.; Thoroddsen, S. T., *J. Mater. Chem. C* **2015,** *3* (11), 2528-2538.
152. Tokito, S.; Smith, P.; Heeger, A. J., *Synth. Met.* **1990,** *36* (2), 183-194.
153. Liu, K.; Sun, Y.; Lin, X.; Zhou, R.; Wang, J.; Fan, S.; Jiang, K., *ACS Nano* **2010,** *4* (10), 5827-5834.
154. Zhang, M.; Atkinson, K. R.; Baughman, R. H., *Science* **2004,** *306* (5700), 1358-1361.
155. Zhang, S.; Koziol, K. K. K.; Kinloch, I. A.; Windle, A. H., *Small* **2008,** *4* (8), 1217-1222.
156. Seyedin, S.; Razal, J. M.; Innis, P. C.; Wallace, G. G., *Smart Mater. Struct.* **2016,** *25* (3), 035015.
157. Qi, H.; Schulz, B.; Vad, T.; Liu, J.; Mäder, E.; Seide, G.; Gries, T., *ACS Appl. Mater. Interfaces* **2015,** *7* (40), 22404-22412.
158. Moulton, J. and Smith, P., *J. Polym. Sci., Part B: Polym. Phys.* **1992,** *30* (8), 871-878.
159. Andreatta, A. and Smith, P., *Synth. Met.* **1993,** *55* (2), 1017-1022.
160. Seyedin, M. Z.; Razal, J. M.; Innis, P. C.; Wallace, G. G., *Adv. Funct. Mater.* **2014,** *24* (20), 2957-2966.
161. Xia, Y.; Yun, L., *Compos. Sci. Technol.* **2008,** *68* (6), 1471-1479.
162. Garg, S.; Hurren, C.; Kaynak, A., *Synth. Met.* **2007,** *157* (1), 41-47.
163. Takamatsu, S.; Kobayashi, T.; Shibayama, N.; Miyake, K.; Itoh, T., *Sensors and Actuators A: Physical* **2012,** *184*, 57-63.
164. Müller, C.; Hamedi, M.; Karlsson, R.; Jansson, R.; Marcilla, R.; Hedhammar, M.; Inganäs, O., *Adv. Mater.* **2011,** *23* (7), 898-901.
165. Balandin, A. A., *Nat. Mater.* **2011,** *10* (8), 569-581.
166. Xu, Y.; Wang, X.; Zhou, J.; Song, B.; Jiang, Z.; Lee, E. M. Y.; Huberman, S.; Gleason, K. K.; Chen, G., *Sci. Adv.* **2018,** *4* (3), eaar3031.
167. Rausch, S.; Rauh, D.; Deibel, C.; Vidi, S.; Ebert, H. P., *Int. J. Thermophys.* **2013,** *34* (5), 820-830.
168. Duda, J. C.; Hopkins, P. E.; Shen, Y.; Gupta, M. C., *Appl. Phys. Lett.* **2013,** *102* (25), 251912.

169. Kroon, R.; Kiefer, D.; Stegerer, D.; Yu, L.; Sommer, M.; Müller, C., *Adv. Mater.* **2017,** *29* (24), 1700930.
170. Kroon, R.; Hofmann, A. I.; Yu, L.; Lund, A.; Müller, C., *Chem. Mater.* **2019,** *31* (8), 2770-2777.
171. Hufnagel, M.; Muth, M.-A.; Brendel, J. C.; Thelakkat, M., *Macromolecules* **2014,** *47* (7), 2324-2332.
172. Gernigon, V.; Lévêque, P.; Brochon, C.; Audinot, J.-N.; Leclerc, N.; Bechara, R.; Richard, F.; Heiser, T.; Hadziioannou, G., *Eur. Phys. J. Appl. Phys.* **2011,** *56* (3), 34107.